Pacific Northwest
NATIONAL LABORATORY

PNNL- 32170-2

DSO+T: Integrated System Simulation

DSO+T Study: Volume 2

January 2022

Hayden M Reeve
Ankit Singhal
Ahmad Tbaileh
Rob Pratt
Trevor Hardy
Jeff Doty
Laurentiu Marinovici
Sadie Bender
Mitch Pelton
Matt Oster

U.S. DEPARTMENT OF ENERGY

Prepared for the U.S. Department of Energy
under Contract DE-AC05-76RL01830

DISCLAIMER

PACIFIC NORTHWEST NATIONAL LABORATORY
operated by
BATTELLE
for the
UNITED STATES DEPARTMENT OF ENERGY
under Contract DE-AC05-76RL01830

Printed in the United States of America

Available to DOE and DOE contractors from the
Office of Scientific and Technical Information,
P.O. Box 62, Oak Ridge, TN 37831-0062;
ph: (865) 576-8401
fax: (865) 576-5728
email: reports@adonis.osti.gov

Available to the public from the National Technical Information Service
5301 Shawnee Rd., Alexandria, VA 22312
ph: (800) 553-NTIS (6847)
email: orders@ntis.gov <https://www.ntis.gov/about>
Online ordering: http://www.ntis.gov

PNNL- 32170-2

DSO+T: Integrated System Simulation

DSO+T Study: Volume 2

January 2022

Hayden M Reeve
Ankit Singhal
Ahmad Tbaileh
Rob Pratt
Trevor Hardy
Jeff Doty
Laurentiu Marinovici
Sadie Bender
Mitch Pelton
Matt Oster

Prepared for
the U.S. Department of Energy
under Contract DE-AC05-76RL01830

Pacific Northwest National Laboratory
Richland, Washington 99354

Abstract

This report summarizes an integrated co-simulation model used by the Distribution System Operator with Transactive (DSO+T) study to represent an electrical generation, delivery, and end-load systems for the purposes of assessing the viability and value proposition of transactive energy coordination of flexible assets versus a business-as-usual case. The integrated co-simulation model includes the bulk generation and transmission system, including the day-ahead and real-time scheduling and dispatch of thermal generators. Forty distribution system operators were modeled in detail, including tens of thousands of residential and commercial buildings and their flexible end loads. These included heating, ventilation, and cooling systems; residential water heaters; electric vehicles; and stationary behind-the-meter batteries. Both wholesale market and end-load results for the business-as-usual case are presented and compared to actual ERCOT system data to assess the accuracy and representativeness of the resulting model.

Summary

The purpose of the Distribution System Operation with Transactive (DSO+T) study is to simulate and analyze how a distribution system operator (DSO) can engage flexible distributed energy resources (DERs) by utilizing a coordination strategy based on transactive energy mechanisms. It seeks to compare two transactive cases (one with flexible loads, the other with batteries) against a business-as-usual case. These three cases are analyzed over two renewable energy scenarios, the first with moderate levels (~15%) of annual renewable generation, the second with high levels of renewable generation (~40%). To successfully understand the impact of this demand flexibility on the distribution and bulk power system operation this study must simulate the fully integrated electrical system, all the way from generators on the transmission system, to individual flexible assets such as heating, ventilation, and cooling (HVAC) units, water heaters, and batteries on the distribution system. The Electric Reliability Council of Texas (ERCOT) region was selected as an ideal system to serve as the basis of this analysis as it has a generation mix representative of the country, is summer peaking, is served by an independent system operator (ISO) wholesale market, and is of tractable size with no interconnections to other regions. This report details the definition of this integrated electrical system model and provides illustrative results showing the level of accuracy obtained. It is one of five reports documenting the DSO+T study.

The bulk generation and transmission system was modeled using Agent-Based Modeling of Electricity Systems (or AMES) to determine the day-ahead scheduling and real-time dispatch of the generation fleet and PYPOWER to solve the optimal power flow equation for the transmission system. A generation mix of coal, natural gas, nuclear, and wind generators was defined for the MR scenario to be representative of ERCOT and the nation as a whole. For the high renewables scenario solar generation was added along with an increase in wind generation capacity to achieve 40% annual renewable generation. Thermal generator startup and production costs, as well as performance parameters, were defined from existing literature. Wind and solar generation output was determined using existing models tuned to historical ERCOT generation and weather data. Forecast uncertainty was applied to day-ahead wind and solar generation estimates. Two synthetic transmission systems were used: an 8-bus model and a 200-bus model.

The resulting performance of the bulk generation and transmission system was compared to historical system data. The generation dispatch and mix was compared to 2016 ERCOT data, while the day-ahead and real-time locational marginal prices were compared to wholesale market prices seen in ERCOT, California (CAISO), and PJM. The calculated locational marginal prices captured the daily and net-load trends seen for prices on the ERCOT system. DSO+T average day-ahead and real-time prices were slightly higher than 2016 ERCOT market prices, similar to PJM market prices, and lower than CAISO market prices. As such, the DSO+T model provides average prices representative of national wholesale markets. The DSO+T results do, however, underpredict the daily range in prices, particularly large irregular price excursions. This may be due to either 1) a need to better define the market model to capture such irregular price escalations, or 2) real market behavior (such as charging of scarcity rent or generator self-scheduling) that is outside the capabilities of current market models. This is an area that warrants further investigation.

The distribution system and end loads were modeled in GridLAB-D™. Forty different DSOs were modeled to capture a range of utility sizes, climate zones, region types (urban, suburban, and rural), and a diversity of residential, commercial, and industrial load mix. Taxonomy

distribution feeders were used to capture distribution losses and miscellaneous loads. These distribution feeders were populated with tens of thousands of residential and commercial building models. To ensure a representative diversity of building types and load profiles was achieved the age, size, envelope insulation, heating fuel type, and occupancy levels were varied for each building based on national survey data and other literature sources. In addition, HVAC units and water heaters had randomized variation in size, performance, and usage schedules. The resulting populations of buildings and their equipment end loads helped ensure diurnal and seasonal load profiles that were representative of the ERCOT region.

The resulting distribution system load profiles were compared to 2016 ERCOT data. The DSO+T simulation model predicted the maximum and average system loads within ~5%. The minimum system load was predicted within 11%. The simulation did overpredict the daily range in system load by 37% on average. Other researchers, using different modeling approaches and datasets have also overpredicted this diurnal load change, particularly in the summer. This suggests that the research community requires either improved building population and parameter definition or the ability to capture additional phenomena in their modeling approaches.

Finally, this report also documents the assumptions and approaches used to define the populations of electric vehicles (EVs) and behind-the-meter batteries used in this study. Because only small numbers of EVs and batteries have been deployed to date they were not implemented in the business-as-usual case for the MR scenario. The low level of adoption also limits available data on the expected population distribution of these DERs in the future. The resulting populations are based on vendor data as well as current sales data and extrapolation assumptions.

Acknowledgments

This project was supported by the Department of Energy, Office of Electricity, Advanced Grid Research and Develop Program. The authors would like to thank Chris Irwin for his support and contributions to shaping the scope and direction of the DSO+T study.

Acronyms and Abbreviations

AMES	Agent-Based Modeling of Electricity Systems
ASHRAE	American Society of Heating, Refrigerating, and Air Conditioning Engineers
BAU	business-as-usual
CAISO	California Independent System Operator
CBECS	Commercial Building Energy Consumption Survey
COP	coefficient of performance
DER	distributed energy resource
DOE	Department of Energy
DSO	distribution system operator
DSO+T	Distribution System Operation with Transactive
EER	energy efficiency ratio
EIA	Energy Information Administration
ELCAP	End-Use Load and Conservation Assessment Program
ERCOT	Electricity Reliability Council of Texas
EV	electric vehicle
FL	full load
HR	high renewable
HUD	U.S. Housing and Urban Development
HVAC	heating, ventilation, and cooling
IECC	International Energy Conservation Code
ISO	independent system operator
LMP	locational marginal price
MCL	minimum compliant load
MR	moderate renewable
NREL	National Renewable Energy Laboratory
NSRDB	National Solar Radiation Database
PJM	Pennsylvania, Jersey, Maryland Power Pool
PNNL	Pacific Northwest National Laboratory
PV	photovoltaic
RECS	Residential Energy Consumption Survey
RTU	rooftop terminal unit
SAM	System Advisory Model
SCED	security-constrained economic dispatch
SCUC	security-constrained unit commitment
SHGC	solar heat gain coefficient

SOC	state of charge
TESP	Transactive Energy Simulation Platform
V1G	Variable Vehicle Charging from the Grid
V2G	Variable Vehicle Charging from the Grid including reverse power flow
WECC	Western Electricity Coordinating Council

Contents

Figures

Tables

1.0 Introduction

The Distribution System Operation with Transactive (DSO+T) study simulates and analyzes how a distribution system operator (DSO) can engage flexible distributed energy resources (DERs), such as air conditioners, water heaters, and batteries, in operation of the electric power system by using a coordination strategy based on transactive energy (Hammerstrom et al. 2007) mechanisms. This study is designed to:

- Design a DSO transactive network capable of coordinating DERs deployed at scale to produce benefits at both the distribution and bulk system levels.
- Test the design and estimate the benefits of a regional deployment at scale for a range of potential future grid scenarios using the valuation (Widergren et al. 2017) and co-simulation (Huang et al. 2019) frameworks developed previously for the U.S. Department of Energy's Transactive Systems Program.
- Issue the simulation and valuation framework to industry as an open challenge to the transactive energy community to develop and improve their designs in preparation for field experiments.

The DSO+T study involves comparing the engineering and economic performance of business-as-usual (BAU) cases representing today's distribution utilities with fixed-price rates for all customer classes and no active participation of price-responsive DERs with that of transactive cases in which the distribution utilities have evolved into DSOs that reflect their operational costs in the form of local retail markets for energy (and eventually other) services. It assumes most customers have installed price-responsive DERs such as batteries, electric vehicles (EVs), or flexible heating, ventilation, and cooling (HVAC) and water heating systems, which interact with forecasts of day-ahead and real-time dynamic prices—i.e., bid into the retail markets that discover optimal and equitable real-time prices in a distributed fashion characteristic of transactive energy systems.

A family of reports documents the study. The primary results are summarized in Volume 1 – Main Report (Reeve et al. 2022a), with considerable additional detail on the results of the analysis provided in Volume 5 – Study Results (Reeve et al. 2022b). The design of the transactive rates, retail markets, and DER control agents, and the presumed regulatory policies associated with the design, are described in Volume 3 – Transactive Energy Coordination Framework (Widergren et al. 2022). Volume 4 – Valuation and Economic Metrics (Pratt 2022) describes the process used to access the *value* of adopting the DSO+T strategy for all primary stakeholders by comparing the change in various metrics between any two cases of the study. This document (Volume 2) describes the instantiation of a large, multiscale, annual time-series co-simulation that is the foundation of the analysis, representing a nationally representative generation fleet, transmission system, and distribution system including retail customer building characteristics and controllable and uncontrollable loads and DERs.

The remainder of this section discusses the scenarios and system that set the requirements of the co-simulation environment which is then discussed. This is followed by a review of prior relevant efforts and a summary of the report structure.

1.1 Analysis Scenarios

At its most basic level, the study consists of two parallel analyses, each with its own BAU case to serve as a baseline. These are illustrated conceptually in Figure 1. The first analysis looks at the combined effect of a DSO engaging a fleet of flexible assets deployed at scale and connected with a transactive network, when there are moderate levels of renewables (moderate renewables [MR] scenario) in the power system. This level of renewable generation can reasonably be achieved for the U.S. as a whole in the absence of federal mandates, based on today's levels in California or Texas (30% and 15%, respectively). The second analysis is similar but assumes a high level of annual renewable generation (high renewables [HR] scenario) corresponding to aggressive renewables portfolio standards set by a number of states (~50% or more).

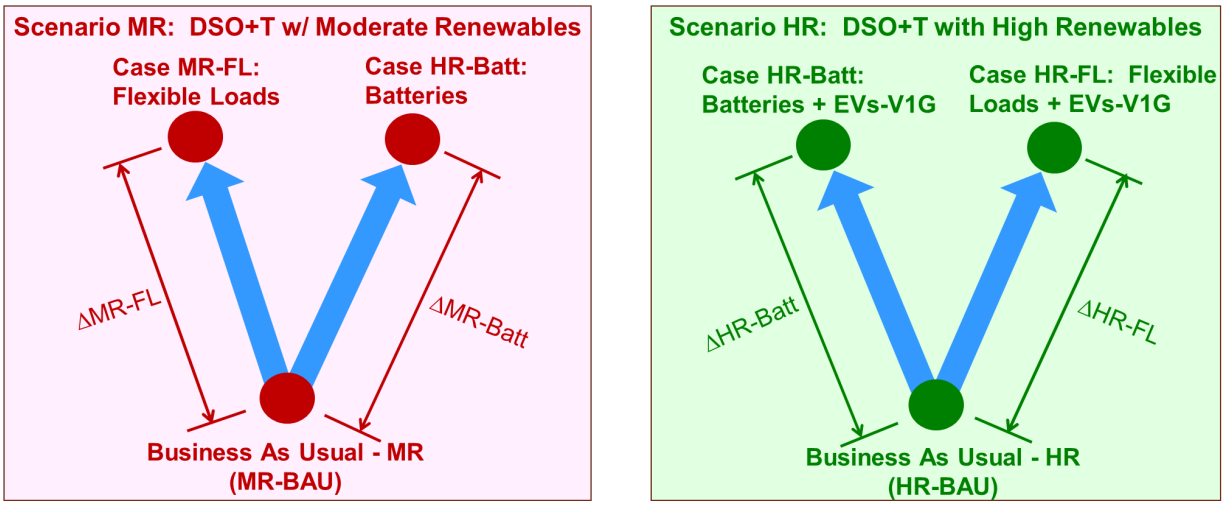

Figure 1. Summary of analysis scenarios: transactive flexible asset fleets with moderate and high levels of renewables.

Each analysis compares two transactive cases against its respective BAU case:

- The flexible load case assumes a high penetration of flexible loads with substantial customer participation as the primary component of the flexible asset fleet. It assumes that a majority of residential and commercial customers (~90%) install grid-responsive controls for primary end-use loads such as heating, cooling, and (residential) water heating.
- The battery storage case assumes that continued breakthroughs in reducing the cost of stationary battery storage and reluctance on the part of most customers to provide flexibility from their loads results in distributed storage dominating the flexible asset fleet. A comparable amount of distributed battery storage will be assumed, sufficient to provide approximately the same size resource as the fleet of flexible assets in the flexible load case.

The HR generation scenario also assumes that low-cost batteries spur a high level of penetration of EVs, with approximately 30% of homes having an EV.

1.2 System Overview

To successfully understand the impact of load flexibility on the distribution and bulk system operation, the study must simulate the fully integrated system, all the way from generators on

the transmission system to individual flexible assets such as HVAC units, water heaters, and batteries on the distribution system. Figure 2 shows the breadth of the DSO+T simulation. The bulk generation system contains a mix of thermal (natural gas, coal, nuclear) generators as well as wind and solar resources. They are connected to the distribution system via a 200-bus transmission model. The distribution system is represented by feeders that connect a combination of residential and commercial buildings, each with a combination of end loads.

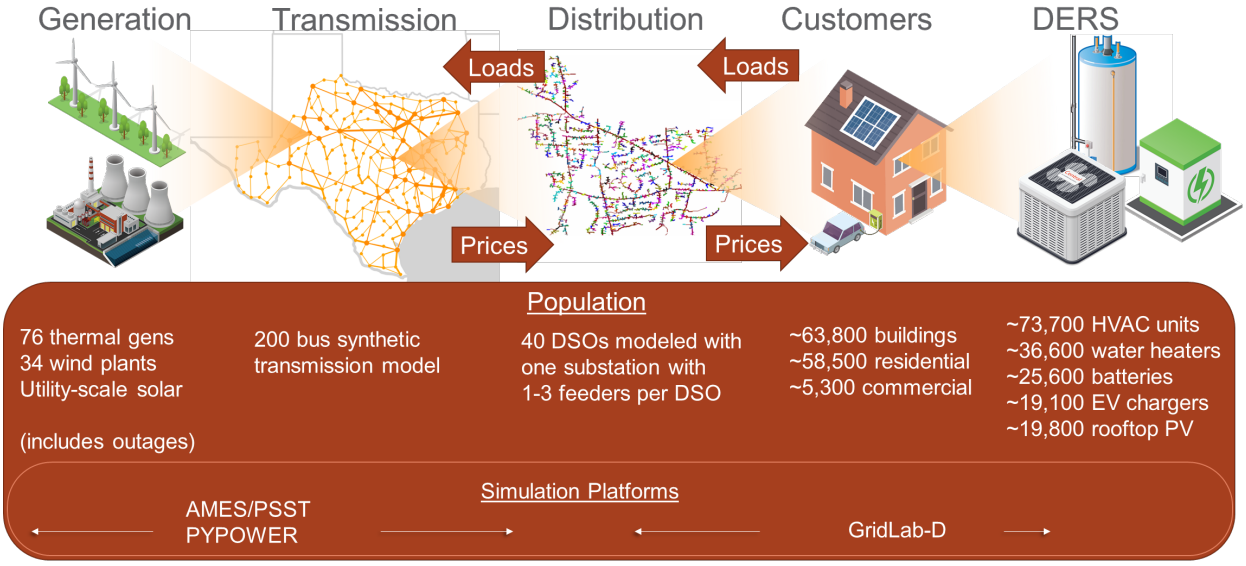

Figure 2. Overview of the system simulation breath, scale, and modeling platforms.

To successfully specify and define this system a number of requirements need to be met to ensure it is tractable and representative of national conditions. For example, a small power system model footprint for the analysis offers the advantage of having fewer generators, transmission lines, and DSOs that must be represented. However, using a typical research transmission network testbed is inappropriate as the basis for this study because realistic loads by customer class, generation mix, level of reserves, etc. are all critical determinants of the relative value of different cases. An actual U.S. bulk power system contains, by definition, real examples of all these infrastructure interactions and is therefore deemed a more realistic topological footprint for the analysis.

A number of desirable characteristics for the footprint were identified for consideration:

- Summer peaking loads are predominant in the United States and ideally would have the hot and humid summer peaks characteristic of the East and South (areas with winter peaks were not considered).
- Smaller is better with fewer generators, transmission lines, and buses being simpler to model and faster to simulate.
- Served by an independent system operator (ISO) wholesale market, which eliminates any bias in infrastructure capacity compared to load that may be associated with vertically integrated utility environments.
- One-to-one correspondence of the ISO and interconnection minimizes the need to model imports and exports.

- Existing renewables penetration comparable to the MR scenario minimizes the need to alter the grid model by retiring some fossil plants and adding more renewables.
- A mix of generation typical of the United States, including steam turbines and natural gas plants, better represents the degree of inherent flexibility of the generation fleet for the MR BAU case.

After considering a number of alternatives and tradeoffs such as size vs. complexity of the modeling effort, the Electric Reliability Council of Texas (ERCOT) region was selected as an ideal infrastructure for analysis of the bulk system in several respects. First, it is an entire interconnection with very little power transfer capability across its boundary. This offers the distinct advantage of allowing power imports and exports with load-serving entities and power generators outside the boundary of the analysis to be ignored. Simulating the entire Western Interconnection, for example, would be a much larger model, and the Eastern Interconnection even larger still. Both have substantial areas not served by ISOs. Limiting the footprint to the California Independent System Operator (CAISO) or New England ISO is more practical logistically but would require extensive modeling of imports and exports further complicated by the Energy Imbalance Market in the case of CAISO.

Further, most of Texas is served by the ERCOT ISO, with the exception of some municipal utilities in medium-sized cities (e.g., Austin, San Antonio) and generation and transmission cooperatives that serve the loads of a number of cooperative rural electric associations. Most of the municipals and generation and transmission cooperatives actively participate in the ERCOT market for at least a portion of their power supply, with 99% of the ERCOT load settled in the 15-minute market.

ERCOT has a wholesale generation mix that is fairly representative of the United States, compared to other ISO regions that are candidates for the study. As shown in Table 1, California (CAISO), New England (ISONE), and New York (NYISO) all have far less coal resources than the United States, and New England and New York ISOs also have significantly more nuclear power.

Table 1. Regional and U.S. generation for 2016 (fraction of wholesale energy produced).

Type of Generation	ERCOT	CAISO	ISONE	NYISO	United States
Natural gas	44%	50%	49%	44%	34%
Coal	29%	0%	2%	1%	30%
Wind	15%	7%	2%	3%	6%
Nuclear	12%	10%	31%	30%	20%
Other*	0%	34%	15%	22%	10%
Solar	0%	10%	1%	0%	1%
Nonsolar	<1%	24%	14%	22%	9%
TOTAL	100%	100%	100%	100%	100%

*Includes solar, hydro, geothermal, petroleum coke, biomass, and landfill gas.

Table 2 examines one important implication of the generation mix more closely, the degree of inherent flexibility in the existing generation fleet, which the transactive DERs will supplement. Examining only the nonintermittent generation (i.e., other than wind and solar), the dispatchable generation fleet is categorized in each region into its flexible (natural gas and hydropower plants) and minimally flexible (coal, nuclear, and other steam-based plants) components. This shows ERCOT as more representative of the U.S. fleet.

Table 2. Regional and U.S. nonintermittent generation for 2016 (fraction of wholesale energy produced).

Type of Generation	ERCOT	CAISO	ISONE	NYISO	United States
Natural and other gas, hydro	51%	75%	59%	65%	43%
Coal, nuclear, other**	49%	25%	41%	35%	57%
TOTAL	100%	100%	100%	100%	100%

**Includes geothermal, petroleum, and biomass.

Only ERCOT and CAISO have wholesale wind and solar renewable resource penetrations (15% and 17%, respectively) that approach the 20% target for the MR scenario. California has an additional 4% supplied by distributed solar photovoltaic (PV), as shown in Table 3, and additionally has renewable geothermal generation of over 4%.

Table 3. Nonutility solar generation for 2016 (fraction of wholesale energy).

Sector	ERCOT	CAISO	ISONE	NYISO	United States
Commercial	0.0%	0.9%	0.9%	0.2%	0.2%
Industrial	0.0%	0.7%	0.1%	0.0%	0.1%
Residential	0.1%	2.6%	0.7%	0.4%	0.3%
TOTAL	0.1%	4.2%	1.7%	0.6%	0.5%

It is important to emphasize that while ERCOT was selected to define the system model, the goal of the study is to develop a nationally representative model. This report will compare the results of the simulation (such as loads and market prices) to ERCOT to provide insight into the representativeness of this model. Comparisons will be made where possible to other regions as well. It is also important to remember that the performance of electricity systems change over time. While we have chosen 2016 as the year of comparison, the performance of ERCOT in other years can vary due to changes in fuel prices, load growth, climate conditions, and transmission and distribution upgrades. The aim of this simulation is to capture the essence of a fully integrated electricity delivery system. ERCOT data are used to gauge how well we have done, but the ultimate goal is to capture nationally representative behavior, not accurately model 2016 ERCOT behavior.

1.3 Co-simulation and Software Stack

Successfully simulating this fully integrated system requires use of a co-simulation platform to integrate and coordinate domain-appropriate tools. To achieve this we leveraged the Transactive Energy Simulation Platform (TESP) that enables the co-simulation of the bulk grid (generation and transmission) systems, distribution system, and end loads (TESP n.d.). More details about the TESP and its usage can be found in prior trial valuation analysis and simulation efforts conducted by Pacific Northwest National Laboratory (PNNL) (Widergren et al. 2017; Huang et al. 2019).

The bulk system is modeled using a combination of Agent-Based Modeling of Electricity Systems (AMES) and PYPOWER. AMES is an open-source tool, developed by Iowa State University (AMES n.d.), that was used to determine the day-ahead scheduling of generators and their real-time dispatch by solving the security-constrained unit commitment (SCUC) and security-constrained economic dispatch (SCED) optimization problems. PYPOWER (PYPOWER 2020) was used to solve the direct current optimal power flow equation for the transmission system.

The electrical distribution system, buildings, and all end loads were modeled using GridLAB-D. The distribution feeders were based on the taxonomy distribution feeders defined by PNNL (Schneider et al. 2008). GridLAB-D has a single-zone house model for simulating building envelope and internal gain loads as well as HVAC performance (GridLAB-D 2017). This house model has been validated and shown to adequately capture overall load shape (Fuller et al. n.d.) and dynamic power consumption at grid-relevant time scales (Gotseff and Lundstrom 2017; Schneider et al. 2016).

This overall co-simulation was run for 12 individual months, with the first three days of each month-long run used to initialize the simulation, and hence not included in the post-processed results. The transmission system (PYPOWER) and distribution system (GridLAB-D) were solved every 15 seconds. Real-time price information was passed between these two systems every 5 minutes. Hourly day-ahead and 5-minute real-time data were recorded for post-processing analysis.

1.4 Relevant Prior Work

This section highlights relevant prior work both in terms of large-scale grid system modeling as well as distribution system and end-load modeling. To the best of our knowledge no one has conducted a fully coupled and integrated co-simulation of price-responsive end loads supporting the operation of the bulk system through real-time and future (day-ahead) markets.

1.4.1 Large-Scale System Analysis

Prior work on large-scale modeling of the electrical delivery system, including simulating the impact of DER flexibility, has typically fallen into two camps. The first has focused on investigating regional impacts (such as system cost) through generation and transmission system modeling. End loads are typically not modeled in detail and are addressed using historical load profiles that have been parametrically adapted to reflect load growth and flexibility response. The second set of work focuses on higher fidelity modeling of end loads and DERs, including control and coordination mechanisms to achieve flexibility while respecting operational constraints. These efforts typically do not include simulation of the bulk system and wholesale considerations, including market prices, are considered boundary conditions that are not altered by changes in distribution system operation.

Examples of bulk system modeling includes work by Graham et al. (2013), who sought to do full electricity delivery system modeling to understand the costs of future scenarios for the Australian electric grid. This work did not address retail costs. In addition, it used a parametric load demand model that assumed load reductions (by device types) to existing and projected load profiles. No market coordination between DERs, the distribution system, and the wholesale market was demonstrated. Work by Vibrant Clean Energy (2019) sought to understand system and customer costs associated with the future decarbonization of generation and electrification of end loads in Colorado. Each scenario considered was evaluated through "*generator siting, transmission expansion, storage capacity additions, demand side resource deployment, transmission power flow, [and] economic dispatch"* across the entire Western Electricity Coordinating Council (WECC). While this work is informative in assumptions made about the adoption of renewables and EVs in the DSO+T study's HR scenario, demand-side resources were considered as an alternative resource that could be dispatched as needed at $60/MWh. Work by the Rocky Mountain Institute (Goldenberg et al. 2018) sought to evaluate the benefits of DER flexibility for enabling the adoption of high amounts of renewables on the ERCOT system in a 2050 scenario. This work applied constant assumptions about the amount of

flexibility per device as well as potential operation strategies. DER flexibility was not modeled in the context of varying adoption and participation rates or operational constraints (for example, comfort limitations on HVAC flexibility or driving patterns prohibiting EV flexibility).

An example of higher fidelity DER models in the context of the distribution system include work by Fuller et al. (2012), who assessed the performance and benefits of demand response of various end loads using GridLAB-D. This work did not include integration into the transmission system and wholesale market (the DERs were price takers, not price makers).

More recently work by Mukherjee et al. (2020) has sought to bridge this transmission/distribution system divide by demonstrating the integrated simulation of DERs responding to and affecting wholesale prices. This work used MATPOWER to model the generation production costs and market of the WECC and was combined with GridLAB-D to model multiple distribution feeders and associated DERs operating under transactive coordination. This work served as a proof point for the co-simulation of the DSO+T study but only simulated one day (not a whole year) and did not investigate the representativeness of the end-load profiles and market prices.

1.4.2 Building Population and Load Modeling

Most relevant prior work on modeling of building performance and electrical end loads has focused on forecasting future load growth for grid resource planning and to estimate the impact of efficiency measures at local or regional scales. For example, Hale et al. (2018) developed a comprehensive bottoms-up model of residential, commercial, industrial, and transportation end loads. Building parameter definitions were based on ResStock and ComStock databases and modeled in EnergyPlus. The results were compared to actual 2012 grid loads to assess the accuracy of such models at the state, regional, and national levels.

The results showed average errors ranging from 20% at the hourly state resolution to 4% at the annual continental United States level. While this work is informative for understanding achievable accuracy, the computational intensity and time resolution of the modeling approach is not as well suited for real-time operational grid modeling. Research by Taylor et al. (2019) also used a vast number of EnergyPlus models to simulate regional grid loads and developed a calibration approach for these system models, then analyzed the regional load over the WECC interconnection in comparison to actual hourly load at 19 balancing authorities. This calibration approach resulted in reduced bias in annual energy consumption (1.8%) and peak loads (6.1%). New et al. (2019) used 15-minute utility data from over 170,000 buildings to develop calibrated EnergyPlus models for 17 classes of residential and commercial buildings. The goal of this work was to estimate the contributions of various building classes to the utility's peak load and identify customers most suitable for demand response. No direct comparison to system load results was presented. Other researchers have also advanced urban-scale building energy modeling capability but do not present direct comparisons to grid loads (el Kontar et al. 2020; Ang et al. 2020; Lei et al. 2021).

Prior work has also assessed the performance of grid distribution modeling tools such as GridLAB-D to model building loads. For example, GridLAB-D can capture grid load profiles with 14.2% average error at the distribution circuit level when calibrated to utility customer data (Fuller et al. n.d.). In addition, it can accurately estimate the increased loads occurring when power is restored after a blackout as many devices (like HVAC units) come on at once (Schneider et al. 2016). Finally, work by Gotseff and Lundstrom (2017) has validated the dynamics of GridLAB-D house models. We are not aware of any assessment of GridLAB-D's ability to estimate region-wide loads over a full annual cycle.

The DSO+T study has developed a method to estimate regional grid loads, based on building models derived from public datasets that are computationally efficient and require no dedicated calibration. The remainder of this paper presents the methodology used to define building parameters, the simulation approach, a comparison of simulation results with actual grid loads, and concludes with a discussion of lessons learned and future work.

1.5 Report Structure

The remainder of the report is split into two parts: the bulk power system and the distribution system (including end loads). The first part details the definition of the generators (Section 2.0) and transmission system (Section 2.4.4). It is concluded in Section 4.0 with presentation of illustrative results of the bulk system compared to actual historical system data. This includes examples of generation dispatch, market prices, and transmission network operation. The second part of the report details the definition of the DSOs and distribution system (Section 5.0) and the approach used to define residential and commercial buildings and their end loads (Sections 6.0 and 7.0). Illustrative results of building system end loads are presented in Section 8.0 and compared to system-level ERCOT data. Finally, Sections 9.0 and 10.0 detail the EV model (only used in the HR scenario) and battery model.

2.0 Generation

2.1 Summary of Generation Fleet and Dispatch Strategy

The number, location, and capacity of the bulk system generators for the MR scenario are based on the ERCOT Test System (Battula et al. 2020), which is available on GitHub (TESP n.d. b). A summary of the generator types, number of sites, and capacities used for the MR case is provided in Table 4.

The HR scenario (also shown in Table 4) maintains the same thermal generation fleet but doubled the wind capacity and added 14.8 GW of utility-scale solar capacity on the transmission system and 21.3 GW of rooftop solar on the distribution system. Thermal plants were not retired *a priori* in the HR order to allow any economically competitive plant to be scheduled and dispatched. This does not impact the dispatch of renewables but allows the simulation to economically utilize plants as needed for reliable operation. The study results can be used to assess the savings from candidate plants for retirement in future work.

Table 4. Summary of generator types, number of locations (200-bus case), and capacity for the MR and HR scenarios.

	MRs			HRs		
Generation Type	Number	Capacity (MW)	Capacity (%)	Number	Capacity (MW)	Capacity (%)
Coal	14	21,900	22%	14	21,900	15%
Natural gas combined cycle	33	40,100	41%	33	40,100	27%
Natural gas internal combustion engine	9	1,800	2%	9	1,800	1%
Natural gas steam turbine	18	13,000	13%	18	13,000	9%
Nuclear	2	5,100	5%	2	5,100	3%
Wind	34	16,300	17%	34	32,600	22%
Solar (utility scale)	-	-	-	200	14,800	10%
Solar (distributed)	-	-	-		21,300	14%
TOTAL	110	98,300	100%	310	150,600	100%

The HR generation fleet was informed, in part, through the use of the Transactive Future Grid State Tool (Bender et al. 2019). This simple capacity expansion tool was configured to target a 50% renewable energy production with at least 20% being produced by wind and 20% by solar (both utility scale and distributed).

The use of thermal generators is based on implementing SCUC and SCED processes for determining day-ahead and real-time market operations. In both cases forecast and actual values for renewable generation were created and used. These processes are executed using AMES V5.0. Unless curtailment (discussed in Section 2.6) is required, all renewable generation is considered to be committed and dispatched and is subtracted from the demand at each bus to create a net load at each bus. Day-ahead and real-time load forecasts are provided by the DSO agent and are discussed in more detail in (Widergren et al. 2022).

The SCUC and SCED processes as modeled in AMES will not capture some real market phenomena. This includes any out-of-market dispatch (either due to self-scheduling or bilateral

contracts). In addition, any scarcity rent (not already inherently captured in the inferred production costs discussed in the next section) is not modeled. Finally, locational marginal prices (LMPs) do not capture uplift costs (startup) or make whole costs that may change (per generator) under HR scenarios and may be impacted by transactive energy approaches. The analysis does track the number of starts per generator as well as startup cost.

2.2 Dispatchable Thermal Generation

This section details the assumptions used for the thermal generator fleet. While the generator capacities and bus locations are identical to the values defined by TESP for the 8- and 200- bus ERCOT test case, the generation production costs, ramp rate limits, and minimum compliant load values were revised to ensure that the resulting LMPs were representative of ERCOT and other markets of interest (as shown in Section 4.2).

2.2.1 Thermal Generation Variable Production and Startup Costs

A number of sources were investigated to determine representative generator heat rates, fuel costs, and resulting variable production costs. For example, heat rate data were used from a recent Californian Energy Commission report on generator energy efficiency measures and production costs (Deaver 2019). As can be seen in Figure 3 these data alone do not capture the resulting change in ERCOT LMP as a function of net system load. Potomac Economics (2017) studied the state of the 2016 ERCOT market and inferred generator heat rates as a function of system load from the observed market prices. This showed a five-times change in heat rate as the system net load changed throughout the year. This suggests other variable system costs (e.g., variable operations and maintenance) or factors beyond heat rate need to be captured.

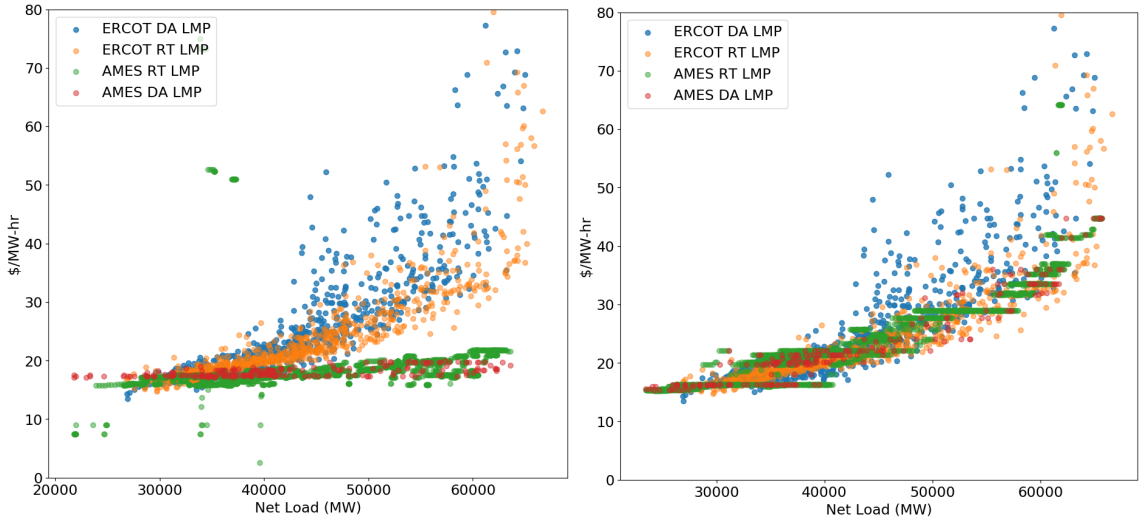

Figure 3. Comparison of LMPs when using Californian Energy Commission heat rates (left) and production costs based on inferred ERCOT heat rates (right).

In an effort to reproduce this effect, a range of generator variable production costs (C1) were assumed by generator type (Table 5). A production cost was determined for each generator by randomly selecting a value between the linear coefficient limits of $C1_{min}$ and $C1_{max}$ using a uniform distribution. This approach seeks to have nominal values that are informed by typical heat rates, while ensuring a diverse range of values resulting in representative generation costs. Aggressive natural gas combined cycle prices were assumed to reflect the low cost of natural

gas in 2016 and represent the resulting generation mix. The quadratic coefficient C2 was assumed to be zero for all thermal generators.

Table 5. Range of variable production costs ($/MWh) by generator type.

Generator Type	C1 (min)	C1 (max)
Conventional steam coal	12.675	29.25
Natural gas combined cycle	13.13	46.46
Natural gas internal combustion turbine	46.32	86.85
Natural gas steam turbine	34.06	78.6
Nuclear	8	8

Estimates of the cost to start each generator were based on Kumar et al. (2012), which was used by the National Renewable Energy Laboratory (NREL) in their Phase 2 Western Wind and Solar Integration Study (Lew et al. 2013). This work estimated the fuel, capital, and maintenance, and other startup costs associated with various generator types and severity of start (hot, warm, or cold). The values used for this study are highlighted in Table 6. Since AMES only does a single day-ahead dispatch there is no way to know if coal and combined cycle and steam gas plants will incur a warm or cold start. Warm start values were assumed as it would cover daily operation. For combustion turbine gas units, cold start values were assumed as any shutdown longer than 1–3 hours is considered a cold start. Note that some generators have large aggregate capacities (e.g., 3 GW) and will have a correspondingly large startup cost based on full-load capacity not minimum compliant load. The potential impact of this warrants further investigation but is outside the scope of this study.

Table 6. Summary of generator startup costs developed by Kumar et al. (2012). Values used in this study are highlighted in bold.

Plant Type		Coal - Small Sub Critical	Coal - Large Sub Critical	Coal - Super Critical	Gas - Combined Cycle	Gas - Large Frame CT	Gas - Aero Derivative CT	Gas - Steam
Capacity (MW)		35-299	300-900	500-1300	-	-	-	50-700
Warm Start Hours		4 to 24	12 to 40	12 to 72	5 to 40	2 to 3	0 to 1	4 to 48
Capital and Maintenance Cost ($/MW)	Hot	58	39	38	31	22	12	26
	Warm	95	61	56	44	28	12	46
	Cold	94	89	99	60	38	12	58
Start Up Fuel Costs (MMBTU/MW)	Hot	5	7.5	10.1	0.19	0.18	1.53	3.67
	Warm	6.67	10	17.1	0.2	0.19	1.53	6.99
	Cold	9.33	14	20.1	0.24	0.22	1.53	8.92
Start Up Fuel Costs ($/MW)	Hot	9.0	13.5	18.2	0.5	0.5	4.0	9.5
	Warm	12.0	18.0	30.8	0.5	0.5	4.0	18.0
	Cold	16.8	25.2	36.3	0.6	0.6	4.0	23.0
Other Startup Costs ($/MW)	Hot	4.58	5.61	5.81		0.95	1.9	3.99
	Warm	6.14	7.98	8.62		0.95	1.9	6.86
	Cold	7.95	10.15	11.58		0.95	1.9	11.44
Total ($/MW)	Hot	71.60	58.14	62.03	31.49	23.41	17.85	39.47
	Warm	113.17	87.02	95.46	44.52	29.44	17.85	70.91
	Cold	118.78	124.40	146.83	60.62	39.52	17.85	92.47

2.2.2 Thermal Generation Minimum Compliant Loads and Ramp Rates

Representative values for generator operating characteristics such as typical full load (FL), minimum compliant load (MCL) and ramp rate were taken from Gonzalez-Salazar et al. (2018), Tables 7, 9, and 12. The representative values used in the study are given in Table 7 below.

Table 7. Assumed thermal generator values (Gonzalez-Salazar et al. 2018).

	Coal	Gas Combined Cycle	Gas Simple Cycle	Gas Aero
Max FL (MW)	500	475	400	60
MCL/FL (%)	40%	45%	37.5%	50
Ramp rate/min (%FL)	3.0%	5.4%	9.6%	100%

All generators of the same type that are located on the same bus are treated as an aggregated generator by AMES. For example, the maximum coal generator in the model exceeds 3 GW. This requires special consideration of how to determine the MCL and ramp rate for generators that have power ratings much higher than typical FL. For this study we assume the following:

$$MCL = \min(P_{Cap}, FL) * F_{MCL} \quad (1)$$

Where MCL is the minimum compliant load (MW), P_{cap} is the generator capacity, and FL is typical of a generator and F_{MCL} is the MCL as fraction of FL, both given in Table 7.

$$Ramp\ Rate = \min(P_{Cap}, FL) * F_{ramp\ rate} \quad (2)$$

The ramp rate (MW/min) is based on the minimum of either the total generator capacity or typical generator FL and typical ramp rate as a fraction of FL given in Table 7.

These assumptions are made to ensure that large aggregated generators do not have very large MCL values (e.g., 1.2 GW) resulting in their scheduling and dispatch being limited due to the large disruption they may bring when first brought online. In addition, we did not want to over represent the flexibility of thermal generators by estimating ramp rates that may also not correctly reflect their flexibility. How best to determine the characteristics of large aggregate generators warrants further investigation.

For reference, the aggregate fleet ramping statistics were determined for 2016 ERCOT system data and summarized in Table 8. These values represent the actual observed ramp rates of the combined fleet by fuel type, not of individual generators. Even so they provide a sanity check for expected behavior. Based on this information nuclear plants were given a ramp rate limit of 0.2% MW_{FL}/min.

Table 8. Fleet ramp rate statistics calculated from 2016 ERCOT data.

	Coal	Gas Combustion Turbine	Gas Combined Cycle	All Gas	Nuclear
Max up (MW/Min)	77.7	79.5	122.5	127.8	5.7
Max down (MW/min)	-1145.7	-84.1	-301.2	358.7	-340
Max up (%)	0.9%	1.9%	1.3%	1.1%	0.20%
Max down (%)	-1.2%	-1.9%	-1.3%	-1.0%	-2.0%

2.3 Wind Generators

The wind power generation used a stochastic model based on an autoregressive integrated moving average process (Chen et al. 2010). This model was trained on 2005 data from a Danish offshore wind farm that consisted of 72 fixed-speed 2.3 MW wind turbines. Given that the variation and capacity factor of wind generation is sufficiently different between the training data and ERCOT, the parameters in the model were adjusted to better match 2016 ERCOT wind performance metrics. Table 9 and Figure 4 show that the resulting model matches key ERCOT wind generation metrics (such as average power generation and load change) within ~6%. The average and maximum hourly change in wind power output is a key feature to match as it drives the required flexibility required from grid operation. The model captures this well and slightly overestimates the wind variation.

Table 9. Comparison of ERCOT wind generator characteristics versus simulation.

	ERCOT	DSO+T	% diff.
Capacity (GW)	17.08	16.30	-4.6%
Peak load (GW)	15.72	16.30	+3.7%
Average generation (GW)	6.048	6.065	+0.2%
Average hourly load change (%)	3.04%	3.2%	+3.1%
Max hourly increase (GW)	3.62	3.78	+4.4
Max hourly decrease (GW)	-3.08	-3.27	+6.2%

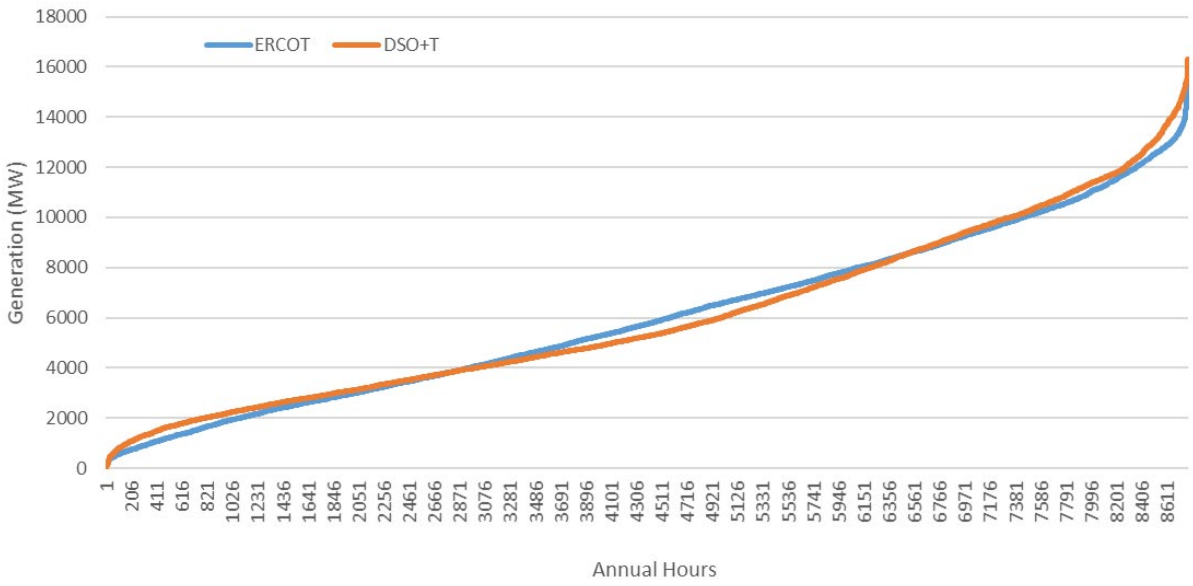

Figure 4. Comparison of ERCOT 2016 wind generation versus duration compared to simulation results.

This level of agreement was achieved by creating five wind power profiles (associated with the 5 buses that have wind generation in the 8-bus model). These profiles were then prorated to the 34 buses that have wind generation in the 200-bus model. This seeks to mimic the regional covariance in wind power output from sites that are closely located. In comparison, creating individual stochastic load profiles for each of the 34 wind generators resulted in much of the

stochastic load variation canceling out at the system level and made it impossible to match the observed ERCOT behavior.

We chose not to use the 2016 ERCOT wind profiles directly as we wanted a general methodology that could be applied to other regions of the country as needed and scaled up to the HR case. If 2016 wind tapes had been used, there was the risk that operational effects (outages, curtailment) in the 2016 ERCOT wind profiles would be scaled without the user's knowledge. This approach also eliminates seasonal variation that is likely to be region specific.

For the HR scenario, the wind generation power production is assumed to be 166% that of the MR scenario. No changes were made to assume higher capacity factors that may be possible from future advanced turbines.

Forecast uncertainty error was applied to the day-ahead hourly wind load profile assuming a Gaussian distribution of error (Figure 5). The uncertainty parameters were based on Hodge et al. (2012), Figure 1, which analyzed 2010 ERCOT data and determined a mean error of 1.117% and an error standard deviation of 11.87% of predicted load.

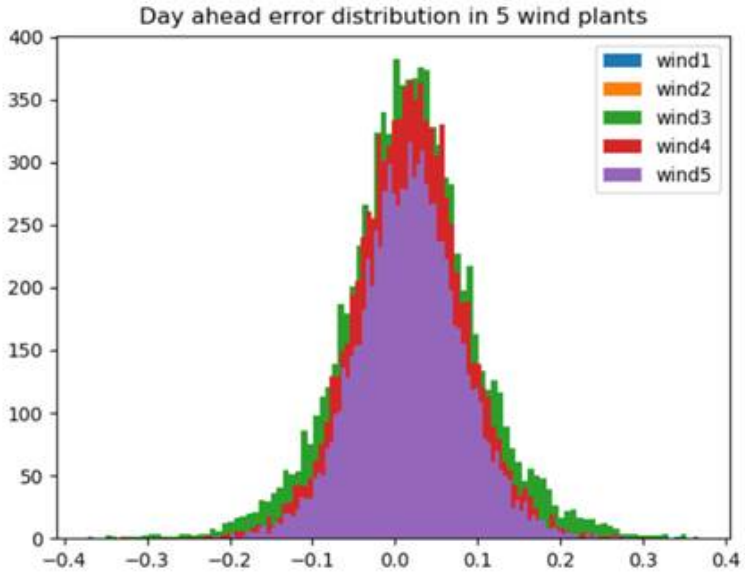

Figure 5. Day-ahead wind forecast uncertainty distribution.

2.4 Solar Photovoltaic Generators

For the HR case, solar PV power generation profiles were developed for both utility and distributed rooftop-scale PV generation. This resulted in four solar generation profiles:

1. 5-minute utility-scale solar PV generation profile for 2016
2. 5-minute distributed solar PV profiles to model rooftop solar installations for 2016
3. Hourly utility-scale solar PV forecasts for 2016
4. Hourly distributed solar PV forecasts for 2016

2.4.1 DSO Solar Capacity Definition

In modeling the HR generation mix, solar generation (both utility and distributed rooftop) was assumed to be present at all transmission buses within the system. The Transactive Future Grid State tool provides an ERCOT-wide estimate of the solar PV installation capacity (Bender et al. 2019); this value came out to be 36.1 GW as shown in Table 4. The total system solar PV generation is assumed to be distributed proportionally to the average load of each DSO. This defines a per-DSO total installed solar PV capacity.

Based on information from the Energy Information Administration (EIA), utility-scale solar PV is assumed to be approximately 40% of the solar PV install base with the remaining 60% being distributed rooftop solar PV installations (DOE-EIA 2017).

2.4.2 Utility-Scale Solar PV

For modeling simplicity, we assumed all utility-scale solar is located at the exact latitude and longitude of the DSO (TESP n.d.). Using the previously defined 40–60% split, we assume this ratio is constant across all of ERCOT and define target nameplate ratings for the utility-scale installation on a per-DSO basis. Using NREL's System Advisory Model (SAM) (Blair et al. 2017) and National Solar Radiation Database (NSRDB) (Sengupta et al. 2018), an hourly profile for 2016 (using actual solar data provided by the NSRDB) was generated and scaled up to satisfy the nameplate requirement. The tilt of the installation was assumed to be 30 degrees for all installations and the azimuth was southerly. Note that no geographic diversity is modeled. These profiles were generated for each of the 200 buses in the production model and summed to form aggregated profiles when working with the 8-bus transmission and generation model.

2.4.3 Distributed Solar PV

For the purposes of this study, the primary difference between utility-scale and distributed solar is geographic diversity. To represent the differences in solar PV production that would occur throughout the geographic footprint of a given DSO, it was necessary to construct a collection of production profiles with varying parameters and then aggregate them to produce a single, average, representative profile to be used in GridLAB-D for all rooftop solar generation.

Diversity in solar PV is captured primarily through three factors appropriate for modeling rooftop installations:

1. Diversity in azimuth angle: No data was readily found that defines common rooftop installation azimuth angle. It is safe to assume that southerly is generally preferred (maximum energy generation) but is far from the only option. Arbitrarily it was assumed that 75% of distributed solar PV was installed facing south and 25% was installed facing west. Though the western-facing installations will produce less annual energy, it is assumed there are customers who would like to meet more of their load with local generation and recognize the need for energy during the afternoon peak.
2. Diversity in tilt angle (corresponding to roof pitch): Based on a review of common home design practices, the roof pitch (and thus tilt angle of the rooftop PV installation sites) for houses was assumed to be uniformly distributed between 18 and 37 degrees.
3. Diversity in geographic location: For each DSO, a distribution of random sites with geographic coordinates +/- 25 km from the DSO location were randomly selected. The

distance of 25 km was based on an examination of the distance between DSO sites in an attempt to avoid overlap in distributed locations among DSOs.

A single profile for the distributed solar PV was created by generating individual profiles for 50 instances within each DSO with random parameters selection (azimuth, tilt, and location) and then averaging the profiles. As in the utility-scale generation calculation, NREL's SAM and NSRDB were used to generate the hourly power profile for all 50 locations. Using the DSO scaling parameter, the penetration rate for distributed solar PV, and the total number of customers represented, the power profile was scaled appropriately and interpolated into 5-minute values before being saved in an appropriate format for use in GridLAB-D.

As a modeling simplification, for each DSO all structures designated to have rooftop solar PV by the physical model instantiation used the same profile. Note that this was a power profile (rather than solar parameters) and was played directly into the physics model of the power system (GridLAB-D) at the point of interconnection of the structure and the rest of the power system. This reduced the number of input files needed while still preserving the greater diversity expected from distributed solar PV generation.

2.4.4 Solar PV Forecast (with Errors)

Using metrics from day-ahead forecasts made in the CAISO system (Zhang et al. 2015), error was introduced to the previously generated hourly values to create a per-DSO solar forecast signal. This forecast signal was evaluated by the metric definitions and values as defined in Zhang et al. (2015).

To create an imperfect solar forecast for use when running the day-ahead energy market, hourly forecast files were generated by adding error to hourly production profiles for both the utility-scale and distributed solar PV generation profiles. (In the case of the latter, the original noninterpolated power profile was used.) The error added to the solar profiles was a random sample from a normal distribution with a mean of zero and a standard deviation (normalized to the solar PV installed capacity) of 0.07. The forecast profile was then run through a cleanup function that performed two roles. The first was to change the forecast value to zero in all periods where the actual solar production was zero. This was based on the assumption that zero solar production hours would occur from sunset to sunrise and the forecast would be able to accurately predict these hours as having no production. The second was to coerce all forecast negative production values to zero.

These cleanup processes affect the statistics of the forecast profile and cause them to deviate from the pure random variation from which they were generated. Thus, the use of a normalized standard deviation of 0.07 when creating the forecast with error was necessary to achieve a normalized standard deviation of 0.04 as derived from Zhang et al. (2015) after the forecast was cleaned up.

Table 10 shows the forecast metrics derived from Zhang et al. (2015) and the min, average, and max values of those metrics over the 416 (208 utility scale, 208 distributed) solar PV forecast files necessary for the analysis.

Table 10. Comparison of solar PV forecast metrics.

	Derived from Zhang et al. 2015	All Generated Solar PV Production Forecasts		
		Minimum	Average	Maximum
Capacity normalized root-mean-square error (MW)	0.04	0.0455	0.0469	0.0491
Capacity normalized standard deviation (MW)	0.04	0.0455	0.0469	0.0496
Correlation coefficient	0.98	0.9802	0.9839	0.9865

2.5 Generation Outages

To simulate the impact of generation outage on bulk system LMP (and potential congestion), we considered two types of outages: planned and unplanned. Planned outages follow the maintenance schedule. Unplanned outages are introduced due to unforeseen failure. Therefore, the day-ahead unit commitment would dispatch those units as usual. However, they might be taken out of service during the day at the top of the hour based on a predefined outage schedule (though the unit commitment has no knowledge of it). The data used were for the WECC system (WECC 2020). Forced outage rate data, which are used for unplanned outages, are generic and based on the plant fuel type.

2.5.1 Using ERCOT Outage Data to Create Events

2.5.1.1 Planned Outages

We used maintenance schedule data to create an outage probability for each month and an average duration by month. Looking at the generator maintenance data by type was inconclusive; generator type and outage duration per type and per month varied across all months. Therefore, the type of generator was not included in the process of creating the events.

In Table 11, frequency refers to the number of generators that had planned outages for that month, average duration is for outages during that month, days out is the total number of day outages for that month (frequency multiplied by average duration), and probability is the number of days of outage for that month divided by the total number of outage days (12,082 days). The values of average outage duration and probability were used in creating the events in this study.

Table 11. Planned outage data (WECC 2020).

	Frequency (Number of outages)	Average duration (Days)	Days out	Probability
January	146.00	8.70	1270.20	0.105128
February	144.00	9.30	1339.20	0.110839
March	214.00	7.75	1658.50	0.137266
April	187.00	10.00	1870.00	0.15477
May	102.00	9.66	985.32	0.08155
June	94.00	7.90	742.60	0.061461
July	38.00	7.60	288.80	0.023902
August	44.00	7.20	316.80	0.02622
September	125.00	4.92	615.00	0.0509

	Frequency (Number of outages)	Average duration (Days)	Days out	Probability
October	104.00	9.40	977.60	0.080911
November	124.00	8.40	1041.60	0.086208
December	120.00	8.14	976.80	0.080845

Using a binomial random number generator, an array was created for every month based on the probability and number of days in that month. After the binomial array was created, we randomly selected a unit from our 120 total units. Once the unit and the day of outage were identified, the outage was given a duration based on the average quantities. Every unit can be used only once, assuming one planned outage for each generator per year. In case it got drawn again, another attempt was made to choose another unit. Based on this procedure, the events in Table 12 were created.

Table 12. Planned outage events.

Day of year	Generator ID	Duration	Type
16	75	8	Conventional steam coal
21	114	8	Natural gas combined cycle
28	55	8	Natural gas combined cycle
35	28	9	Wind turbine
45	13	9	Natural gas combined cycle
59	117	9	Wind turbine
74	32	7	Wind turbine
76	54	7	Natural gas combined cycle
93	0	10	Natural gas internal combustion engine
112	100	10	Wind turbine
114	70	10	Natural gas internal combustion engine
117	85	10	Wind turbine
124	31	9	Wind turbine
148	9	9	Natural gas combined cycle
150	73	9	Conventional steam coal
162	93	7	Solar photovoltaic
199	72	7	Natural gas steam turbine
252	27	4	Natural gas combined cycle
264	29	4	Wind turbine
267	33	4	Wind turbine
269	115	4	Wind turbine
283	99	9	Wind turbine
295	69	9	Natural gas steam turbine
296	6	9	Natural gas steam turbine
337	26	8	Wind turbine
353	30	8	Conventional steam coal
371	15	8	Conventional steam coal

For the implementation in DSO+T, the above data were populated in a CSV file for each unit for each day of the year, 1 indicating an outage and 0 indicating the unit was available (the day-ahead could still not commit it).

2.5.1.2 Unplanned Outages

From the data provided, we used a forced outage rate and duration to create the unplanned outage events. The data was mapped based on generator types as shown in Table 13.

Table 13. Forced outage rate data used to create unplanned outage events.

Type	Forced Outage Rate	Duration (hours)
Natural gas – combined cycle	0.0306	26
Natural gas – combustion turbine	0.035	51
Natural gas – steam turbine	0.023	30
Natural gas – internal combustion engine	0.0345	37
Coal – steam turbine	0.0418	48
Nuclear – steam turbine	0.0309	190
Photovoltaic	0.001	1
Wind turbine	0.0012	1

For every unit, a binomial random number generator was used to create an array of 8,760 hourly elements based on the forced outage rate divided by the outage duration for that generator type. If an event was present, it was given the duration of hours based on the type. Following the above procedure, the events in Table 14 were created.

For the implementation in DSO+T, these events were populated in a CSV file for every unit for every hour of the year, 1 indicating an outage and 0 indicating the unit is available. In case an event was tripping on a unit that was already out of service, nothing would be done and the event was skipped. Some units had more than one unplanned outage event, but no more than two incidents were present. Indices 1 and 2 following Hour and Duration indicate the event number.

Table 14. Unplanned outage events.

Generator Type	Generator ID	Hour1	Duration1	Hour2	Duration2
Natural gas – combined cycle	5	346	26		
Natural gas – combined cycle	8	175	26		
Natural gas – combined cycle	13	383	26	1257	26
Natural gas – combined cycle	20	4518	26		
Natural gas – combined cycle	38	4474	26		
Natural gas – combined cycle	49	2061	26		
Natural gas – combined cycle	51	2016	26		
Natural gas – combined cycle	60	5372	26		
Natural gas – combined cycle	81	5763	26		
Natural gas – combined cycle	98	4370	26		
Natural gas – combined cycle	106	184	26	848	26
Natural gas – combustion turbine	4	7247	51		

Generator Type	Generator ID	Hour1	Duration1	Hour2	Duration2
Natural gas – steam turbine	10	8170	30		
Natural gas – steam turbine	11	2213	30		
Natural gas – steam turbine	66	1879	30		
Natural gas – steam turbine	69	661	30	6471	30
Natural gas – internal combustion engine	7	8536	37		
Coal – steam turbine	14	7765	48		
Coal – steam turbine	15	5529	48		
Coal – steam turbine	19	2853	48		
Coal – steam turbine	56	210	48		
Photovoltaic	1	311	1		
Photovoltaic	37	714	1		
Photovoltaic	68	868	1	2005	1
Photovoltaic	89	5551	1		
Photovoltaic	91	7874	1		
Photovoltaic	93	212	1		
Photovoltaic	101	127	1	5232	1
Photovoltaic	118	949	1		
Photovoltaic	35	70	1	4373	1
Photovoltaic	44	4250	1	7216	1
Photovoltaic	45	5335	1		
Photovoltaic	48	3731	1	3921	1
Photovoltaic	78	1544	1		
Photovoltaic	84	4935	1	8663	1
Photovoltaic	85	2704	1	7692	1
Photovoltaic	96	1828	1	4866	1

2.5.2 Outage Implementation

For planned outages, the generator was removed from the generator list so AMES would not dispatch it. This also included unplanned outages that were continuing from the previous day; if the generator was not available at the time of bidding (when the day-ahead unit commitment was created) it would not be considered for that day and would be treated as a planned outage until it came back into service. We considered the day-ahead unit commitment problem to have full knowledge about them and those generators were removed out of service at midnight and came back in service at midnight. A schedule with one-day resolution was used to represent the outage events.

For unplanned outages, right before the dispatch was implemented, the unplanned generator outage would be implemented by setting that unit to out of service for that hour. This was seen as it not being committed by the day ahead. A one-hour resolution schedule was created to represent those outage events.

2.6 Reserve Margins and Generation Curtailment

The analysis assumed (up and down) reserve margins of 15%. For the HR scenario the large amount of variable renewable generation could result in AMES being unable to maintain reserve

margin resulting in a lack of convergence and a solution. While these instances were rare (~5% of simulated points) a renewable curtailment strategy was implemented to curtail both wind and utility-scale solar in equal proportions to ensure solution convergence. The need for curtailment was most prevalent when the total amount of dispatchable thermal generation became small relative to the overall system load. For this reason, renewables were curtailed to ensure there was always more than 8 GW of dispatchable thermal generation.

3.0 Transmission System Definition

This section describes the methodology used to define the transmission system model. The study leveraged transmission networks models available in the TESP platform (TESP n.d. b) and described in Battula et al. (2020). Two different transmission networks were leveraged in this study (as shown in Figure 6): a leaner 8-bus test-bench model and a 200-bus production model. The 8-bus model was used to debug the simulation and perform trial analysis, while the 200-bus model was used to generate the primary study results. These synthetic networks were developed by determining 8 or 200 buses using a clustering algorithm that aggregated existing generation and estimated load centers based on latitude and longitude. This previous work then applied the Delaunay Triangulation method to build the line topology, which was then manually adjusted to improve realism. For example, for the 8-bus grid, three lines along the southern and western borders were trimmed for greater realism. For the 200-bus system, Battula et al. (2019) pruned lines, added parallel lines, incremented transformer sizes, and added shunt compensation to eliminate overloads and voltage violations at peak load. (More details are provided by Battula et al. (2019), Section 5.) As a result, the 200-bus ERCOT transmission model includes 47 extra-high-voltage buses at 345 kV and 200 high-voltage buses at 138 kV.

For the study these transmission system definitions were used as-is except for specific line resizing required to ensure feasible solutions with MR and HR generation performance and load profiles that differed from that used by Battula et al. (2019). Finally, the characteristics of the bus loads (distribution system definition, population, load mix, etc.) are discussed in more detail in Section 5.0.

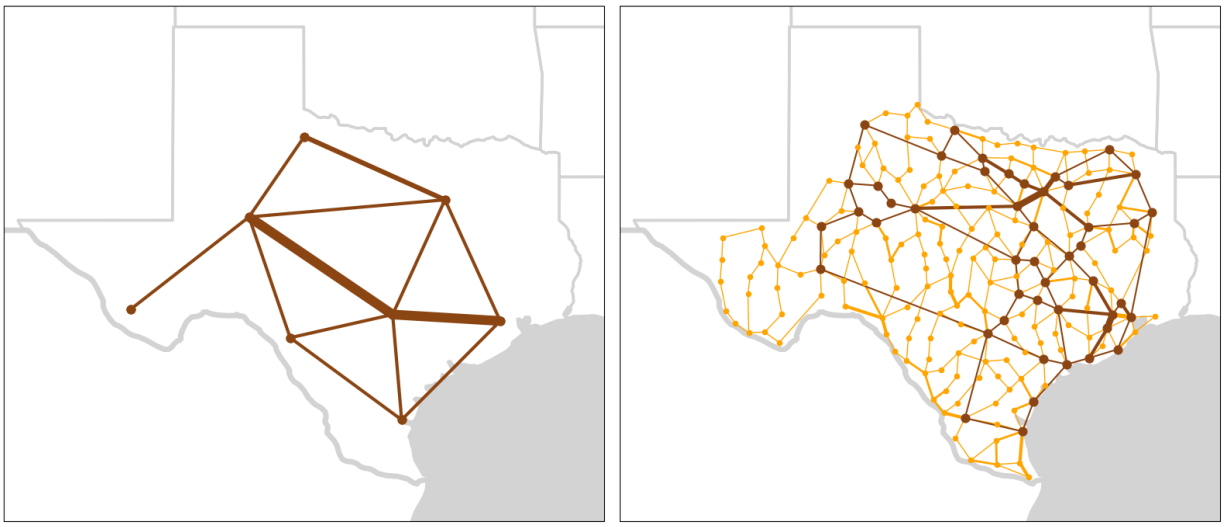

Figure 6. Example of 8-bus (left) and 200-bus (right) transmission networks. 345 kV lines are shown in brown and 138 kV lines in orange. The line thickness is proportional to its MVA rating.

4.0 Bulk System Results

This section presents select results of the bulk system illustrating the representativeness of the generation dispatch, market price, and transmission system models. The results focus on three key areas:

1. The daily dispatch of the generation fleet and the resulting annual generation mix.
2. The resulting LMPs determined for the day-ahead and real-time markets.
3. Performance of the transmission system, any occurrence of congestion, and resulting geographic variation in LMPs.

4.1 Summary of Generation Dispatch and Mix

Comparisons of the DSO+T real-time generator dispatch with actual ERCOT values are shown in Figure 7 for the MR BAU case. The load profiles and the overall generation dispatch trends and resulting fuel mix suggests that the simulation is representative. A detailed analysis of the load profiles is presented in Section 8.0; however, it can be seen here that the overall load shape and weather-dependent changes throughout the month are well captured. In addition, the dispatch of nuclear, coal, and gas generators is trend-wise accurate. The simulation appears to enact more aggressive ramping of the coal fleet than was observed in the ERCOT case. This may be due to larger diurnal load changes in the simulation or the lack of a soft constraint in AMES to minimize ramping on these generators. It should be noted that since the wind generation profiles are stochastically generated and not based on 2016 data a direct daily comparison of the wind profiles is not appropriate. The annual generation capacity and production values are summarized in Table 15. This indicates that the simulation dispatches more coal generation (at the expense of gas) than would be expected based on the 2016 ERCOT system data. The overall level of natural gas generation is representative of the nation as whole.

Table 15. Summary of system capacity and production by generator type for the MR and HR scenarios versus ERCOT and the nation.

	Capacity				Generation			
Fuel	ERCOT	U.S.	MR	HR	ERCOT	U.S.	MR	HR
Nuclear	5%	9%	5%	3%	12%	20%	13%	11%
Coal	20%	25%	22%	15%	29%	30%	38%	26%
Natural gas	58%	41%	56%	37%	44%	34%	35%	23%
Wind	15%	7%	17%	22%	15%	6%	14%	26%
Solar (utility scale)	1.0%	2%	-	10%	0.2%	1.0%	-	6%
Solar (distributed)	-	1%	-	13%	-	-	-	8%
Other	5%	15%	5%	3%	12%	20%	13%	11%

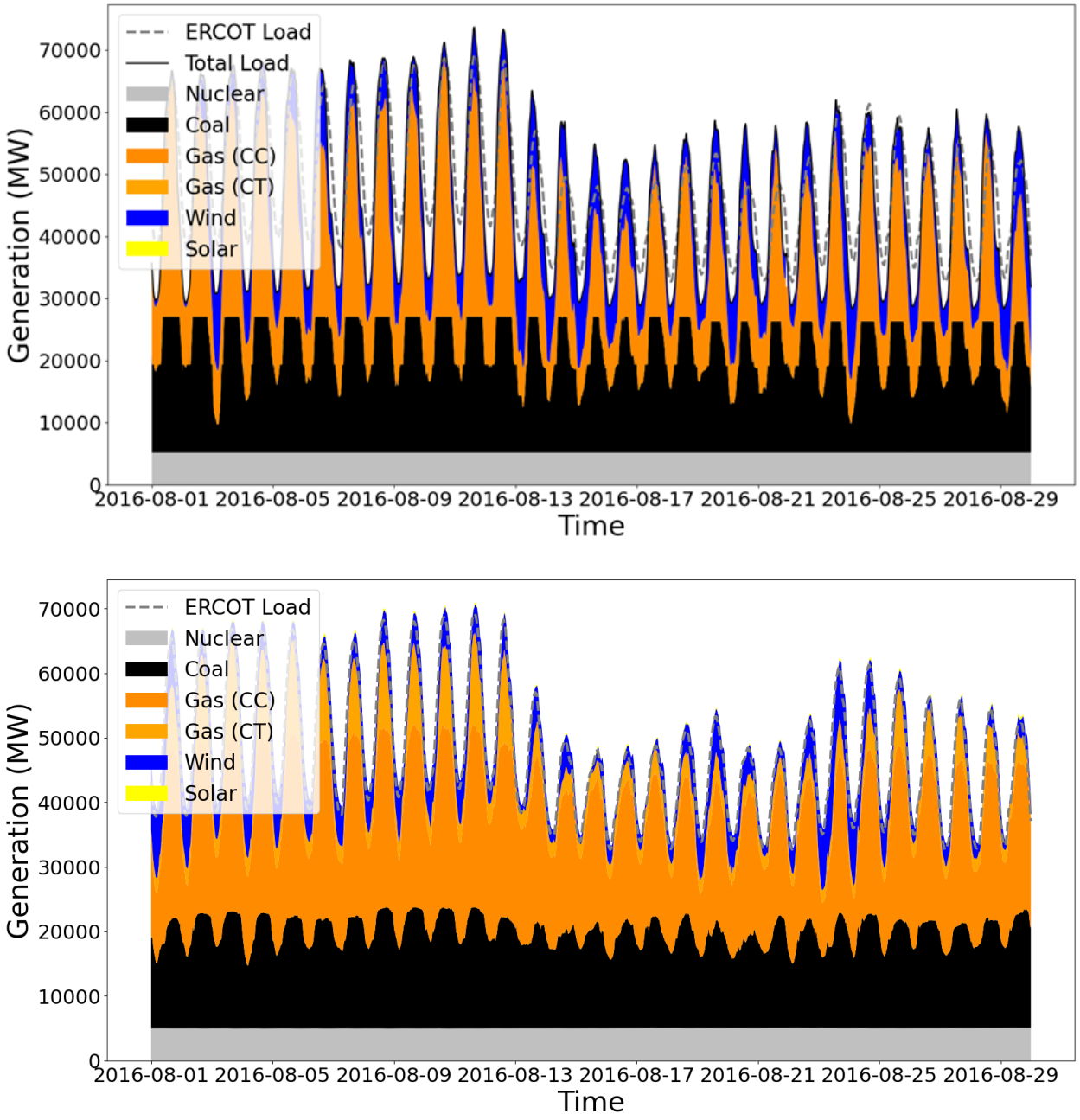

Figure 7. Comparison of AMES real-time generation dispatch for the MR scenario (top) versus actual ERCOT dispatch (bottom) for August 2016.

As example of the generation dispatch during the peak summer load for the HR scenario is shown in Figure 8. The net peak loads are reduced by the contributions of rooftop solar located on the distribution system (the difference between the MR BAU dashed gray reference line and the black total load line in Figure 8). In addition, utility-scale solar and wind generation reduce the total required dispatchable generation requirement further. The result is significantly higher ramping of natural gas and coal generation (particularly in the late afternoon and evening). In some cases abundant renewable generation can reduce the need for dispatchable generation to 8 GW (as shown on August 13 in Figure 8) at which point utility solar and wind generation is curtailed.

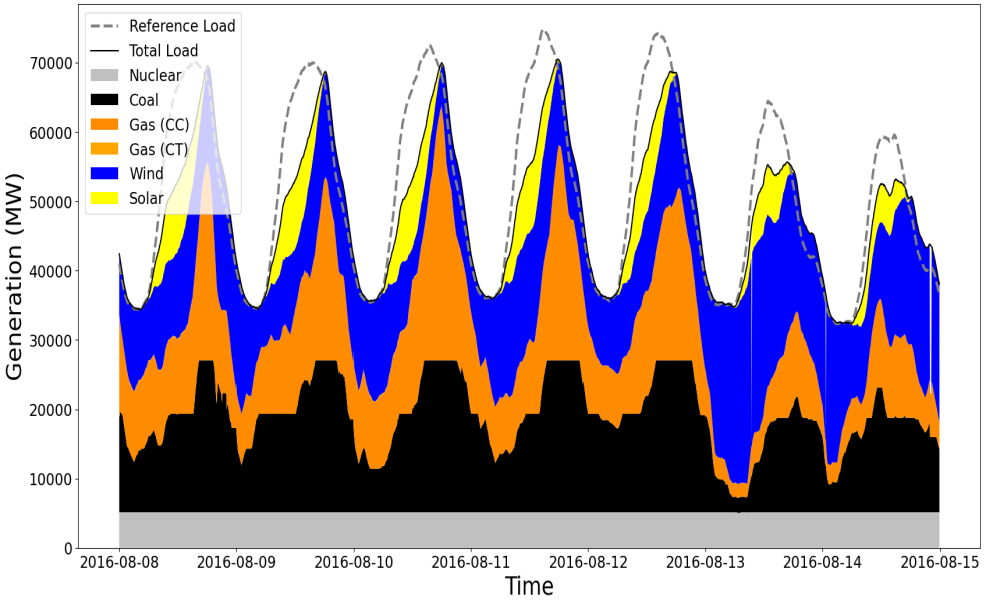

Figure 8. Example AMES real-time generation dispatch for the HR scenario. (The MR total load is shown as the gray 'reference load'.)

4.2 Summary of Locational Marginal Prices

This section discusses the representativeness of the resulting day-ahead and real-time wholesale market prices. Figure 9 shows a time history of real-time prices during the summer peak. In addition, Figure 10 shows a comparison between DSO+T and ERCOT of real-time and day-ahead prices as a function of net load (total load minus renewable generation). This illustrates that the simulation captures the overall daily trends and variation with system load. As will be seen later, however, the simulation does not do as well at capturing isolated price spikes beyond typical ranges (and often going off the vertical axis scales shown on the figures).

To ensure that the market prices generated by the simulation were not over-fitted on one region of the country, the annual data was also compared to data from the PJM and CAISO markets. 2016 data was used for ERCOT and PJM and, due to availability, 2017 data was used for CAISO. In addition, since these prices vary by location, zones had to be selected in each region to compare data. For ERCOT, the Houston zone data is presented, for PJM the PJM node is presented, and for CAISO the SNTHLNE_6_N001 node is shown. For results from DSO 3 are shown for the 8-bus case.

Figure 11 through Figure 14 show detailed comparisons of day-ahead and real-time prices throughout the year. They also show summaries of the daily range in price experienced throughout the year. (The daily range in price is the maximum price for the day minus the minimum price.) The box and whisker plots show that the simulation accurately captures average LMPs that are representative of typical wholesale markets. The quantity versus duration curve for the day-ahead price (Figure 13, left) emphasizes this, showing that the study prices are similar in magnitude to PJM and are bounded by CAISO (which experienced high prices at the zone in question) and ERCOT (which had cheaper prices). The graphs do show, however, that the simulation does not capture the average and extreme daily ranges in price, particularly in the shoulder seasons. As can be seen in Figure 11 (bottom) and Figure 13 (left) the DSO+T market model consistently underpredicts the daily range in day-ahead prices and

overall price volatility seen in national electricity markets. Similar trends are seen for real-time prices as well.

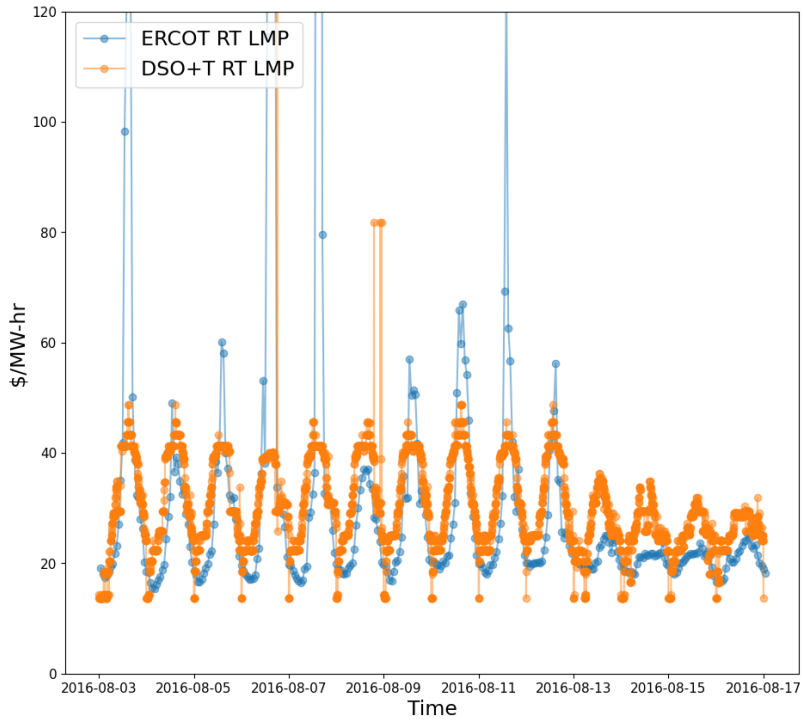

Figure 9. Comparison of DSO+T and ERCOT real-time prices in August.

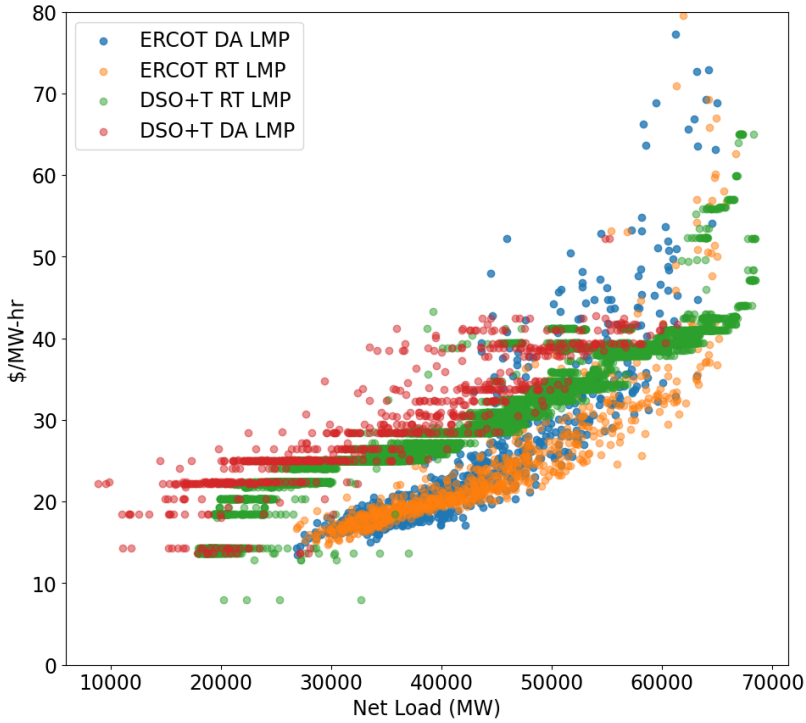

Figure 10. Comparison of DSO+T and ERCOT real-time and day-ahead prices in August as a function of net system load.

There are potentially two main causes for the DSO+T market model not capturing this price volatility: first, the model may not be calibrated and configured correctly; and second, the price behavior may be due to market behavior that is outside the capabilities of the model. Further effort to calibrate and tune the generator performance and production cost parameters (detailed in Section 2.2) combined with investigation of the effect of system parameters (such as reserve margins) could improve the representativeness of the market model. For example, requiring the system to dispatch more expensive peaker plants to address reserve shortfalls (due to outages or stricter fleet ramping constraints) could increase price variation. However, given the complex integrated nature of the SCUC and SCED optimization processes successfully identifying key parameters and tuning them may be challenging. Alternatively, the price features seen in real markets may be due to behavior by market actors that is outside the capabilities of SCUC and SCED modeling approaches and assumptions. For example, out-of-market operation and self-scheduling by generators may alter prices in a way that diminishes market efficiency. In addition, the ability to exercise scarcity pricing (Meyn et al. 2018, page 89) could explain market volatility in the ERCOT market (but may not explain the results in PJM and CAISO).

Better understanding the practical and theoretical limits on capturing real market behavior warrants further investigation given the important role that market prices (value signals) play in transactive energy systems. In addition, understanding the acceptability (and impact) of these limits on valuing transactive approaches needs to be kept in mind.

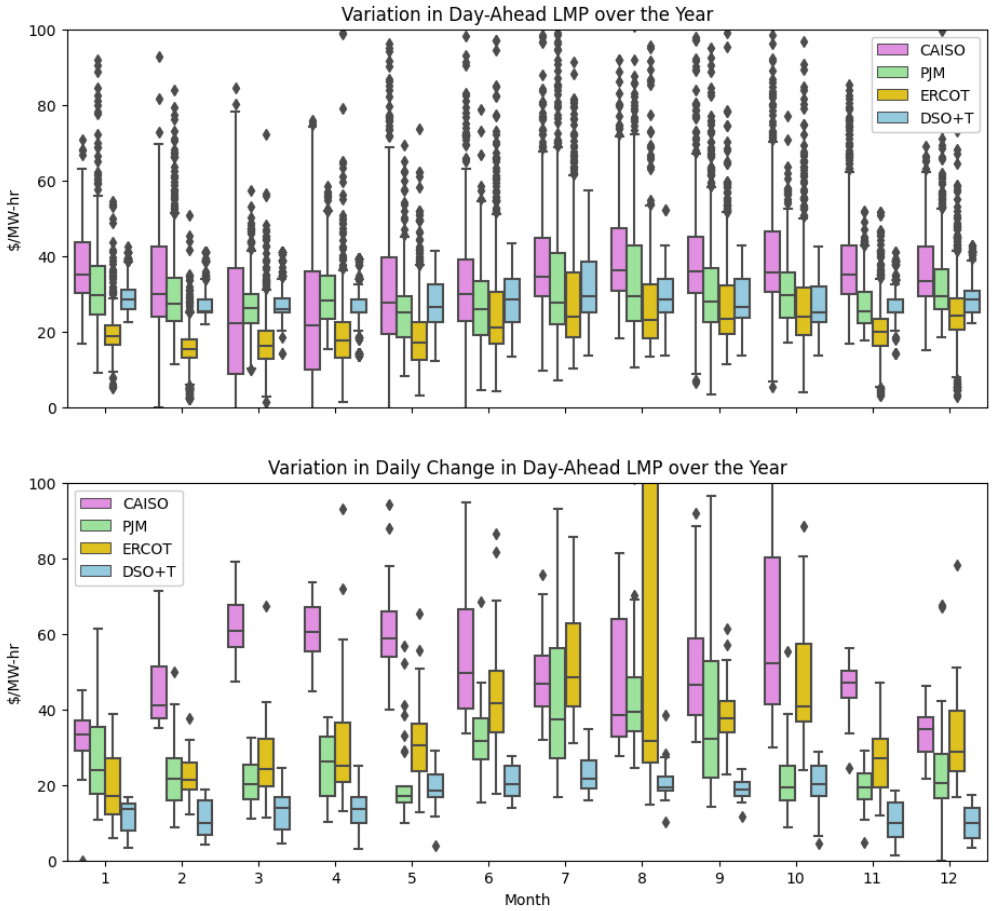

Figure 11. Comparison of day-ahead market prices (top) and daily range in day-ahead market price (bottom) for various regions and the simulation.

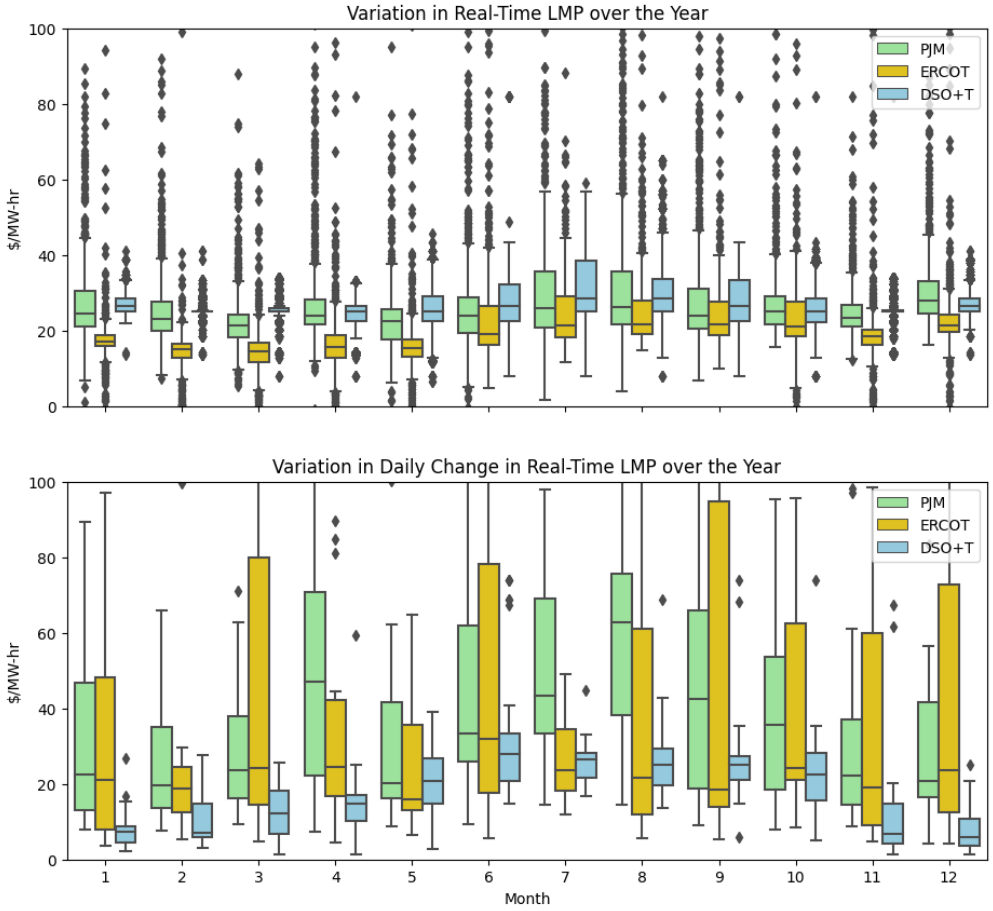

Figure 12. Comparison of real-time market prices (top) and daily range in real-time market price (bottom) for various regions and the simulation.

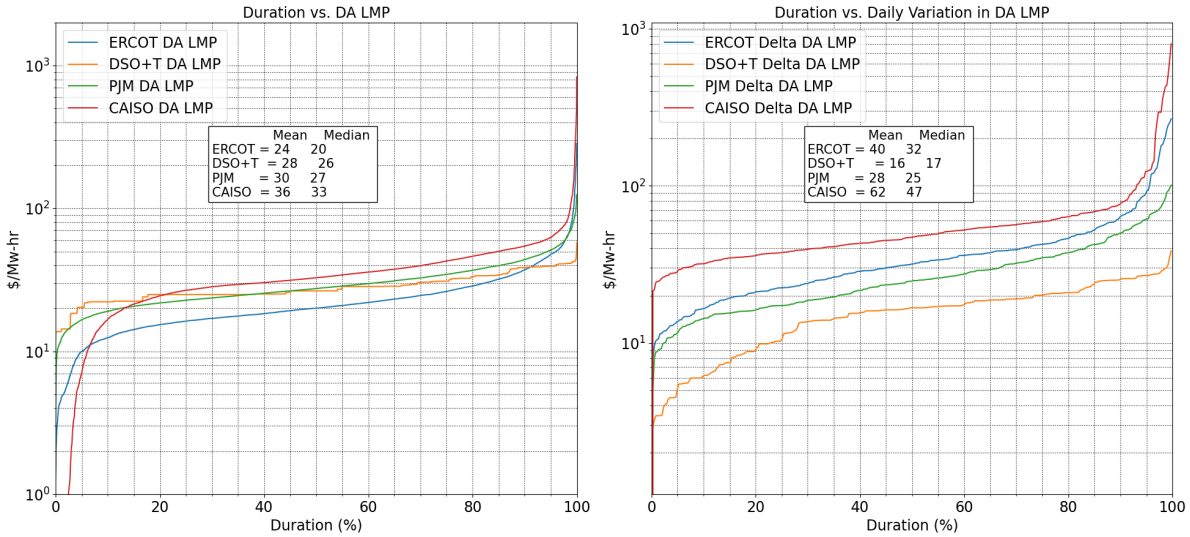

Figure 13. Duration vs. quantity curves for day-ahead market prices (left) and daily range in day-ahead market price (right) for various regions and the simulation.

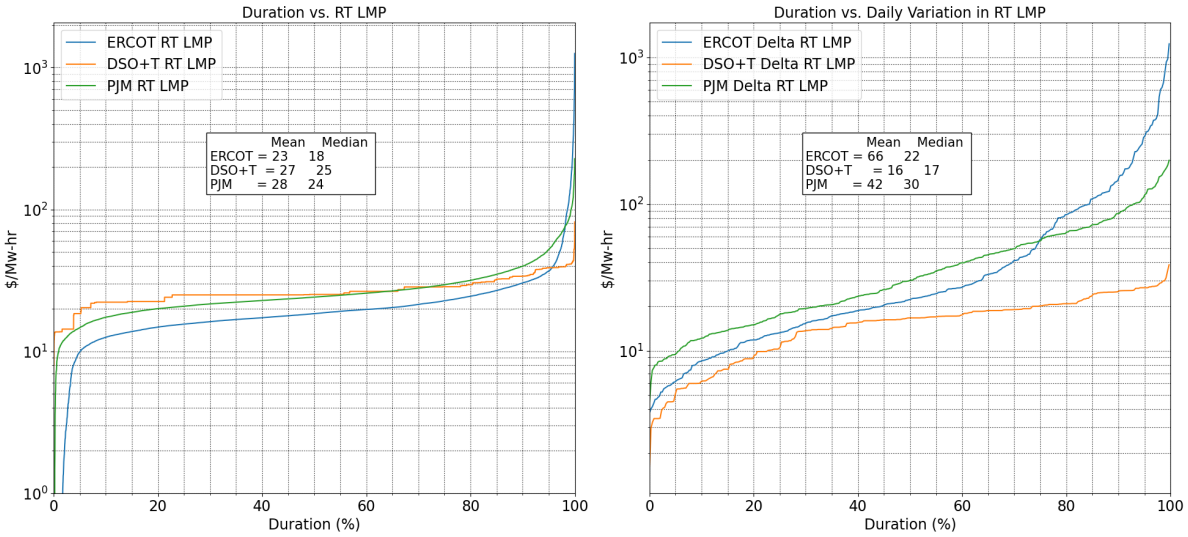

Figure 14. Duration vs. quantity curves for real-time market prices (left) and daily range in real-time market price (right) for various regions and the simulation.

4.3 Summary of Transmission System Results

This section provides illustrative results of the geographic distribution of the system loads, generation dispatch, resulting transmission system utilization and, ultimately, resulting market prices. Results are shown for the system peak generation (73.4 GW) that occurs at ~4 p.m. on August 12. Figure 15 shows the geographic distribution of the peak load and the resulting transmission system loading. The contour plot shows the load for each bus and highlights that (as will be discussed in Section 5.6) over 50% of the system load occurs on just 5 buses, representing population centers in the north and east of Texas. In comparison, the more rural western Texas region has much lower loads. The fractional utilization of the transmission lines is also illustrated using a color gradient, with fully utilized lines (that is, a line capacity of 1.0) shown as red. This shows that there is higher transmission line utilization and congestion in lines serving and adjacent to the major load centers.

Figure 16 and Figure 17 show similar plots for the geographic distribution of thermal generation capacity and resulting dispatch. There is significant generation capacity adjacent to the major load centers and during the system peak load these generations see a high level of dispatch. (Note that not all system nodes have dispatchable generation and therefore may not be able to have generation dispatch fractions greater than zero). Finally, Figure 18 shows the resulting variation in real-time prices during the system peak. The LMP distribution is dominated by a single node (DSO 127) whose real-time LMP has reached the market cap of $2000/MW-hr for several hours during the afternoon. Figure 19 shows example real-time LMPs in the transmission system later in the day (5 p.m.) when lower loads result in fewer transmission constraints and a return to typical price ranges ($30-50/MW-hr).

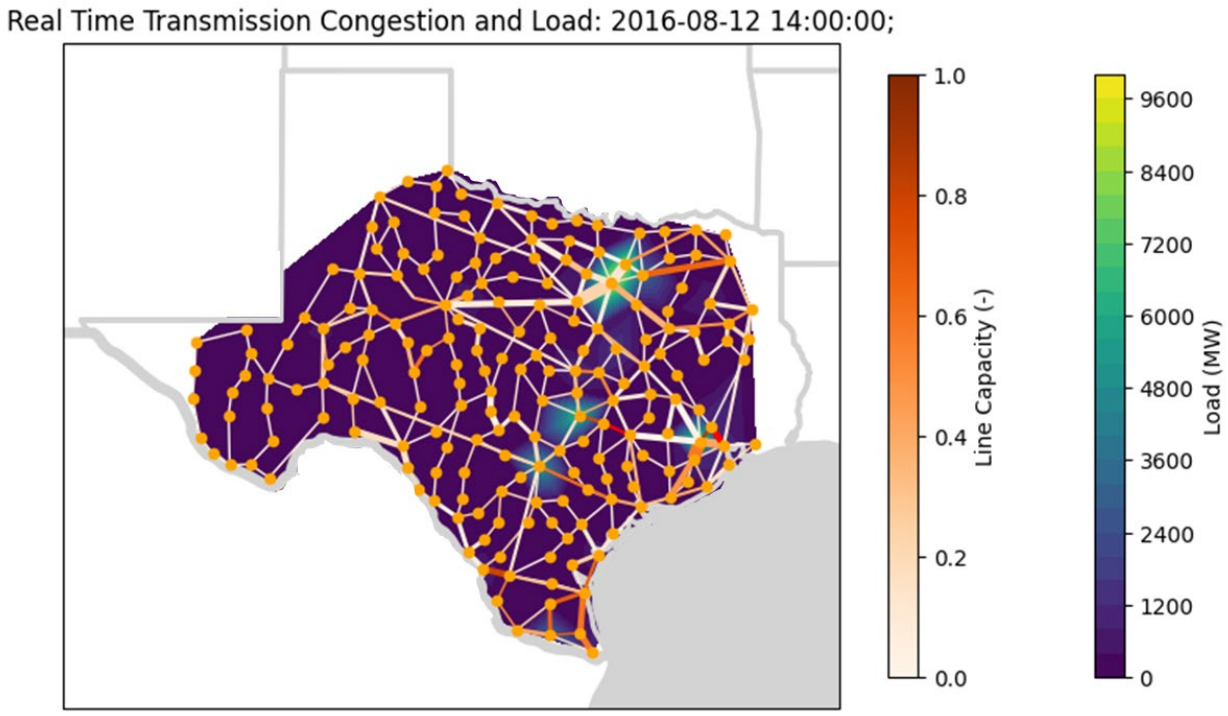

Figure 15. Geographic distribution of real-time load in the DSO+T system model during the system peak load.

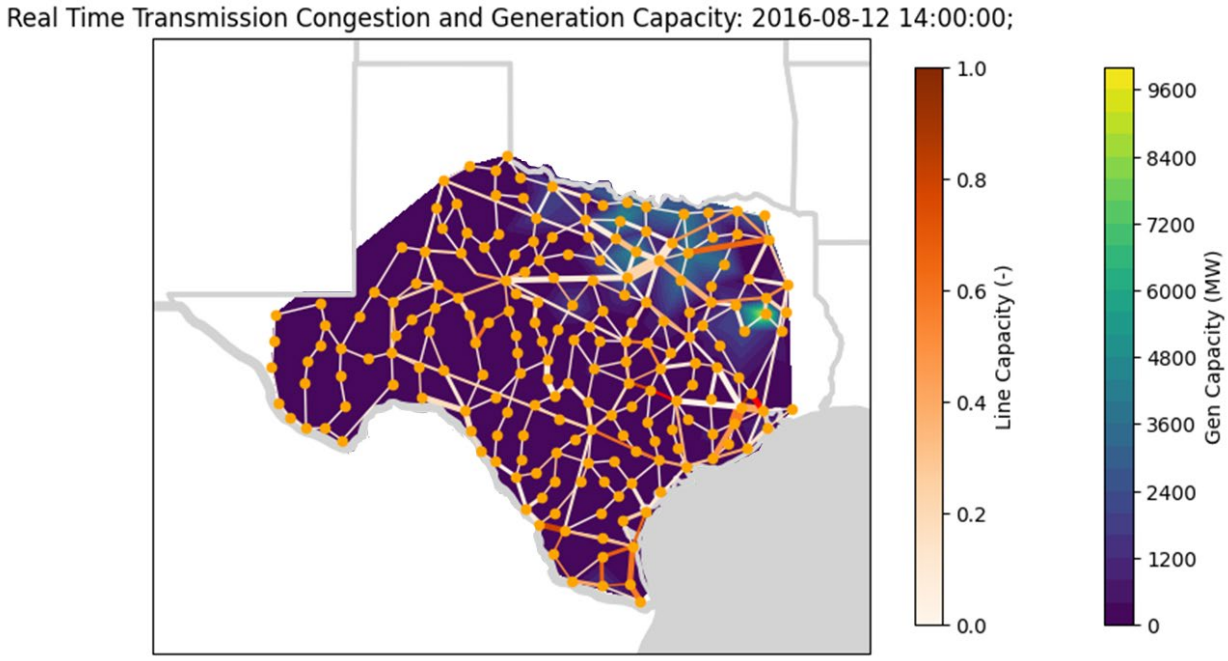

Figure 16. Geographic distribution of generation capacity in the DSO+T system model during the system peak load.

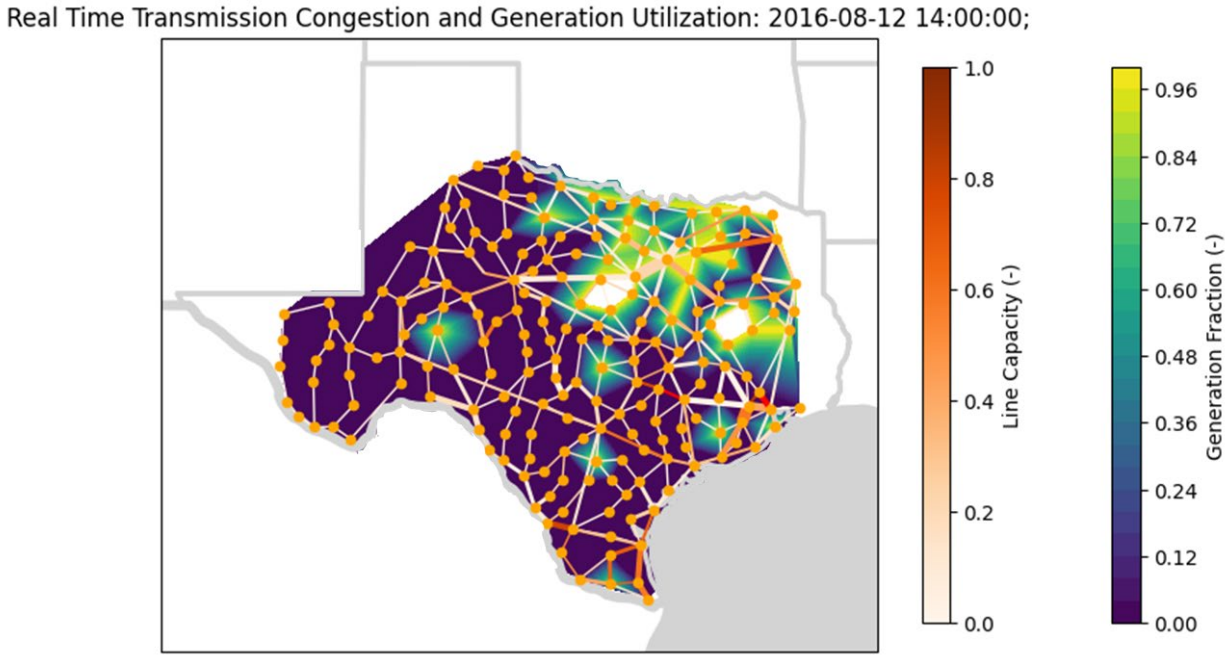

Figure 17. Geographic distribution of dispatchable generation utilization in the DSO+T system model during the system peak load.

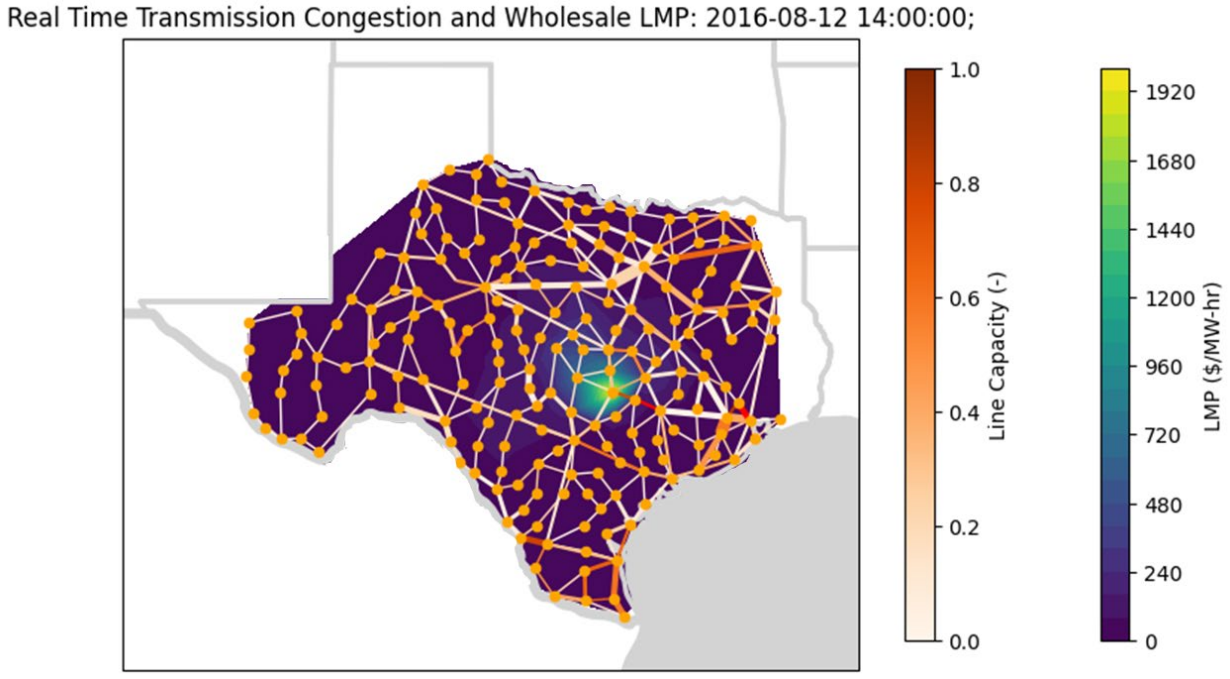

Figure 18. Geographic distribution of the resulting real-time LMPs in the DSO+T system model during the system peak load.

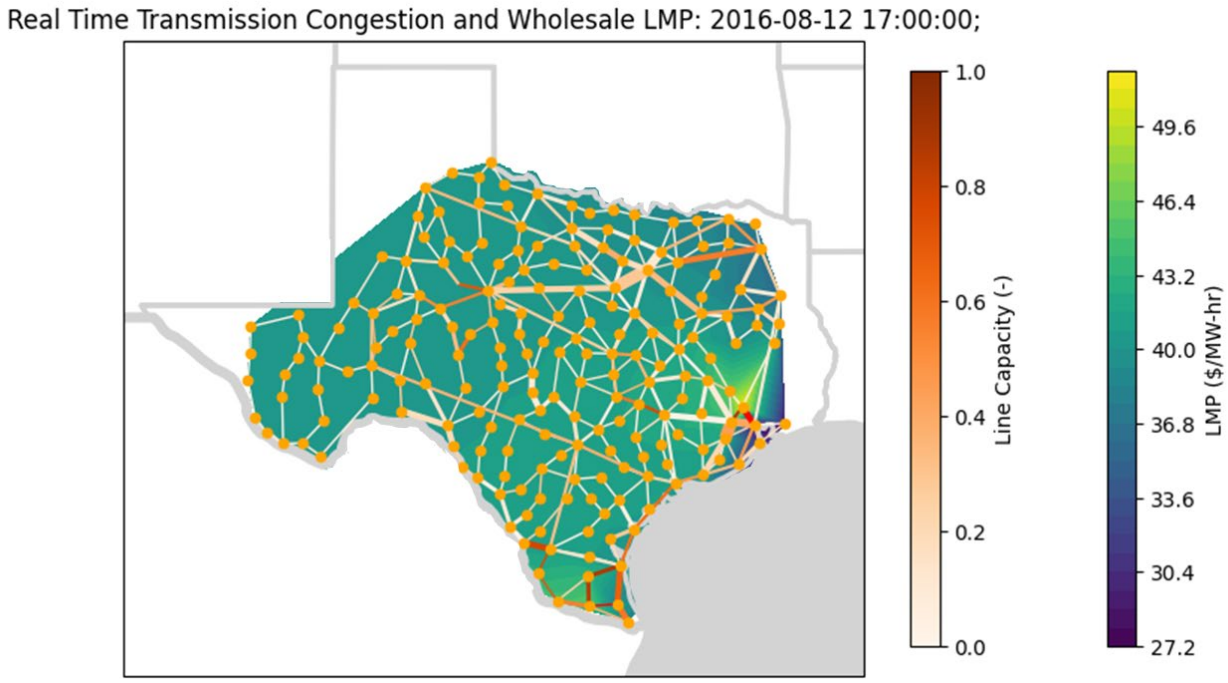

Figure 19. Geographic distribution of real-time LMPs in the DSO+T system model at 5 p.m. on August 12, 2016.

5.0 Distribution System Definition

This section details the data and processes used to define the characteristics of the transmission buses and attributes of the associated DSOs and their distribution system.

5.1 Bus Definitions

The key bus characteristics that determine distribution loads and performance include:

- Utility type (urban, suburban, and rural) which affects the type of distribution feeders and proportion of various building classes
- Latitude and longitude, which dictates the bus's climate zone and resulting 2016 weather profile
- Number and mix of residential, commercial, and industrial customers and loads
- Distribution system capacity constraints, for example substation capacity limits.

Utility types, bus loading, and load mix were designed using data reported to EIA (DOE-EIA n.d.), historical loading data reported by ERCOT (ERCOT, n.d.), and the existing TESP model of the ERCOT transmission system (TESP n.d. b) as described in Table 16.

Table 16. Data sources for bus definitions.

Source	Data
EIA 2016 Utility Data (DOE-EIA n.d.)	For each ERCOT utility: 1. Energy consumption in MWh broken into customer type 2. Customer count broken into customer type 3. Load/customer averages
ERCOT 2016 Historical Loading Data (ERCOT, n.d.)	1. Hourly load data for eight weather zones within ERCOT 2. Boundaries of the eight weather zones
TESP 200-Bus Data (TESP n.d. b)	For each bus: 1. Latitude and longitude coordinates 2. Solved load flow data in MW

5.2 Utility Types in ERCOT

Electric utilities in Texas consist of cooperatives, municipals, investor-owned utilities, and retail marketers. Each utility reported the energy delivered in 2016 to the EIA (DOE-EIA n.d.), with the values broken into three customer types: residential, commercial, and industrial. For the 200-bus case, each bus was assigned a utility type by mapping the latitude and longitude coordinates to the utility that services that location. The utility data were used to define the mix of residential, commercial, and industrial customers and loads.

5.2.1 Cooperatives

Cooperatives in West Texas are primarily rural, with many of the main offices in towns with populations less than 10,000 and service areas that span up to 10 counties. Outside of a few outliers, it is appropriate to categorize West Texas cooperatives as rural, with occasional suburban feeders for larger towns served by the region. The population density is higher in East Texas than in West Texas. As such, it is appropriate to include a higher number of suburban

feeders to represent these cooperatives. Figure 20 shows the service area boundaries of each of the cooperatives in Texas.

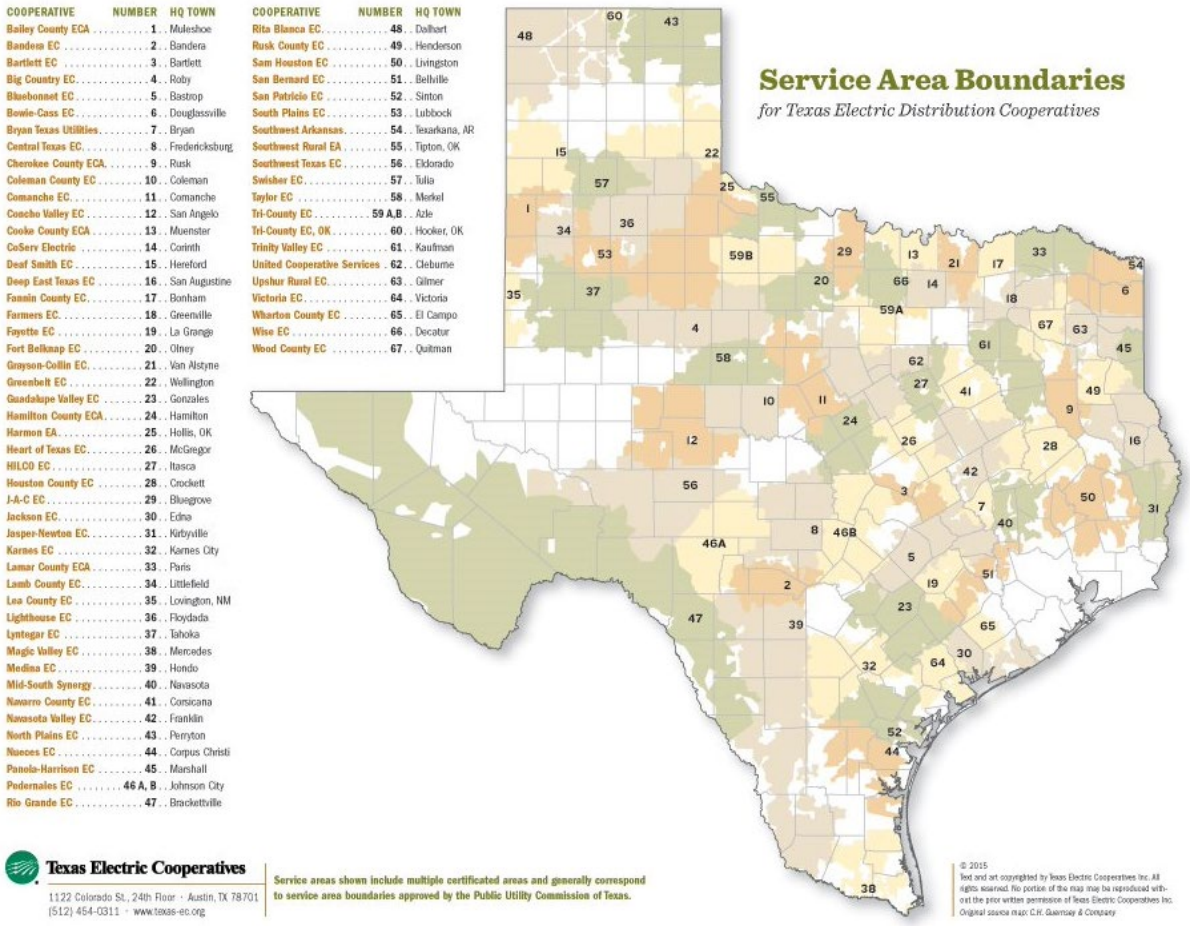

Figure 20. ERCOT cooperative service boundaries.

5.2.2 Municipals

Municipals are considered suburban for medium-sized cities or urban for larger cities. Municipal service areas are tied to city limits, so feeders would be shorter in distance than those in rural areas. In addition to shorter feeder lengths, customer density is higher than cooperatives and feeders would have the ability to switch load from one adjacent feeder to another.

5.2.3 Investor-Owned Utilities

Investor-owned utilities are shareholder-owned and operated for profit. Most investor-owned utilities within ERCOT do not cover contiguous areas, but rather provide service for areas outside the boundaries of the cooperative and municipal utilities. Figure 21 shows the service areas of the investor-owned utilities within ERCOT.

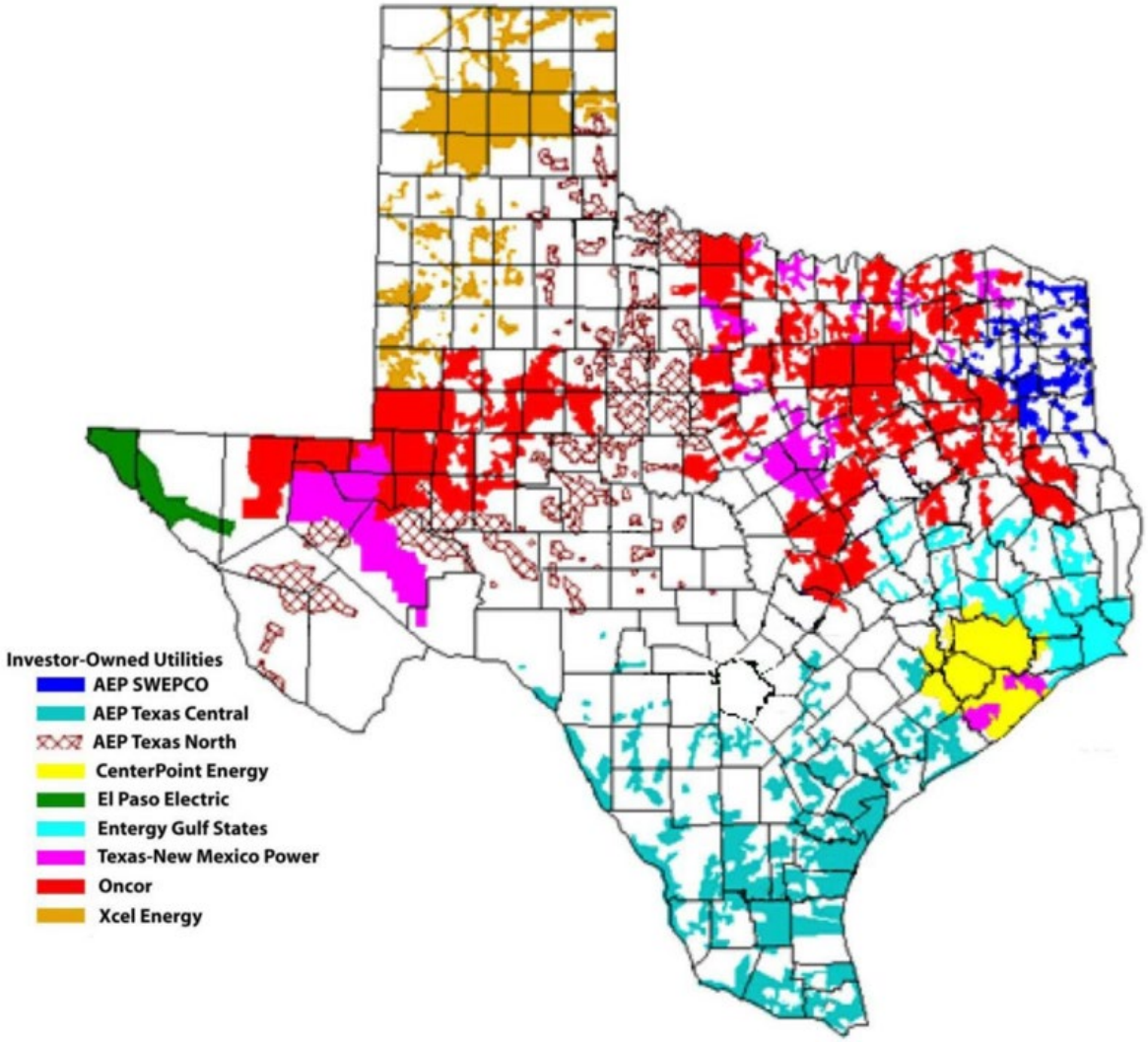

Figure 21. Service areas of investor-owned utilities in ERCOT.

5.2.4 Retail Marketers

Retail marketers deliver power to the end user, but most marketers do not own or maintain any actual infrastructure. Marketers are scattered throughout Texas, making it difficult to associate customers with a specific region, city, or county. Marketers that service specific cities or regions, such as Centerpoint in Houston, can be incorporated into existing suburban or urban DSO models. For the sake of the DSO+T study, retail marketers are considered to be investor-owned utilities.

5.3 Climate Zones and Weather Profiles

Each bus was assigned a climate zone and 2016 weather profile based on its latitude and longitude coordinates. The American Society of Heating, Refrigerating, and Air Conditioning Engineers (ASHRAE) divides the nation into seven zones based on temperature. These are further subdivided into humid (A), dry (B), and marine (C) environments. Texas experiences five zones: Zones 2 and 3 are defined based on the annual cooling degree days, while Zone 4 is defined by both annual cooling degree days and heating degree days as shown in Figure 22.

Table 17 lists the ranges for each climate zone. Most of the territory in Zone 4B is outside the ERCOT service area, which excludes that climate zone from the study; the small area for 4B is incorporated into Zone 3.

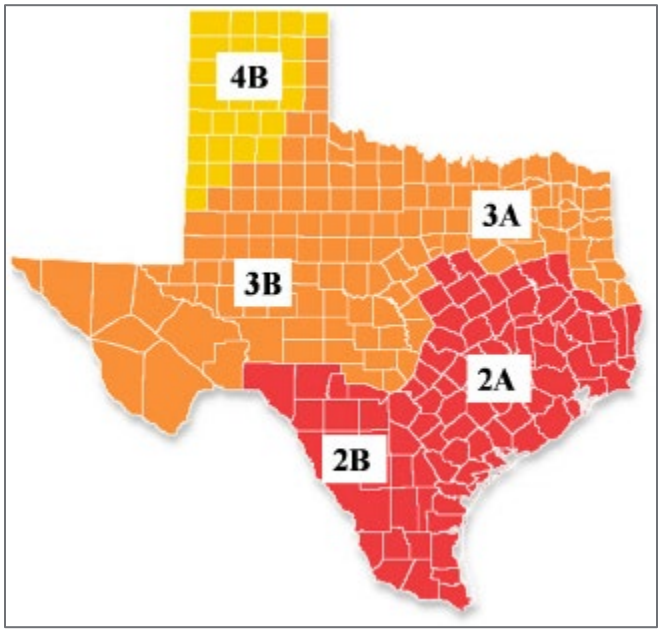

Figure 22. Map of ASHRAE-defined climate zones in Texas.

Table 17. Climate data in Texas.

Climate Zone	Moisture	Cooling/Heating Degree Day Ranges
2A	Humid	6300 < CDD50°F ≤ 9000
2B	Dry	6300 < CDD50°F ≤ 9000
3A	Humid	4500 < CDD50°F ≤ 6300
3B	Dry	4500 < CDD50°F ≤ 6300
4B	Dry	CDD50°F ≤ 4500 and 3600 < HDD65°F ≤ 5400

5.4 Customer and Building Population Mix

5.4.1 Residential and Commercial Customer and Building Populations

Each simulated utility has a mix of residential, commercial, and industrial customers based on EIA utility data (DOE-EIA n.d.). The data were used to determine the total number of residential and commercial buildings that make up the load at a bus. We assume a one-to-one relationship between a residential customer and a residential unit. That is, each residential customer is assumed to occupy a single-family home, apartment unit, or manufactured home. The proportions and definitions of the residential buildings are defined in more detail in Section 6.0.

This study found that a one-to-one relationship between commercial customers and commercial buildings is not valid. Investigation of EIA utility data (DOE-EIA n.d.) and commercial building energy survey data (DOE-EIA 2012) identified many more commercial customers in ERCOT than commercial buildings. For example, utility data indicate approximately 1.3 million commercial customers in ERCOT; however, there are only an estimated 620,000 commercial buildings. Therefore, this study assumed one commercial building for every 2.09 commercial

customers. The classes, proportions, and definitions of commercial buildings are defined in more detail in Section 7.0.

5.4.1 Industrial Load Profile and Magnitude

Individual industrial customers were not modeled in this study. Each DSO assumed an average industrial load based on the load mix reported to the EIA. Initially, the industrial load profile was determined by subtracting the residential and commercial building load profiles (calculated in the BAU case) from the hourly ERCOT load data (discussed in Section 5.8). This profile would then be the basis of the industrial load profile for all scenarios and cases. This approach was chosen in part because we could not find a satisfactory open, parametric industrial load profile model in the literature. Unfortunately, this approach resulted in unrealistic load profiles and values (including periods of negative industrial load on individual buses). This is due to the industrial load accounting for less than 5% of load on some buses. Therefore, if the predicted residential and commercial building load profiles over-estimate ERCOT loads by more than 5%, the industrial load profile would need to be negative to sum to the required system load. Achieving better than 5% accuracy is beyond the current capability of building modeling. The average modeled building loads matched ERCOT data within ~12% with daily load variation off by an average of 40% as discussed in Section 8.3.

As an alternative, this study used a constant (flat) industrial load profile shape. This was based on the low variation seen in (Hale et al. 2018) and feedback from industry experts who cite large industrial loads as typically being flat. The development of a representative and open parametric industrial load profile model warrants further investigation and development.

5.5 Definition of Distribution Feeder Models

To simulate distribution losses, feeders were included in the distribution system model. Table 18 summarizes the taxonomy feeders (Schneider et al. 2008) that were used, as a function of DSO type and taxonomy feeder climate zone (which is different from the ASHRAE climate zone definition) as shown in Figure 23. The feeder definition was selected to capture the range of feeder types that may be present (for example, dense, short urban feeders versus longer, more sparsely populated rural feeders) while maintaining a reasonable number of building models and therefore a balance between computational effort and accuracy. The selected feeders result in between ~900 and ~1,500 residential customers being modeled per DSO.

Table 18. Summary of taxonomy feeders implemented by DSO type.

Region Type	Zone 3	Zone 4	Zone 5
Urban	R4-12.47-1 R5-12.47-1	R4-12.47-1 R4-12.47-2	R5-12.47-1 R5-12.47-2
Suburban	R5-12.47-5	R5-12.47-5	R5-12.47-5
Rural	R5-12.47-5	R5-12.47-5	R5-12.47-5

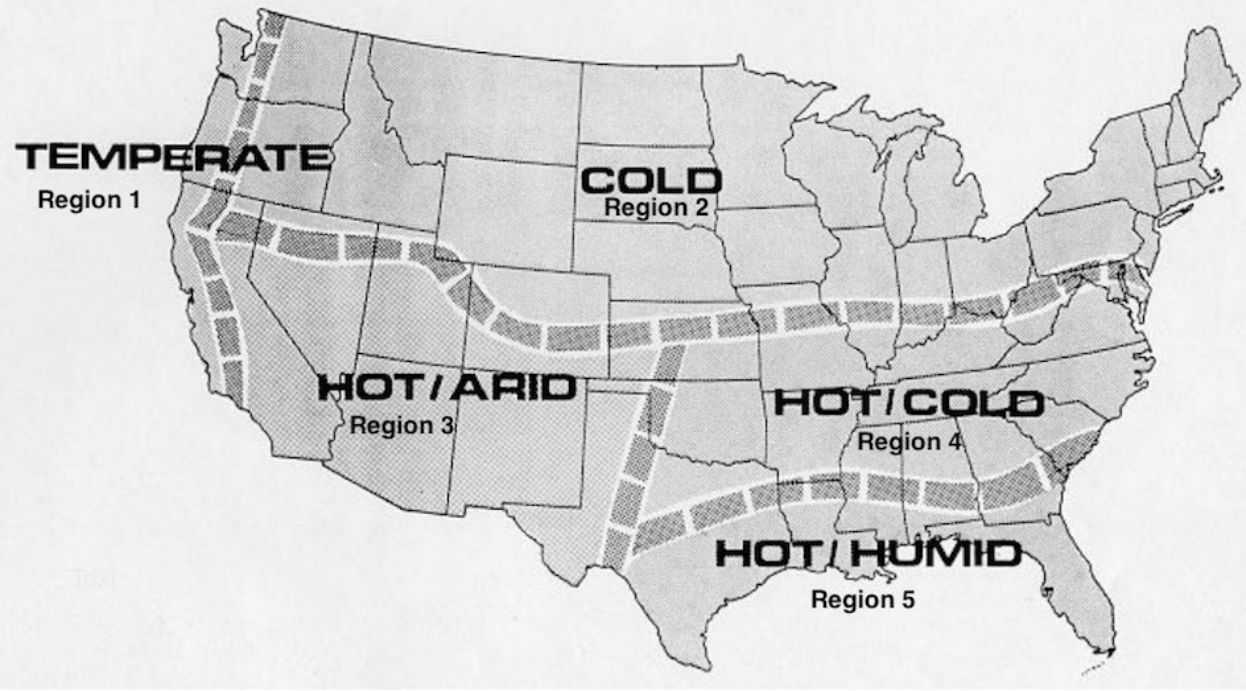

Figure 23. Region definitions used for taxonomy feeders.

The required number of residential and commercial building populations are randomly generated (as described in Sections 6.0 and 7.0) based on the expected feeder population and designated ratio of residential to commercial customers for that utility. Residential and commercial buildings are then assigned to nodes on the feeder based on matching building size (sq. ft.), as a proxy for expected electrical rating, to the capacity of the feeder node in question. This process typically results in a surplus of commercial buildings as the taxonomy feeders often have insufficient commercial nodes with the required ratings. When this happens a 'copper-plate' feeder is instantiated and used to feed the remaining commercial buildings, ensuring the correct population mix is achieved. All feeders representing a DSO are then merged into a combined GridLAB-D model that is used to simulate the distribution system and building loads.

The selected taxonomy feeders only simulate a small fraction of the total customers on any given DSO. To account for this, a weighting factor is utilized on the resulting distribution load when applied to the bus in the bulk system transmission model. The weighting factor is the ratio of the number of actual DSO residential customers divided by the number of simulated residential customers as shown below:

$$weighting\ factor = \frac{Residential\ Customers_{DSO}}{Residential\ Customers_{Sim}} \quad (3)$$

As expected, large urban DSOs with many customers have large weighting factors, while smaller rural cooperatives can have small weighting factors. Ultimately the simulations resulted in 11,929 and 63,729 individual customer buildings being simulated for the 8- and 200-bus models. For the 8-bus model the DSO weighting factors range from 23.5 to 3,816 with a system-wide weighting factor of 952. For the 200-bus model, where only 40 DSOs are simulated (see Section 5.6) the DSO weighting factors range from 13.5 to 2,008 with a system-wide weighting factor of 172.

5.6 DSO Selection and Demographics

This section describes how the simulated DSOs were selected and the resulting demographics captured in the study. For the 200-bus model the vast majority of buses and associated DSOs have few customers and small loads. Figure 24 shows the proportion of total system load represented by the largest buses. This shows that the largest 5 buses have over 50% of the system load, while the largest 40 and 66 buses represent 89.8% and 94.9% of the system load. Simulating the loads on all 200 buses represents diminishing improvements in accuracy at considerable computational expense. Furthermore, some rural buses have so few customers that more customers would be simulated than actually exist (that is, a weighting factor of less than one). For this reason, it was decided to simulate 40 DSOs. This results in approximately 90% of the system load being simulated but reduces the computational size of the model by a fifth. The 160 buses that are not simulated were modeled using unresponsive load profiles (as described in Section 5.8).

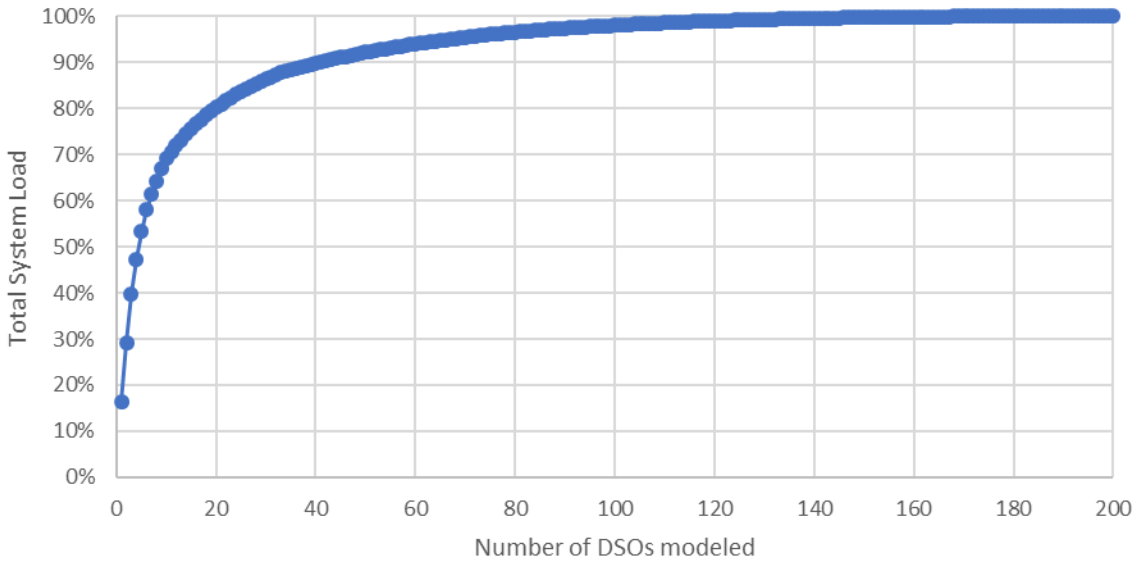

Figure 24. Cumulative system load vs. bus count.

The selection of the 40 buses was not based solely on size. Selecting the largest 40 DSOs resulted in a selection that slightly overrepresented urban regions, investor-owned utilities, and summer peaking DSOs while underrepresenting cooperatives. Some adjustments in the DSO selections were made in an attempt to counteract this. Six cooperative DSOs were added, five of which were rural. The resulting DSO selection still captured >87% of the system load.

Table 19, Table 20, and Table 21 show the resulting demographic mix and representativeness of the selections. Rural cooperatives are still underrepresented but less so than with a selection based solely on load. More importantly, this selection substantially increases the number of samples for both cooperatives and rural utilities, increasing the statistical significance of the study results for future analysis. Key attributes of all 40 simulated DSOs are provided in Table 22.

Table 19. Comparison of simulated buses by region type.

	Total Buses	Simulated Buses	Total Load	Sim Load	Difference
Urban	15	9	65%	71%	-5.9%
Suburban	79	22	29%	26%	3.1%
Rural	100	9	6%	3%	2.7%

Table 20. Comparison of simulated buses by DSO ownership type.

	Total Buses	Simulated Buses	Total Load	Sim Load	Difference
Investor-owned	43	15	66%	71%	-4.1%
Cooperative	142	17	17%	11%	5.4%
Municipal	15	8	17%	18%	-1.3%

Table 21. Comparison of simulated buses by peaking season.

	Total Buses	Simulated Buses	Total Load	Sim Load	Difference
Summer	129	27	89%	92%	-2.9%
Winter	35	9	6%	5%	1.0%
Dual	36	4	5%	3%	1.9%

Table 22. Details of key attributes for all 40 simulated DSOs.

Bus	Utility Type	Ownership Type	Peak Season	ASHRAE Zone	BLM Zone	Average Load (MW)	Congestion Factor (-)
1	Urban	Investor-owned	Summer	2A	3	4720	0.939
2	Suburban	Cooperative	Winter	2A	7	260	0.93
3	Suburban	Municipal	Summer	2A	6	1664	0.938
4	Urban	Investor-owned	Summer	2A	4	5135	0.939
5	Rural	Cooperative	Dual	2A	6	294	0.949
7	Rural	Cooperative	Winter	3B	2	127	0.93
8	Suburban	Municipal	Summer	2A	5	107	0.938
15	Suburban	Cooperative	Winter	3B	1	333	0.938
16	Rural	Cooperative	Dual	3A	3	89	0.93
23	Suburban	Cooperative	Summer	3B	3	133	0.938
26	Suburban	Investor-owned	Summer	2A	6	497	0.93
43	Rural	Cooperative	Winter	3B	5	261	0.949
48	Suburban	Investor-owned	Dual	2A	4	383	0.93
51	Suburban	Investor-owned	Dual	2A	4	643	0.938
52	Suburban	Municipal	Summer	2A	6	150	0.938
54	Suburban	Cooperative	Winter	2A	8	723	0.938
55	Rural	Cooperative	Winter	2A	4	135	0.948
59	Suburban	Cooperative	Winter	3A	3	142	0.938
69	Suburban	Investor-owned	Summer	2B	2	196	0.938
76	Urban	Investor-owned	Summer	2A	5	5260	0.939
77	Urban	Investor-owned	Summer	3A	5	968	0.93
78	Urban	Investor-owned	Summer	3A	7	924	0.939
79	Suburban	Investor-owned	Summer	3A	6	670	0.938
80	Suburban	Investor-owned	Summer	3A	5	310	0.938

Bus	Utility Type	Ownership Type	Peak Season	ASHRAE Zone	BLM Zone	Average Load (MW)	Congestion Factor (-)
83	Rural	Cooperative	Summer	2A	7	138	0.93
86	Suburban	Municipal	Summer	2A	5	263	0.938
89	Suburban	Cooperative	Summer	2A	2	224	0.938
98	Rural	Cooperative	Winter	3A	5	130	0.949
100	Suburban	Municipal	Summer	3A	5	117	0.938
104	Urban	Municipal	Summer	2A	5	2673	0.939
110	Suburban	Investor-owned	Winter	3B	3	479	0.938
115	Suburban	Municipal	Summer	2A	5	292	0.938
117	Urban	Investor-owned	Summer	3A	6	489	0.939
123	Suburban	Cooperative	Summer	2B	4	1807	0.938
125	Suburban	Cooperative	Summer	2A	4	258	0.938
127	Urban	Investor-owned	Summer	3B	3	3331	0.939
140	Rural	Cooperative	Summer	3B	3	166	0.949
161	Rural	Cooperative	Summer	2A	5	512	0.949
166	Urban	Investor-owned	Summer	2A	6	423	0.939
197	Suburban	Municipal	Summer	2A	6	565	0.937

5.7 Definition and Determination of Substation Limits

This study simulates one substation per DSO. It is assumed that this substation has a capacity constraint, the value of which is used by the transactive retail market to determine if congestion pricing should be applied. As a result of this limitation, the DSO capacity constraint assigned to any simulated substation represents the more severe of two constraints reflecting the DSO's objectives in reducing both of these capital expenses:

1. Every substation is assigned a capacity limit that, at least, reflects its share of limiting the DSO's and region's peak demand (and resulting transmission fees and generation capacity payments).
2. When a substation's peak demand is limited by its own capacity, an additional reduction in the capacity limit is assigned to give customers on congested substations an incentive to increase their response when necessary to limit peak demand, reflecting the fact that more value is at stake, i.e., the value of avoided generation plus the value of additional avoided substation capacity.

The process to determine the fraction of substation capacity for the DSO type that is congested in any given year, was based on the methodology documented in Appendix B of (Pratt et al. 2022). The substation capacity constraint factors for all 40 simulated DSOs are provided in Table 22. These are shown as a fraction of annual peak load determined in the BAU case. For example, if the congestion factor is 0.93, congestion pricing will be applied to any day-ahead or real-time load that exceeds 93% of the peak load from the BAU case.

5.8 Generating Hourly Load Profiles from ERCOT Data

Load profiles for buses that were not simulated were based on ERCOT historical hourly load data (ERCOT n.d.) that is disaggregated into the 8 weather zones for which ERCOT data is reported (Figure 25). These hourly datasets are used to define load curves for each of the 200 buses through the following steps. First, the ERCOT 2016 hourly data is normalized for each of the 8 zones. Next, each bus is assigned one of the weather zones based on its latitude and

longitude coordinates. Then the average bus loading results from TESP (TESP n.d. b) are scaled such that the summation of all bus loads equals the average hourly load from the historical ERCOT data. The normalized vector for each bus is then multiplied by the scaled load flow solution in the TESP bus case, resulting in hourly load profile tapes for each bus.

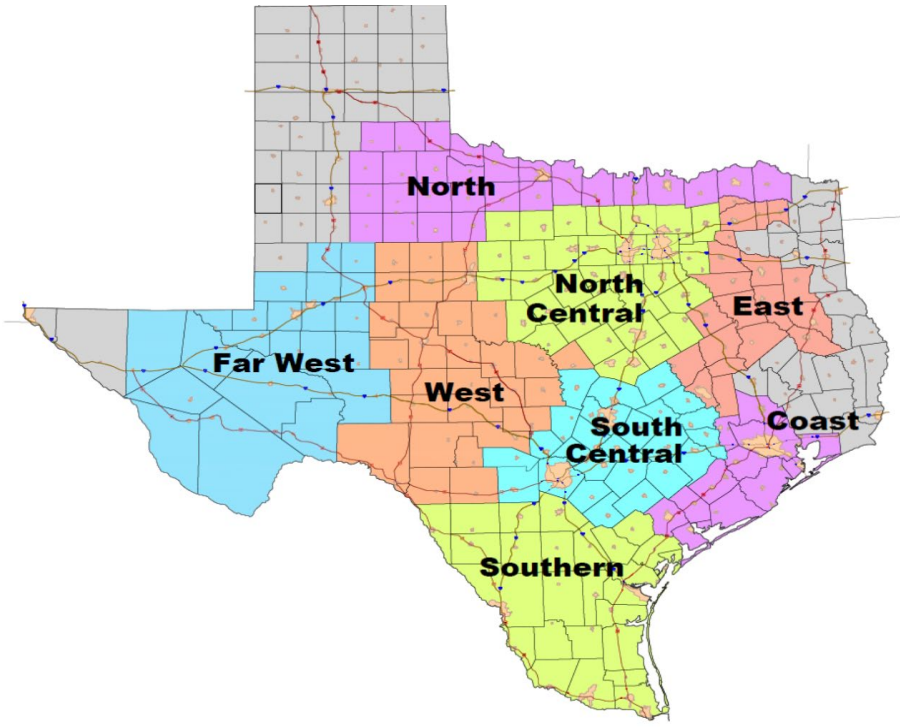

Figure 25. ERCOT load data is divided into eight weather zones.

6.0 Residential Buildings

This section describes how a residential building population, representative of the ERCOT market, is instantiated for each DSO region. Distributions of key characteristics of homes, such as building type, vintage, day/night and winter/summer thermostat settings, heating fuel source, number of stories and floor areas for building types were drawn from the EIA's Residential Energy Consumption Survey or RECS (DOE-EIA 2015) for the South Census Division. Thermal integrity (e.g., window and wall R-values) and air conditioner and heat pump efficiency are suggested by vintage, building codes, and historical construction practices. Reasonable distributions of other key home characteristics that were not available from the survey had to be assumed, such as the amount of thermal mass, level of internal heat gains, window-to-wall ratios, footprint aspect ratios, and outside air infiltration rates. Using detailed distributions of key building design and operation characteristics is important to ensure that both the resulting system load profile as well as the distribution of customer energy usage and retail electricity costs are representative. The residential building distributions used in this study are described in the following sections.

6.1 Determining Building Type and Vintage

Statistical distributions of residential building type and vintage for each DSO type (urban, suburban, and rural) building population was based on the 2015 RECS dataset from the South Region, which is inclusive of the following states: TX, OK, AR, LA, MS, AL, GA, FL, TN, NC, SC, KY, VA, WV, DC, MD, DE.

RECS data include U.S. Census Bureau classification for Urban Areas and Urban Clusters and data that do not fit either of these criteria are classified as Rural. An Urban Area is defined as a densely settled group of blocks or tracts with a population of 50,000 or more. Urban Clusters are defined as areas with a population between 2,500 and 50,000. Buildings in areas with populations under 2,500 are considered to be in a Rural setting. This classification is used to define three DSO types, i.e., Urban (Urban Areas), Suburban (Urban Clusters), and Rural. Of the RECS microdata used for this study, 64 percent of the observations were in Urban settings, 11 percent in Suburban, and 25 percent in Rural settings.

RECS data are classified as belonging to one of five building types: manufactured home, single family detached, single family attached, apartment 2-4 units, and apartment >5 units. This study combined data from single family attached and detached homes and combined both apartment categories to form three building types, i.e., single family, apartment, and manufactured home. Based on these data, a likelihood was determined for each building type to fall in one of eight vintage bins. These likelihoods for each DSO type are shown in Figure 26, with apartments being less prevalent in rural DSOs which would be expected based on the definition of a rural building being in a less densely populated area.

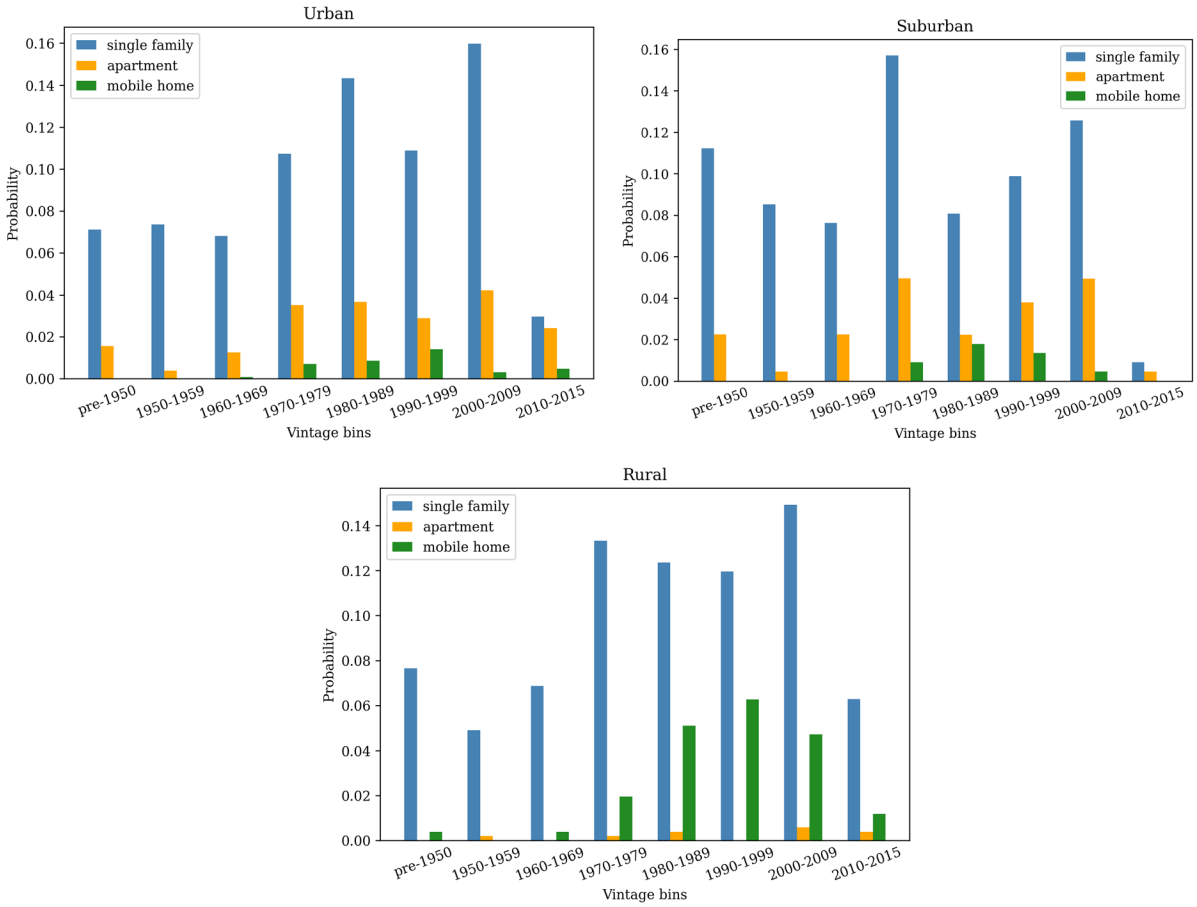

Figure 26. Probability distribution of building types for eight vintage bins within DSO type.

6.2 Determining Building Form Factor

GridLAB-D uses the following key variables to define the building form: gross floor area, ceiling height, number of stories, aspect ratio, window-to-wall ratio, exterior wall fraction, exterior ceiling fraction, and exterior floor fraction. A constant ceiling height of 8 feet is used for manufactured homes and apartments, whereas for single family it is uniformly distributed between 8 and 9 feet. A constant 15% window-to-wall ratio is assumed for all building types. The single family homes are considered either single or double story based on the RECS data as shown in Table 23, whereas all apartment and manufactured home buildings are considered single story.

The footprint aspect ratio (width-to-depth ratio) of single family and apartment buildings are randomly chosen from a truncated normal distribution with a mean of 1.5. Manufactured homes are considered either single-wide (67%) or double-wide (33%) with mean aspect ratios of 5.5 and 2.2 respectively (see Table 24). Since double-wide manufactured homes usually are bigger in floor area than single-wide, the separation single- and double-wide is performed based on a floorspace threshold (1,080 sq. ft.) that is determined based on industry average sizes for manufactured homes.

Table 23. Probability of single and double story level for single family homes for each region type as per RECS 2015 dataset.

Story level	Urban	Suburban	Rural
Single Story	0.62	0.80	0.75
Double Story	0.38	0.20	0.25

Table 24. Statistical parameters used to construct a truncated normal distribution of aspect ratio for each building type.

Aspect Ratio	min	max	mean	std
Single family	1	2	1.5	0.5
Apartments	1.2	1.8	1.5	0.1
Manufactured homes single wide	4.5	5	5.5	0.1
Manufactured homes double wide	1.8	2.5	2.2	0.2

To account for common walls, ceilings, and floors between dwelling units, we used GridLAB-D's exterior wall, ceiling, and floor fractions—the fraction of the gross exterior surface area that is not in common with another unit. These fractions are considered 100% for all single family and manufactured home buildings as they do not share any walls, ceilings, or floors with other buildings. However, for apartments we consider that each unit is part of either an eight-unit or a 16-unit apartment complex as shown in Figure 27.

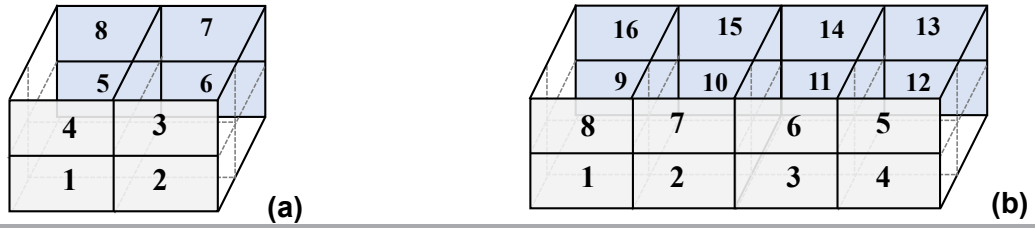

Figure 27. Schematics of apartment complexes with (a) 8-units and, (b) 16-units, in order to estimate exterior wall fraction, exterior ceiling fraction, and exterior floor fraction.

In an eight-unit complex, the upper units (3, 4, 7, 8) have exterior ceiling but not floor (exterior ceiling fraction = 1, exterior floor fraction = 0) and the lower units (1, 2, 5, 6) have exterior floor but not ceiling (exterior ceiling fraction = 0, exterior floor fraction = 1). All eight units have 50% of their walls as exterior (exterior wall fraction = 0.5). Similarly, in a 16-unit complex, the upper units (5-8,13-16) have exterior ceiling fraction = 1 and exterior floor fraction = 0; whereas the lower units (1-4, 9-12) have exterior ceiling fraction = 0 and exterior floor fraction = 1. In this case, all eight corner units have 50% exterior walls (exterior wall fraction = 0.5). Whereas, all middle units have only one wall along the length as exterior, therefore exterior wall fraction (*EWF*) can be given as function of aspect ratio (*AR*):

$$EWF = \frac{AR}{2(1+AR)} \quad (4)$$

Floor area for a given building type within a certain vintage bin is randomly picked from a specific truncated normal distribution based on the statistical parameters (mean, minimum, maximum, and standard deviation) shown in Figure 28. These parameters are estimated from the RECS dataset. Note that there are not enough samples to get these parameters for manufactured home buildings for first three vintage bins.

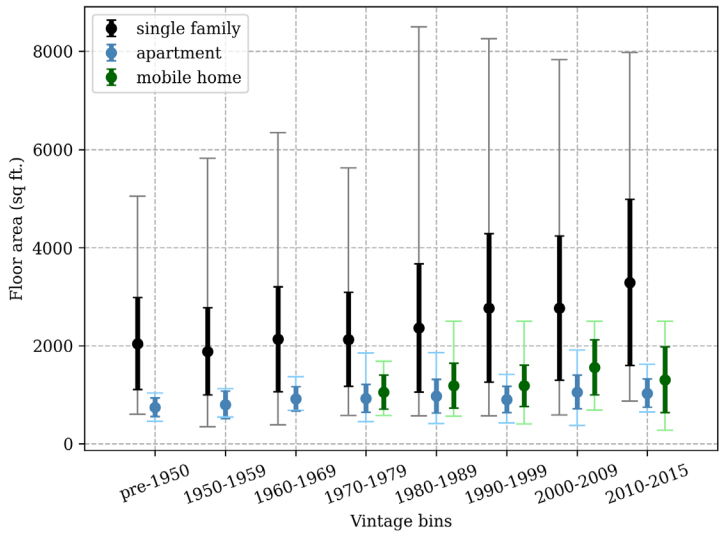

Figure 28. Floor area truncated normal distribution parameters: mean, minimum, maximum and standard deviation per vintage bin for each building type based on RECS data.

6.3 Determining Building Thermal Properties

6.3.1 Envelope

The thermal integrity parameters of the building envelope for all three building types are shown in Table 25, Table 26, and Table 27. These tables show the equivalent parallel-path heat flow R-value for the ceilings, walls, and slab floor, and the window characteristics for each integrity level.

Table 25. Thermal integrity levels for single family homes.

Integrity Level	Frac. of Population	Description	Ceiling R-value (hr-°F-ft²/Btu)	Wall R-value (hr-°F-ft²/Btu)	Floor R-value (hr-°F-ft²/Btu)	Window Characteristics				Door R-value (hr-°F-ft²/Btu)	Infiltration air exchange (1/hr)
						Layers	Glazing	Treatment	Frame		
0	5%	old, uninsulated	11	4	4	1	Glass	Clear	aluminum	3	1.5
1	20%	old, insulated	19	11	4	2	Glass	Clear	aluminum	3	1.5
2	20%	old, weatherized	19	11	15	2	Glass	Clear	aluminum	3	1.0
3	40%	old, retrofit upgraded	30	11	15	2	Glass	Clear	thermal break	3	1.0
4	10%	2003 IECC code	38	16	22	2	Low-e glass	Clear	thermal break	5	0.5
5	5%	2009 IECC code	48	22	30	3	Low-e glass	Heat-absorbing	insulated	11	0.5

Table 26. Thermal integrity levels for manufactured homes.

Integrity Level	Frac. of Population	Description	Ceiling R-value (hr-°F-ft²/Btu)	Wall R-value (hr-°F-ft²/Btu)	Floor R-value (hr-°F-ft²/Btu)	Window Characteristics				Door R-value (hr-°F-ft²/Btu)	Infiltration air (1/hr)
						Layers	Glazing	Treatment	Frame		
0	49%	old (1976-1994)	13.4	9.2	11.7	1	Glass	Clear	aluminum	2.2	1.5
1	51%	new (1994-present)	24.1	11.7	18.1	2	Low-e glass	Clear	thermal break	2.2	0.4

Table 27. Thermal integrity levels for apartments.

Integrity Level	Frac. of Popula-tion	Description	Ceiling R-value (hr-°F-ft²/Btu)	Wall R-value (hr-°F-ft²/Btu)	Floor R-value (hr-°F-ft²/Btu)	Window Characteristics				Door R-value (hr-°F-ft²/Btu)	Infiltration air exchange (1/hr)
						Layers	Glazing	Treatment	Frame		
0	5%	old, uninsulated	11	4	4	1	Glass	Clear	aluminum	3	1.5
1	20%	old, insulated	19	11	4	2	Glass	Clear	aluminum	3	1.5
2	25%	old, weatherized	19	11	15	2	Glass	Clear	aluminum	3	1.0
3	40%	old, retrofit upgraded	30	11	15	2	Glass	Clear	thermal break	3	1.0
4	10%	2003 IECC code	38	16	22	2	Low-e glass	Clear	thermal break	5	0.5

The U-values for single family homes in Table 24 are based on ceiling construction consisting of 2x10 joists 24 in. on center, with a 2% miscellaneous framing fraction. Cavity insulation levels are R-11, R-19, or R-30 depending on the integrity level. Integrity Level 4 meets the 2003 International Energy Conservation Code (IECC). Integrity Level 5 (based on the 2009 IECC) is used for all buildings in the 2009-2015 vintage bin. Level 5 has an additional R-8 covering for the entire assembly. The wall construction is 2x4 studs 16 in. on center, except for Integrity Level 6 which has 2x6 studs 24 in. on center. A 5% miscellaneous framing fraction is used in every case. Cavity insulation levels are none (R-1), R-11, R-13, or R-19 depending on the integrity level. The U-values for the floor above the crawlspace are based on 2x10 joists 24 in. on center, with a 5% miscellaneous framing fraction. Cavity insulation levels are none (R-4), R-11, R-19, or R-30 depending on the integrity level. Single family homes are assumed to have four solid doors, each with an area of 19.5 ft^2.

For manufactured homes, the component integrity levels do not vary independently because they are associated with the U.S. Housing and Urban Development (HUD) building code (HUD, 2009). The overall heat loss levels required by the code changed in 1994. The resulting change in component insulation levels for HUD Zone 1 are shown in Table 27. These characteristics were verified to meet the HUD code for Zone 1 at 15% window area (an overall heat loss coefficient of 0.116 Btu/ft^2-°F). There were 37% assumed built to the 1976 standards and 63% to the improved 1994 standards. The U-values for manufactured homes in Table 25 are based on truss ceiling construction, which is assumed to be the thermal equivalent of 2x10 joists 24 in. on center, with a 2% miscellaneous framing fraction. Insulation levels are R-11 or R-14 with an R-8 cover, depending on the integrity level. The floor assembly is also assumed to be the thermal equivalent of 2x10 joists 24 in. on center, with a 2% miscellaneous framing fraction. Floor insulation levels are R-7 or R-11. The wall construction is 2x4 studs 16 in. on center. A 5% miscellaneous framing fraction was used. Cavity insulation levels are R-7 or R-11. Manufactured homes are assumed to have four solid doors, each with an area of 19.5 ft^2.

The thermal integrity of the building envelope is shown in Table 26, paralleling that of single family homes, except no multifamily homes are at the highest integrity level. The U-values for multifamily homes in Table 26 are based on ceiling construction consisting of 2x10 joists 24 in. on center, with a 2% miscellaneous framing fraction. Cavity insulation levels are R-11, R-19, or R-30 depending on the integrity level. The wall construction is 2x4 studs 16 in. on center, except for Integrity Level 3 which has 2x6 studs 24 in. on center. A 5% miscellaneous framing fraction is used in every case. Wall cavity insulation levels are R-11 or R-13 depending on the integrity level. Multifamily homes are assumed to have one solid door with an area of 19.5 ft^2, with a sliding glass door (counted as a window) as the other egress point.

The number of layers of glazing, type of glazing, and any tinting or reflective treatments for each integrity are shown in Table 24. The glazing properties are translated into U-values and solar heat gain coefficients (SHGCs) as described in GridLAB-D (2017), Tables 1 and 2. The nominal rate of infiltration of outside air is also provided for each integrity level, ranging from 1.5 times

the volume of the house each hour for old, leaky homes, to 0.5 air changes per hour for modern homes and 0.25 air changes per hour for extremely tight homes. Effective seasonal infiltration rates were assumed to be 50% of the nominal infiltration. A window exterior transmission coefficient is selected from a truncated normal distribution (50% mean with 10% standard deviation) to simulate the effect of window shading due to screen or trees.

Table 28. HUD code insulation levels for manufactured homes (Zone 1).

	1976 Standards		1994 Standards	
	Single-Wide	Double-Wide	Single-Wide	Double-Wide
Ceiling	R-11	R-11	R-14	R-14
Walls	R-7	R-7	R-11	R-11
Floor	R-7	R-7	R-11	R-14

6.3.2 Thermal Mass and Heat Transfer

There are four primary properties of the thermal mass in a building that must be specified for the GridLAB-D simulations of each building type:

- Total thermal mass of the home, mostly consisting of interior partitions and furnishings
- Total surface area of the thermal mass in the home
- Heat transfer coefficient for the surface of the thermal mass
- Mass of the air in the home, plus a small portion of the furnishings and interior surface mass, that is affected by short-term temperature fluctuations within the thermostat's deadband during on/off cycles of the space conditioning equipment.

For residences, the thermal mass was estimated based on the surface areas of the ceilings, interior surface of exterior walls and partition walls, less the area of windows, exterior doors, and interior doors or openings in the partition walls. The area of the partition walls was estimated based on the number of rooms. The number of rooms was estimated as a function of the floor area on each story of the home. From the number of rooms, the interior partition wall area was computed as the gross area, less 20% for interior doors or openings. The results of these calculations are that single family homes have 0.7 ft^2 of interior wall surface area per unit of gross exterior wall area. For single-wide and double-wide manufactured homes, this ratio was 0.7 and 0.8, respectively. For apartments, the ratio was 0.7.

The primary component of the thermal mass of these surfaces is the gypsum board on the surface. A small amount of mass is added by the framing of the partition walls. In addition, the thermal mass of home furnishings was estimated based on data from household moving companies, which indicated 12,000 lbs. for a 3,500 ft^2 home, i.e., 3.4 lbs/ft^2. Five major appliances were also assumed at an average of 200 lbs. each. Assuming the thermal properties of the furnishings are equivalent to soft wood, these assumptions produced a total thermal mass per unit floor area of 3.4 Btu/^{o}F-ft^2 for single family homes, and estimates of 3.7 Btu/^{o}F-ft^2, 3.4 Btu/^{o}F-ft^2, and 3.4 Btu/^{o}F-ft^2 for single-wide and double-wide manufactured homes and multifamily homes, respectively. Based on these values, thermal mass per unit floor area is uniformly distributed between a range from 2.5 to 4 Btu/^{o}F-ft^2.

The average heat transfer coefficient for the surface of the thermal mass was estimated as the weighted average for horizontal and vertical surfaces and surface areas of the ceilings and

interior surfaces. For vertical surfaces, the heat transfer coefficient was assumed to be 0.59 Btu/hr-^{o}F-ft^{2}; for horizontal surfaces, we assumed 0.49 Btu/hr-^{o}F-ft^{2}. The furnishings were assumed to reduce the interior surface area by cover up some of it up. With these assumptions, the effective interior mass surface conductance per unit interior surface area for single-family homes was estimated to be 0.38 Btu/hr-^{o}F-ft^{2}. For single-wide and double-wide manufactured homes and multifamily homes, it was estimated to be 0.39 Btu/hr-^{o}F-ft^{2}, 0.37 Btu/hr-^{o}F-ft^{2}, and 0.37, Btu/hr-^{o}F-ft^{2}, respectively.

6.3.3 Plug Loads and Internal Gains Schedules

Homes vary significantly in their use of appliances, which are a considerable source of heat gain inside a residence. To model this source of diversity in heating and cooling loads, we first developed a simple regression model that accounts for the average level of internal heat gains in homes of various floor areas using data from the End-Use Load and Conservation Assessment Program (ELCAP), the largest end-use metering project in the United States (Pratt et al. 1989). The "Other" end use is defined as the total consumption, less space conditioning and water heating.

The internal gains as a function of floor area are approximated as a regression against mean annual consumption data for the "Other" end use by floor area categories. A model was developed of the average annual energy consumption as a function of floor area of the form:

$$\text{Other} = a\, x^{b} \qquad (5)$$

This can be converted to a linear regression by an axis transformation into the form:

$$\log_e(\text{kWh/yr}) = \log_e(a) + b \log_e(\text{floor area, ft}^2) \qquad (6)$$

The mean ELCAP consumption for four categories of floor area and the resulting fit to these data points is shown in Table 29. Converting the units from kWh/yr to average power in watts, the internal gains as a function of floor area for the average home is estimated as

$$\text{Other} = 324.9 * (\text{floor\_area})^{0.442} * 1000 / 8760 \qquad (7)$$

Table 29. Regression of ELCAP "Other" Annual End-Use Load vs. Floor Area

End Use	Size of Home (ft^2)				Regression: ln(Other) = ln(a) + b ln(x)		
	850	1350	2100	2475	Parameter	Value	Std. Error
Other	6730	7298	9066	11079	ln(a)	5.7834	0.8017
ln(End Use)	ln(Size of Home (ft^2))				b	0.4420	0.1088
	6.745	7.208	7.650	7.814	r2	0.8918	
ln(Other)	8.814	8.895	9.112	9.313	a	324.9	45.0
Predicted End Use	Size of Home (ft^2)				$EU = a\, x^{b}$		
	850	1350	2100	2475	$\ln(EU) = \ln(a) + \ln(x^{b})$		
Other	6403	7856	9550	10269	$\ln(EU) = \ln(a) + b \ln(x)$		

The mean load shape for the internal heat gains was also taken from this metering project based on the "Other" end-use load shape (Figure 29). The magnitude and pattern of the "Other" loads change seasonally as shown. In the GridLAB-D simulations, the season was assumed to correspond to the calendar quarters.

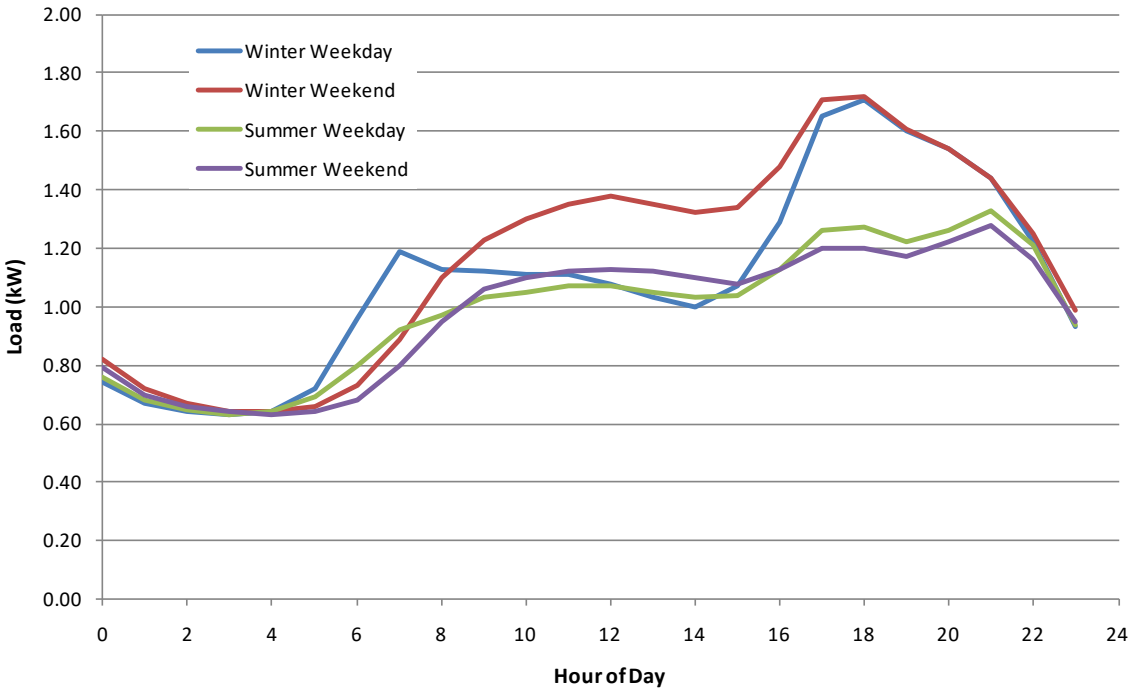

Figure 29. Average load shape for internal heat gains in residences.

The average internal gains load shape for any given residence is then defined as the product of two dimensionless scalar multipliers and the average load shape

$$\text{Internal\_gains(hr)} = S_{\text{random}}\, S_{\text{floor area}}\, \text{Load\_shape(hr)} \quad (8)$$

Then, the scaling factor for the floor area is

$$S_{\text{floor area}} = \text{Other} / \text{Mean(Load\_shape)} \quad (9)$$
$$= 324.9\ (\text{floor\_area})^{0.442}\ 1000 / 8760 / \text{Mean(Load\_shape)}$$

The random scaling factor (S_{random}) was then varied from a value of 1.0 by $\pm$20% to create further randomized diversity in the internal heat gains.

In the GridLAB-D simulations, 50% of the heat gains from the appliances were delivered directly to the air inside the home and 50% emanated from the mass. (100% of the heating or cooling supplied by the HVAC system was delivered to the air.)

6.4 Set Points for HVAC Units

A combination of RECS data and assumptions were used to determine heating and cooling set points for HVAC units. Each house was assumed to have a maximum of four set-point preferences in one day for the following periods:

1. Morning time occupied represents the time of the day prior to occupants leaving for work or school
2. Day time unoccupied represents the daytime hours when nobody is consistently in the residence.

3. Evening time occupied represents when a typical work or school day is over and the residence is occupied again, it is considered to be the same as the morning set point
4. Nighttime occupied represents when people are in the home, different from the morning and evening occupied set points.

The RECS data directly report the winter and summer indoor temperatures for the daytime when someone is home, daytime when no one is home, and nighttime. No specific times are provided along with these data. The original survey data for each of the RECS set-point categories for the winter space heating portion of the year were recorded in bins with unbounded extremities:

- 63 degrees or less
- 64 to 66 degrees
- 67 to 69 degrees
- 70 degrees
- 71 to 73 degrees
- 74 degrees or more
- Does not use heating equipment.

For the purpose of determining winter set points, the responses were evenly distributed to whole degrees within the RECS bins and the unbound extremities were bounded to be the same size as most of the other temperature bins. Table 30 and Figure 30 show the distribution of setpoints for the three times outlined by RECS. The data supports a reasonable assumption that during winter the set point is lower while the home is unoccupied and relatively higher while people are home.

Table 30. RECS survey data on residential occupant winter thermostat set points.

Indoor Temp	Daytime Occupied	Daytime Unoccupied	Nightime
61	1.0%	4.8%	2.4%
62	1.0%	4.8%	2.4%
63	1.0%	4.8%	2.4%
64	1.4%	5.8%	4.1%
65	1.4%	5.8%	4.1%
66	1.4%	5.8%	4.1%
67	6.8%	7.0%	7.2%
68	6.8%	7.0%	7.2%
69	6.8%	7.0%	7.2%
70	18.8%	15.9%	18.1%
71	6.8%	4.1%	5.1%
72	6.8%	4.1%	5.1%
73	6.8%	4.1%	5.1%
74	9.7%	5.1%	7.0%
75	9.7%	5.1%	7.0%
76	9.7%	5.1%	7.0%
Did not use	3.6%	3.6%	3.6%

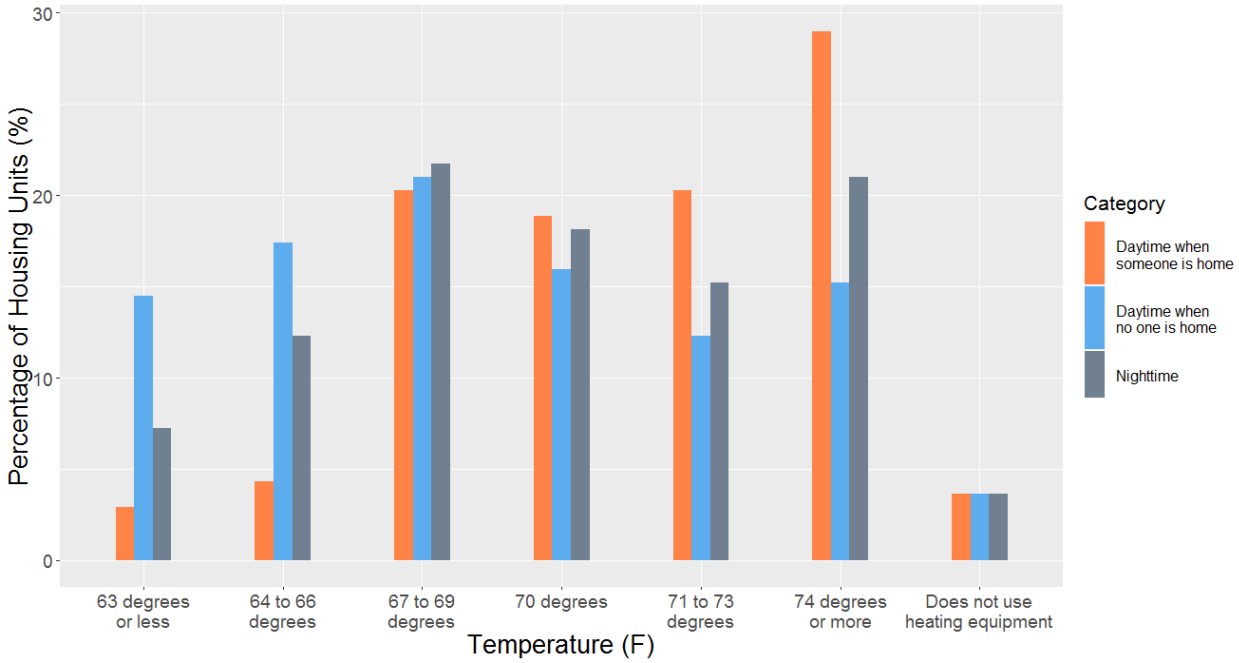

Figure 30. Distribution of residential occupant winter thermostat set points.

The same process was done to interpret the summer set-point data from RECS. It should be noted that the set-point values differ between the space heating and cooling data. The original survey data for each of the RECS set-point categories for the summer space cooling portion of the year were recorded in bins with unbounded extremities:

- 69 degrees or less
- 70 degrees
- 71 to 73 degrees
- 74 to 76 degrees
- 77 to 79 degrees
- 80 degrees or more
- Does not use air conditioning equipment.

For the purpose of determining summer set points, the responses were evenly distributed to whole degrees within the RECS bins and the unbound extremities were bounded to be the same size as most of the other temperature bins. Table 31 and Figure 31 show the distribution of set points for the three times outlined by RECS. Again the data support the expectation that the summer set points for unoccupied times would be relatively higher than the occupied set points.

Table 31. RECS data on residential occupant summer thermostat set points.

Indoor Temp	Daytime Occupied	Daytime Unoccupied	Nighttime
67	3.6%	2.2%	6%
68	3.6%	2.2%	6%
69	3.6%	2.2%	6%
70	14.5%	13.0%	17%
71	6.8%	3.4%	6.5%
72	6.8%	3.4%	6.5%
73	6.8%	3.4%	6.5%
74	9.2%	8.9%	8.5%
75	9.2%	8.9%	8.5%
76	9.2%	8.9%	8.5%
77	5.6%	6.5%	3.9%
78	5.6%	6.5%	3.9%
79	5.6%	6.5%	3.9%
80	1.7%	6.5%	1.2%
81	1.7%	6.5%	1.2%
82	1.7%	6.5%	1.2%
Did not use	4.3%	4.3%	4.3%

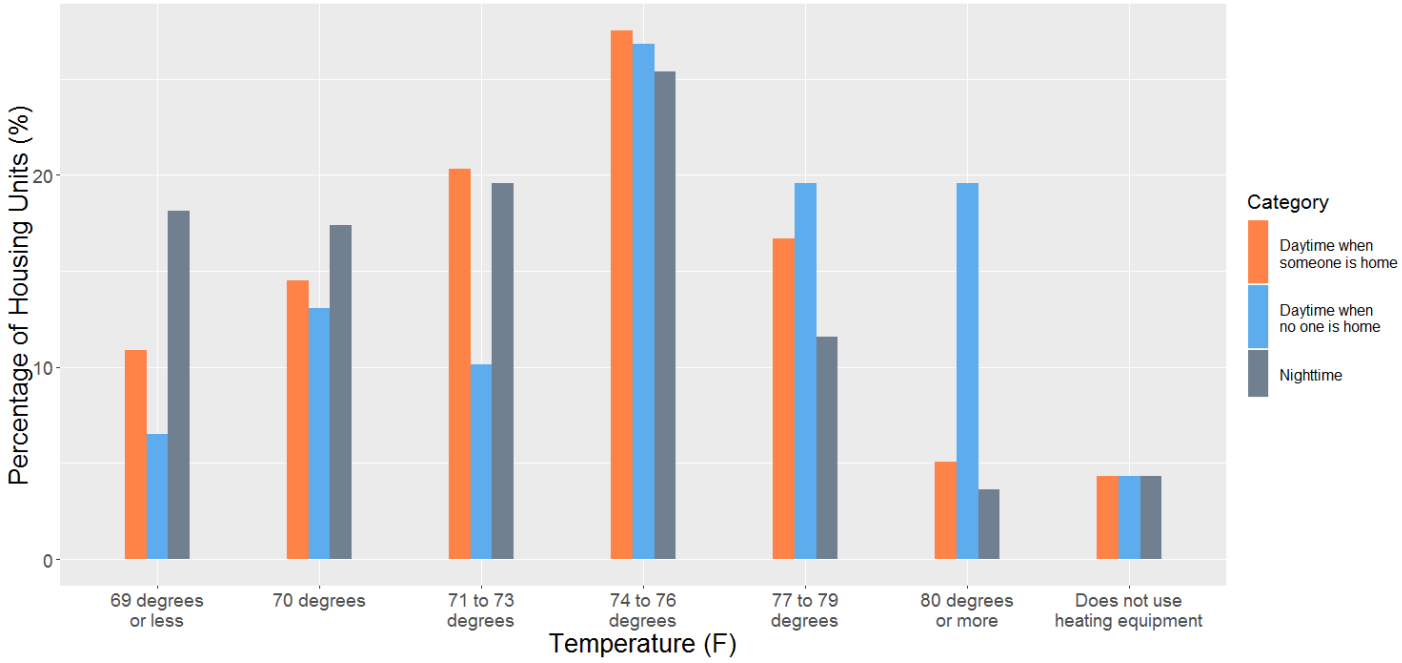

Figure 31. Distribution of residential occupant summer thermostat set points.

Using the percentages outlined above to instantiate residential set points would result in an accurate modeling of the residential population as an aggregate but may not necessarily be a reasonable instantiation of any individual residence. For example, it likely would not be realistic to model a residence with a summer set point of 74 degrees while occupied and 70 degrees while unoccupied. In order to avoid this a procedure was put in place for distributing the set points for individual houses in all the time categories. The format of the data for space heating and cooling is identical, so the procedure is identical for both datasets.

First a random draw is taken from the distribution of temperature values for when someone is home during the day. This value is taken to be the ideal temperature. Then a random draw is

taken from the daytime when no one is home temperatures, which has been partitioned into subset distributions. The subsets were created to track behaviors of individual respondents. For each temperature reported in the daytime when someone is home category, there is a corresponding distribution for the daytime when no one is home data. For example, if there were 23 temperatures reported in the daytime when someone is home microdata for space heating, 23 distributions were generated for the daytime when no one is home category.

Then a random draw is taken from the nighttime temperatures, which has been partitioned into subset distributions. The subsets were created to track behaviors of individual respondents. For each temperature combination possible for the daytime when someone is home and daytime when no one is home, there is a corresponding distribution for the nighttime data. For example, if there were 55 unique combinations of daytime when someone is home and daytime when no one is home temperatures, there would be 55 nighttime distributions.

Furthermore, the following checks and adjustments are also being applied to each house set points scheduling:

- Ensure that daytime cooling set point when no one is home is never lower than when someone is home.
- Ensure that daytime heating set point when no one is home is never more than when someone is home.
- Ensure that the highest heating set point throughout the day is always lower than the lowest cooling set point by margin of 3°F, performed to avoid simultaneous heating and cooling in the same day.

A summary of the average weekaday cooling and heating setpoints for a population of 100 residential buildings is shown in Figure 32.

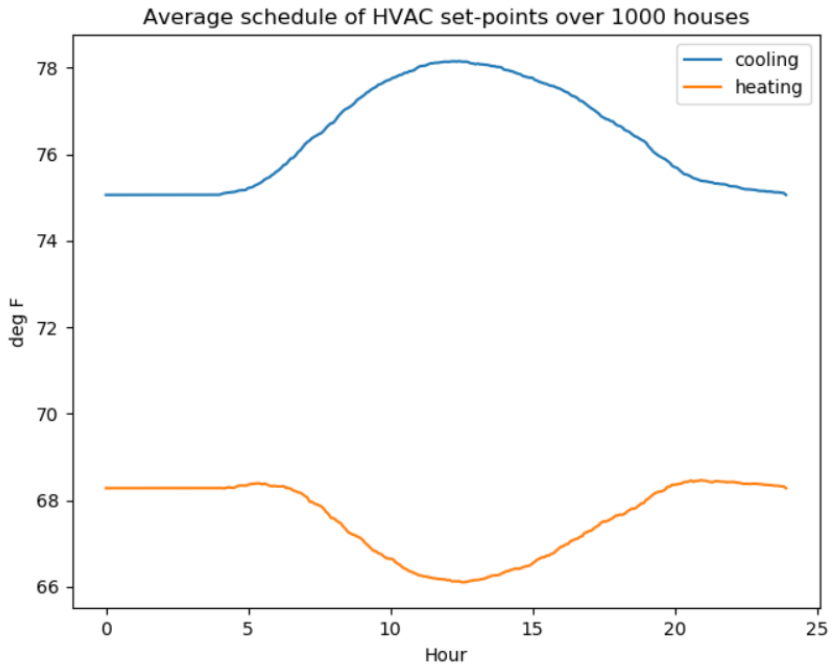

Figure 32. Example average heating and cooling set-point schedules for a population of residential buildings.

6.5 Determining HVAC Equipment Parameters

6.5.1 Residential HVAC Unit Performance

The efficiency of an air conditioner is rated by its energy efficiency ratio (EER), the ratio of its cooling output to its power input. Furthermore, efficiency standards for air conditioners are based on a seasonal average EER rather than a single condition. Air conditioner efficiencies have steadily increased during the past 30 years due to improved appliance standards (Figure 33). Therefore, the HVAC unit efficiency is based on the age of the unit and associated energy efficiency standards at the year of purchase. The seasonal EER performance rating was based on shipment and efficiency data provided in Navigant (2015). Air conditioning and heat pump units are assumed to be upgraded on an 18-year lifecycle. Therefore, for houses built in the last 18 years, the efficiency is based on performance standards in effect at the year of construction. For older houses it is assumed that the HVAC unit would have gone through one or more replacement cycles. For example, a house constructed in 2000 would have an air condition with 2018 performance, and a 1980 house would have an air conditioner with 2016 performance. Finally, a Gaussian random distribution of with a standard deviation of ±10% was applied to all resulting coefficient of performance values.

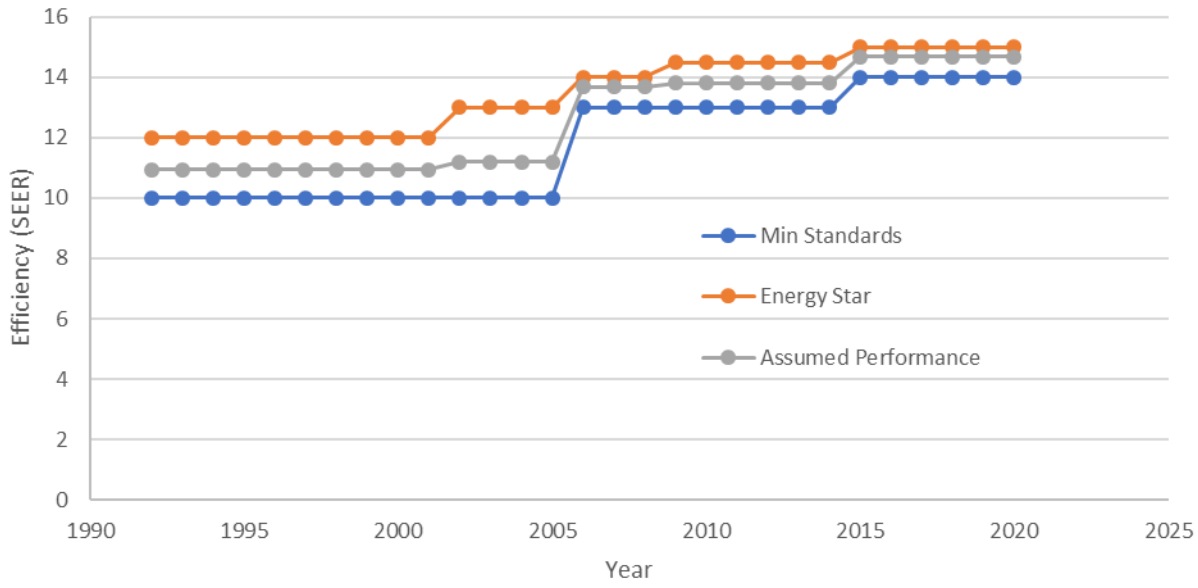

Figure 33. Shipment-weighted assumed residential air conditioning performance (Navigant 2015).

The GridLAB-D simulation uses the dimensionless coefficient of performance (COP) instead of EER to indicate air conditioner efficiency. This distribution of seasonal EERs was converted to COPs and used in the simulations. To estimate distribution, we assumed that a heat pump's heating and cooling EERs are approximately equal.

The oversizing of air conditioning units is an important feature that impacts the cycling and pulldown capability of the unit. Oversizing is based on the work of James et al. (1997), who investigated 368 recently built Florida homes and found over 50% of the homes had installed systems with a cooling capacity greater than 120% of their maximum cooling load. Based on

this, a Gaussian distribution was used with an average oversizing factor of 1.23 (with a standard deviation of 0.108) bounded at values of 1 and 1.6.

6.5.2 Prevalence of Electric Heating

2015 RECS data were used to determine the prevalence of homes that used electricity to provide space heating. In this study, electric heating is considered a function of DSO region type (urban, suburban, and rural) rather than the building type. For this particular use of RECS data only the West South Census Division was included rather than the entire South Region. The West South Census Division only includes the states of TX, OK, AR, and LA. This building characteristic was believed to differ significantly enough between this division and the other divisions within the South Region to justify using a smaller sample of data for this instantiation assumption with the outcome being a more realistic assumption for the ERCOT system. The data show that 48%, 38%, and 36% of urban, suburban, and rural homes, respectively, use electricity as their main space heating fuel. RECS data also conclude that 19%, 24%, and 31% of urban, suburban and, rural homes use heat pumps for heating. The remaining electric heating homes are considered as resistance heating in GridLAB-D.

6.6 Determining Water Heater Parameters

Although the 2015 RECS data did not include specifics on the water heater tank, sizing based on number of occupants is used as shown in Table 32. The number of occupants for each home are decided based on the floor area of the house. For each family size category, the tank size is randomly selected from five uniformly distributed discrete size bins within the corresponding range. The tank overall heat transfer rate is uniformly distributed in a range from 2–4 Btu and the heating element rating is distributed between 3–6 kW. The tank set point is distributed between 110–126°F. There are 12 water demand schedules prepared, six each for small and large water demand. Based on the home size (Table 31), a randomly selected schedule from small and large schedules is attached to the water heater.

Table 32. Residential water heater sizing guide based on floor area and number of occupants.

Family Size	Floor Area Range (sq.ft.)	Gallon Capacity Range	Water Demand Type
1-2 people	0-1000	30-50	Small
2-3 people	1000-2000	40-50	Small
3-4 people	2000-4000	40-75	Large
5+ people	4000-10000	50-75	Large

6.6.1 Prevalence of Gas Water Heating

In this study, the same fuel source is assumed for both HVAC and water heater. Every home has either gas or electric; therefore, the gas water heater prevalence is considered same as HVAC gas prevalence.

7.0 Commercial Buildings

This section describes how a random population of commercial buildings is instantiated for each DSO's region. The primary independent parameters defining the building population composition and characteristics of each individual building are the region of the country (in this case the West South Central Census division), the DSO type (urban, suburban, or rural), and the ASHRAE climate zone of the DSO. The following subsections describe how the overall building population was determined and how the form factor, thermal properties, internal gains schedule, and HVAC properties of each building were defined. The vast majority of commercial buildings were less than 10,000 sq. ft. and were instantiated using the single-zone GridLAB-D house object. Buildings over 10,000 sq. ft. were represented using multizone models comprised of multiple GridLAB-D house objects. The final subsection provides more details on this approach.

7.1 Determining Building Type and Vintage

The overall prevalence of various commercial building types was determined by using the 2012 Commercial Building Energy Consumption Survey (CBECS) dataset (DOE-EIA 2012). The more than 50 principal building activity subcategories reported by CBECS were consolidated into the 11 building types presented in Table 33. Where possible the raw CBECS survey data and weightings were used to generate the parameter data in this study. This process used the most granular CBECS data available, provided the associated survey micro data included sample sizes of at least 20 buildings for summation characteristics and 100 buildings for characteristic splits. For example, if the West South Central Census division provided sufficient samples it was used, if not the South Census region or complete U.S. dataset were used.

Table 33 shows the resulting prevalence of building type. The split by DSO type (urban, suburban, and rural) was based on the total commercial customer counts of these DSOs from ERCOT data. The distribution of building types within each DSO is assumed to be identical except that large offices and inpatient healthcare (hospitals) are only present in urban regions.

Finally, CBECS data were used to determine the likelihood that a building fell within a certain vintage (Table 33). When instantiating the population, a vintage bin was randomly selected based on its probability and a year of construction was then randomly selected from within that range using a uniform distribution. Figure 34 show an example building age distribution.

Table 33. Summary of commercial building attributes by building type.

Building Type	Building Prevalence				Vintage	Total Area	Ceiling Height (Floor-to-floor)	No. Stories	Aspect Ratio	Window-Wall Ratio	Wall Construction	Roof Construction	Ventilation req.		Interior/exterior Shading Coefficient
	Total	Urban	Sub.	Rural	[<1960, 1960-1979, 1980-1999, 2000-2009, 2010-2015]	1000 sq. ft. [1-5 5-10 10-25 25-50 >50]	(ft)	[% 1 2 3 4 … 14 15-25 >25]	-	%	[Mass Wall, Metal Building, Steel-frame, Wood-frame]	[Insulation above deck, Attic & other]	CFM/ft2	Air Changes / hour	% Awnings
	98.90%	71.2%	15.6%	13.2%											
Office, Large (> 50,000 sq. ft.)	0.7%	0.70%	0%	0%	Custom	Custom	13	Custom	1.5	40%	[42% 17% 24% 17%]	[28% 72%]	0.1	0.46	31%
Office, Medimum/Small (<50,000 sq ft)	20.2%	14.4%	3.2%	2.7%	[21% 17% 36% 22% 3%]	[65% 18% 10% 7% 0%]	13	[79% 18%]	1.5	33%	[32% 29% 20% 20%]	[16% 84%]	0.1	0.46	34%
Warehouse and Storage	16.1%	11.5%	2.5%	2.1%	[8% 15% 45% 31% 0%	[67% 12% 10% 3% 8%]	28	[95% 4%]	2.2	0.7%	[14% 78% 4% 4%]	[11% 89%]	0.052	0.11	17%
Big box	23.6%	16.8%	3.7%	3.1%	[20% 25% 33% 20% 2%]	[52% 25% 17% 4% 3%]	20	[85% 13%]	1.28	7%	[37% 39% 12% 12%]	[19% 81%]	0.28	0.84	51%
Strip	1.8%	1.28%	0.28%	0.24%	[0% 53% 21% 26% 0%]	[9% 45% 1% 16% 29%]	17	[83% 17%]	4	11%	[62% 13% 13% 13%]	[43% 57%]	0.3	1.06	100%
Education	7.4%	5.3%	1.15%	0.98%	[16% 21% 49% 12% 2%]	[36% 14% 18% 14% 18%]	13	[75% 17%]	1.4	33%	[34% 28% 19% 19%]	[11% 89%]	0.53	2.45	24%
Food Service	6.1%	4.3%	0.95%	0.81%	[17% 23% 46% 15% 0%]	[71% 20% 8% 0% 0%]	10	[83% 17%]	1	17%	[27% 23% 25% 25%]	[13% 87%]	1.04	6.24	57%
Food Sales	3.6%	2.56%	0.56%	0.48%	[0% 25% 56% 11% 7%]	[78% 14% 4% 4% 0%]	20	[86% 14%]	1.28	7%	[48% 18% 17% 17%]	[22% 78%]	0.28	0.84	47%
Lodging	3.1%	2.21%	0.48%	0.41%	[10% 25% 49% 13% 4%]	[23% 22% 23% 18% 14%]	11	[62% 10%]	3	11%	[42% 13% 18% 18% 18%]	[7% 93%]	0.13	0.71	14%
Heathcare Inpatient	0.2%	0.20%	0.00%	0.00%	[14% 41% 23% 9% 12%]	[0% 0% 4% 15% 81%]	14	Custom	1.31	16%	[42% 15% 25% 15%]	[49% 51%]	0.18	0.77	43%
Low Occupancy	16.1%	11.46%	2.51%	2.13%	[35% 23% 32% 9% 2%]	[48% 26% 13% 7% 5%]	14	[82% 15%]	1.5	33%	[44% 20% 18% 18%]	[5% 95%]	0.052	0.22	25%

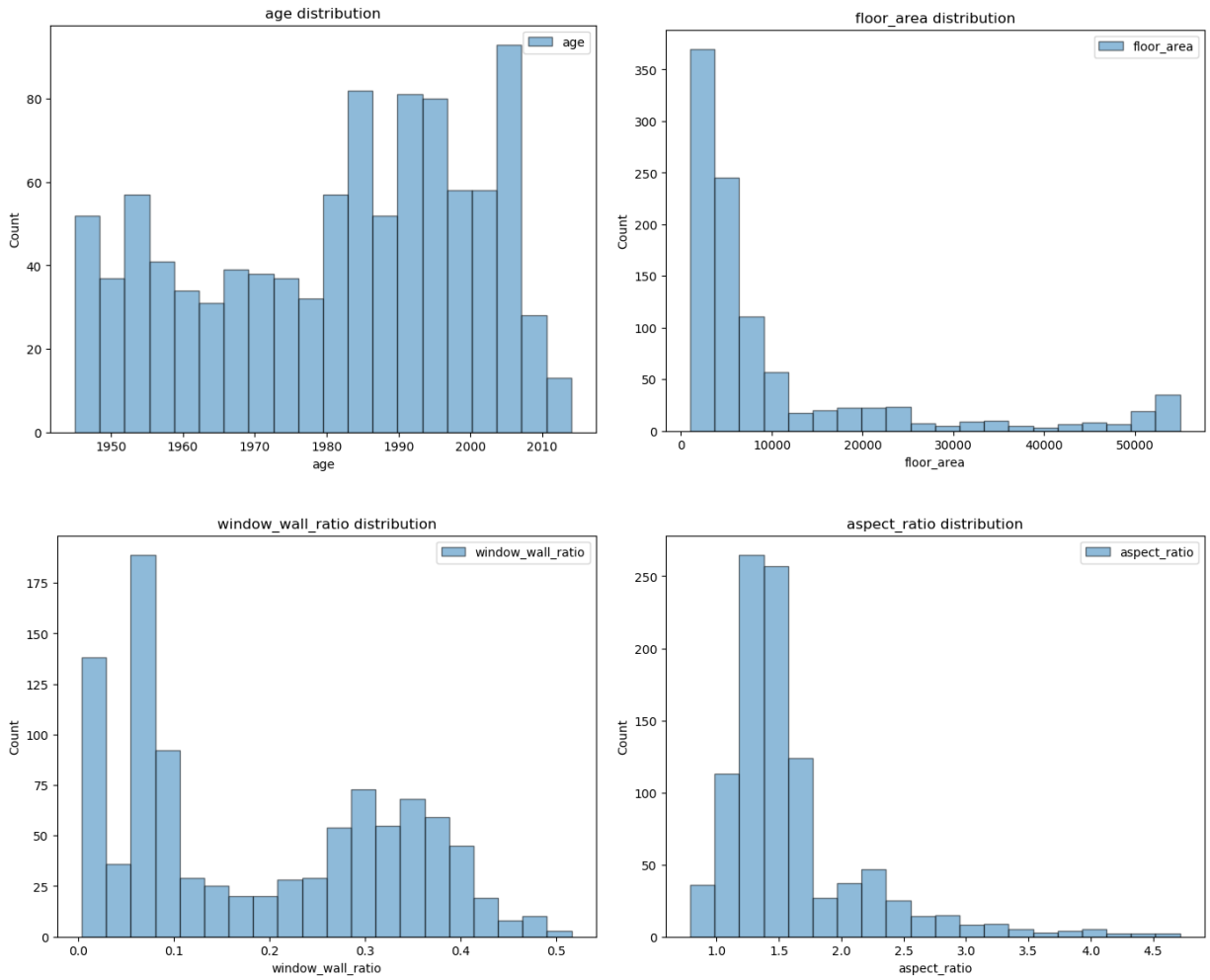

Figure 34. Example distributions of building age, floor area, window-wall ratio, and aspect ratio for a population of 1,000 commercial buildings on a suburban DSO.

7.2 Determining Building Form Factor

The building form is defined by five key variables: gross floor area, floor height, number of stories, aspect ratio, and window-to-wall ratio. These values were informed by the 2012 CBECS as well as the DOE reference building definitions (Deru et al. 2011). Summary values are provided in Table 32. The floor height was kept constant for each respective building type based on the reference building definitions, while the aspect ratio and window-to-wall ratio were randomly varied around mean values from the reference model buildings with a Gaussian distribution and standard distributions of 10% and 20% respectively. Since the majority of buildings surveyed only had one or two floors, the model performs a discrete random choice of one or two floors based on the likelihood by building type. Finally, the total floor area is determined by randomly selecting an area bin and then randomly selecting a floor area within that bin assuming a uniform distribution. Example distributions of 1,000 commercial buildings on a suburban DSO are shown in Figure 33. Note that the instantiation strategy for larger buildings (>10,000 sq. ft.) did alter some parameters. More details are provided in Section 7.6.

7.3 Determining Building Thermal Properties

7.3.1 Envelope

The modeled thermal envelope performance of the commercial buildings is a function of vintage, construction type, and ASHRAE climate zone. Summary values are provided in Table 34, Table 35, Table 36, and Table 37. For buildings constructed after 1999, Texas building energy codes were used to estimate the nominal envelope performance (Texas Comptroller, n.d.). The 2000 International Energy Conservation Code (IECC) was adopted in 2001, the 2009 IECC was adopted in 2011 and the 2015 IECC was adopted in 2016. The 2009 IECC values for wall, roof, and window performance are assumed for buildings constructed between 2010-2015. While not present in the CBECS 2012 dataset, the 2015 IECC can be used for buildings constructed after 2015. For simplicity 2000 IECC compliance is modeled by using the post-1980 values provided in Deru et al. (2011) as they follow ASHRAE Standard 90.1-1989, an approved method to meet the 2000 IECC. Note that 90.1-1989 only had one prescribed U-value for "light-weight" walls so all wall types except mass walls have identical values.

Prior to 2000, Texas did not have mandatory statewide energy codes and instead the parametric models developed by Briggs et al. (1987, Appendix C) were used. This work assumed that building walls "built prior to 1960 were built based on uninsulated, structural masonry wall assemblies." Buildings built after 1980 were assumed to meet ASHRAE 90.1P (a simplification for the more cumbersome 90A-1980). Interpolation was used for dates between 1960 and 1980. Briggs et al. calibrated these models to billing data, which indicated the original assumptions overstated the difference between vintages and were corrected. A similar approach was used for roof U-values interpolating between values for 1946, 1975, and 1988.

For this work we assume that values prior to 1960 are an average or 1946 and 1975, the values for 1960-1979 use the 1975 equation (based on ASHRAE 90-75), and the 1980-1999 values use the 1988 value (ASHRAE 90.1P). Similar assumptions were made for window U-values. Finally, the SHGC parametric model was developed by Briggs et al. (1987, Appendix C) as a function of building age and size. The relationship of SHCG as a function of building size was implemented by Briggs et al. to reflect that "*the use of tinted and reflected glass was assumed to be more extensive in… large buildings than in small buildings.*" This relationship was not directly implemented as it gives nonphysical values for larger buildings (i.e.,100,000 sq. ft.) Therefore, an average size of 20,000 sq. ft. was assumed for the values used.

The values from these various sources are generally self-consistent and monotonically improving over time; however, for some reference city and climate zone combinations the U-values can have local minima. This is due to some sources being parametrically based on heating and cooling degree days for reference cities rather than averaged for a climate zone. Also, the construction types used in the standards above do not always have a one-to-one mapping with the construction types reported by the CBECS. To address this the mappings provided in Deru et al. (2011, Tables 15 and 16) were used. It was assumed that an equal weighting was applied when a CBECS construction type mapped to multiple building code construction types. The construction method distribution by building type is provided in Table 32. Gaussian distributions with a standard deviation of 10% where applied to R-wall and R-roof values. A 5% standard deviation was applied to SHGC and R-window values.

Table 34. Roof U-values as a function of climate zone, vintage, and construction type.

ROOF U-Value (BTU/hr-sqft-F)				Pre 1960	1960-1979	1980-1999	2000-2009	2010-2015		After 2015	
Location			90.1-2004 Climate Zone	All Types				Insulation entirely above deck	Attic and Other	Insulation entirely above deck	Attic and Other
Miami	FL	1A	0.20	0.100	0.072	0.074	0.063	0.034	0.048	0.027
Houston	TX	2A	0.20	0.100	0.067	0.066	0.048	0.027	0.039	0.027
Phoenix	AZ	2B	0.20	0.100	0.041	0.046				
Atlanta	GA	3A	0.20	0.100	0.068	0.072	0.048	0.027	0.039	0.027
Los Angles	CA	3B-CA	0.20	0.100		0.100				
Las Vegas	NV	3B-other	0.20	0.100	0.054	0.048				
San Francisco	CA	3C	0.19	0.100		0.088				
Baltimore	MD	4A	0.17	0.086	0.061	0.058	0.048	0.027	0.032	0.027
Albuquerque	NM	4B	0.16	0.089	0.066	0.059				
Seattle	WA	4C	0.16	0.085	0.072	0.064	0.048	0.027	0.032	0.027
Chicago	IL	5A	0.13	0.072	0.056	0.053				
Denver	CO	5B	0.12	0.076	0.057	0.051				
Minneapolis	MN	6A	0.08	0.060	0.047	0.045	0.048	0.027	0.032	0.021
Helena	MT	6B	0.08	0.060	0.049	0.049				
Duluth	MN	7	0.08	0.060	0.045	0.040	0.039	0.027	0.028	0.021
Fairbanks	AK	8	0.08	0.060	0.033	0.031	0.039	0.027	0.028	0.021

Table 35. Wall U-values as a function of climate zone, vintage, and construction type.

WALLS - Above Grade U-Value (BTU/hr-sqft-F)				Pre 1960	1960-1979	1980-1999	2000-2009				2010-2015				After 2015			
Location			90.1-2004 Climate Zone	All Types			Mass Wall	Metal Building	Steel Framed	Wood Framed	Mass Wall	Metal Building	Steel Framed	Wood Framed	Mass Wall	Metal Building	Steel Framed	Wood Framed
Miami	FL	1A	0.230	0.230	0.230	1	1.000	1	1	0.58	0.093	0.124	0.089	0.151	0.079	0.077	0.064
Houston	TX	2A	0.230	0.230	0.230	0.34	0.150	0.15	0.15	0.151	0.093	0.124	0.089	0.151	0.079	0.077	0.064
Phoenix	AZ	2B	0.230	0.230	0.230	0.41	0.240	0.24	0.24								
Atlanta	GA	3A	0.227	0.225	0.223	0.29	0.130	0.13	0.13	0.123	0.084	0.084	0.089	0.123	0.079	0.064	0.064
Los Angles	CA	3B-CA	0.230	0.230	0.230	1	0.220	0.22	0.22								
Las Vegas	NV	3B-other	0.230	0.230	0.230	0.29	0.160	0.16	0.16								
San Francisco	CA	3C	0.226	0.224	0.223	0.49	0.130	0.13	0.13								
Baltimore	MD	4A	0.204	0.191	0.178	0.12	0.089	0.089	0.089	0.104	0.084	0.64	0.089	0.104	0.052	0.064	0.064
Albuquerque	NM	4B	0.197	0.181	0.165	0.19	0.100	0.1	0.1								
Seattle	WA	4C	0.197	0.180	0.163	0.1	0.092	0.092	0.092	0.09	0.069	0.064	0.064	0.09	0.052	0.064	0.064
Chicago	IL	5A	0.186	0.164	0.141	0.1	0.082	0.082	0.082								
Denver	CO	5B	0.184	0.161	0.138	0.14	0.082	0.082	0.082								
Minneapolis	MN	6A	0.173	0.145	0.117	0.071	0.065	0.065	0.065	0.08	0.069	0.064	0.051	0.08	0.52	0.064	0.051
Helena	MT	6B	0.173	0.145	0.116	0.079	0.072	0.072	0.072								
Duluth	MN	7	0.169	0.139	0.108	0.061	0.058	0.058	0.058	0.071	0.057	0.064	0.051	0.071	0.52	0.064	0.051
Fairbanks	AK	8	0.160	0.125	0.090	0.047	0.045	0.045	0.045	0.071	0.057	0.064	0.036	0.061	0.52	0.045	0.036

Table 36. Window U-values as a function of climate zone and vintage.

WINDOW U-Value (BTU/hr-sqft-F)	Location		90.1-2004 Climate Zone	Pre 1960	1960-1979	1980-1999	2000-2009	2010-2015	After 2015
	Miami	FL	1A	1.13	1.22	1.22	1.22	1.2	0.5
	Houston	TX	2A	1.13	1.22	1.22	1.22	0.75	0.5
	Phoenix	AZ	2B	1.13	1.22	1.22	1.22		
	Atlanta	GA	3A	1.13	1.22	1.22	0.72	0.65	0.46
	Los Angles	CA	3B-CA	1.13	1.22	1.22	1.22		
	Las Vegas	NV	3B-other	1.13	1.22	1.22	1.22		
	San Francisco	CA	3C	1.13	1.22	0.62	0.72		
	Baltimore	MD	4A	1.13	1.22	0.62	0.59	0.55	0.38
	Albuquerque	NM	4B	1.13	1.22	0.62	0.72		
	Seattle	WA	4C	1.13	1.22	0.62	0.72	0.55	0.38
	Chicago	IL	5A	0.83	0.62	0.52	0.59		
	Denver	CO	5B	0.83	0.62	0.52	0.59		
	Minneapolis	MN	6A	0.83	0.62	0.52	0.52	0.55	0.36
	Helena	MT	6B	0.78	0.52	0.32	0.52		
	Duluth	MN	7	0.78	0.52	0.32	0.52	0.45	0.29
	Fairbanks	AK	8	0.78	0.52	0.32	0.52	0.45	0.29

Table 37. Window SHGC as a function of climate zone and vintage.

WINDOW - SHGC (-)	Location		90.1-2004 Climate Zone	Pre 1960	1960-1979	1980-1999	2000-2009	2010-2015	After 2015
	Miami	FL	1A	0.495	0.310	0.218	0.25	0.25	0.25
	Houston	TX	2A	0.495	0.345	0.269	0.25	0.25	0.25
	Phoenix	AZ	2B	0.495	0.310	0.218	0.25		
	Atlanta	GA	3A	0.495	0.385	0.330	0.25	0.25	0.25
	Los Angles	CA	3B-CA				0.44		
	Las Vegas	NV	3B-other	0.495	0.354	0.284	0.25		
	San Francisco	CA	3C				0.39		
	Baltimore	MD	4A	0.495	0.387	0.333	0.36	0.4	0.4
	Albuquerque	NM	4B	0.495	0.407	0.363	0.36		
	Seattle	WA	4C	0.495	0.430	0.397	0.39	0.4	0.4
	Chicago	IL	5A	0.495	0.407	0.363	0.39		
	Denver	CO	5B	0.495	0.415	0.374	0.39		
	Minneapolis	MN	6A	0.495	0.415	0.374	0.39	0.4	0.4
	Helena	MT	6B	0.495	0.423	0.388	0.39		
	Duluth	MN	7	0.495	0.428	0.395	0.49	0.45	0.45
	Fairbanks	AK	8	0.495	0.434	0.403	NR	0.45	0.45

While the above sources address window SHGC factors, they do not account for the additional contribution of internal or external shading. For this we assume that the percentage of buildings with shading is equal to the percentage of buildings that report having awnings in the CBECS micro data (Table 32). Based on a review of modeling of awnings and window treatments performed by Lawrence Berkeley National Laboratory (Kohler et al. 2017; Curcija et al. 2013), buildings with shading are then considered to have a median 50% reduction in SHGC values with a random Gaussian distribution with standard deviation of 10 percentage points. Finally, building ventilation rates are based on the average values for the DOE reference buildings (Table 32). No additional infiltration is assumed and GridLAB-D default values are assumed for door and floor U-values. Example distributions are shown in Figure 35.

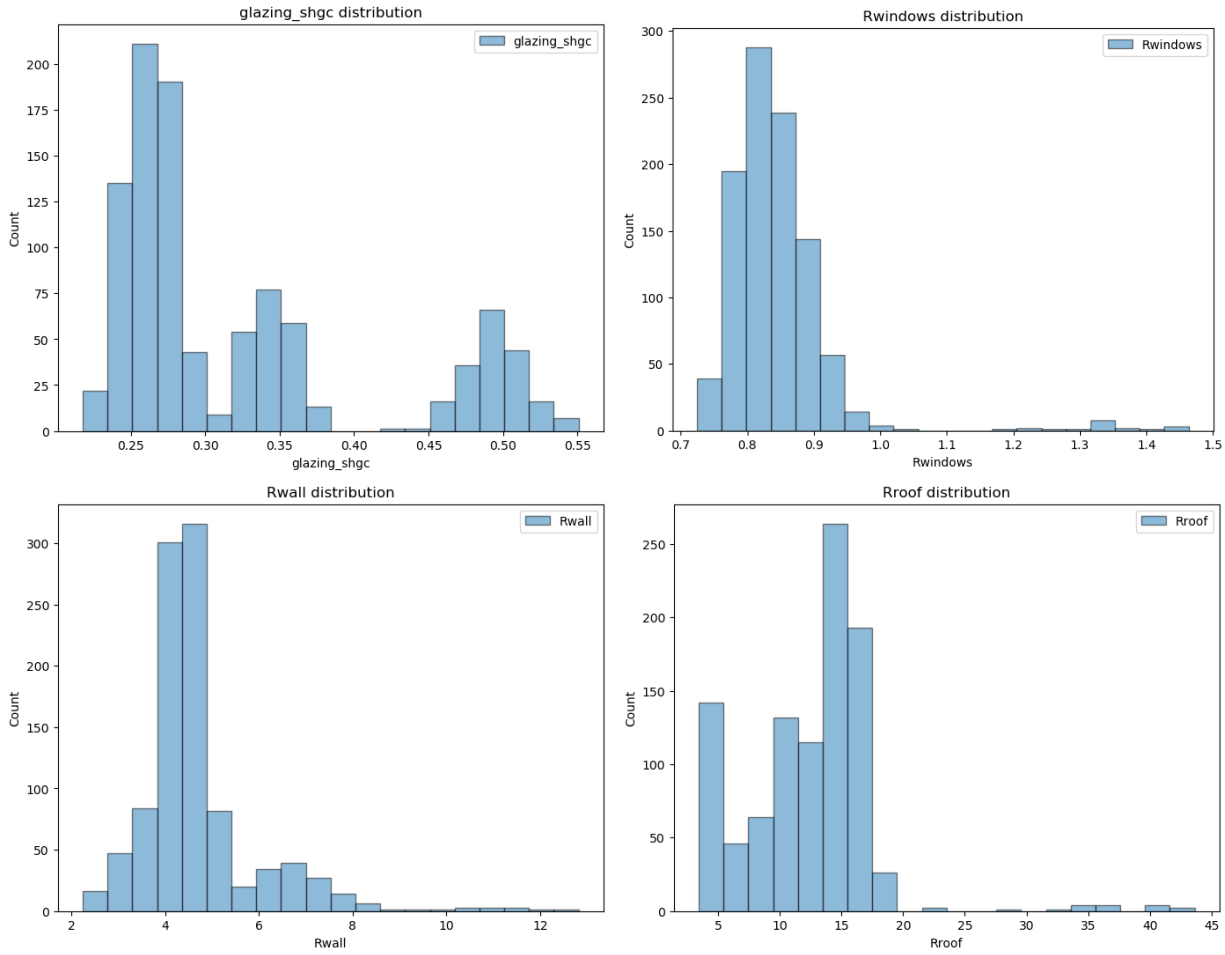

Figure 35. Example distributions of window SHGCs (-) and thermal resistance (R-values; h·ft^2 ºF/Btu) for windows, walls, and roofs for a population of 1,000 commercial buildings on a suburban DSO in ASHRAE Climate Zone 2A.

7.3.2 Thermal Mass and Heat Transfer

The internal thermal mass of a building and its associated heat transfer coefficient are critical parameters influencing the building's ability to provide flexibility in load demand via the HVAC system. Unfortunately the range of values typical in commercial buildings has not been well studied with much of the work to date focused on parametric modeling investigations (Johra and

Heiselberg 2017a). To verify commonly used assumptions, Johra et al. (2017b) surveyed the contents of 12 residential and office rooms in Denmark. This determined values in the range of 10–100 kgs/m^2 of net floor area and did not include the thermal mass of internal structural elements such as walls. They then calculated an effective thermal capacity of approximately 13–45 kJ/K.m^2 (0.73, 1.5, 2.2 BTU/F-ft^2). This work also used the following parametric estimates for light, medium, and heavy wall construction: 30, 55, 100 Wh/K.m^2 (5.3, 9.7, and 17.6 BTU/F-ft^2). These were slightly higher than the values calculated by Briggs et al. (1987) based on wall material properties by year of construction (13.6 BTU/F-ft^2 prior to 1947, 8.9 BTU/F-ft^2 in 1970, and 4.6 BTU/F-ft^2 for 1985 and after) and the code cutoff for mass walls (>5-7 BTU/F-ft^2).

Based on the values above it was assumed that the internal thermal mass (M_{Int}) had a mean value of 1.5 BTU/F-ft^2 and standard deviation of 0.2 BTU/F-ft^2. To this was added the wall thermal mass (M_{Ext}) as a function of perimeter and window-to-wall ratio. The wall thermal mass was assumed to be a linear interpolation of the values provided in Briggs et al. (1987) for values between 1947 and 1985 and held constant outside those years. Because only a portion of the exterior wall's thermal mass is thermally coupled to the interior zone temperature only a fraction (F=0.5) is applied. Therefore, the total thermal mass of the building is calculated as:

$$M_T = 0.9\, M_{Int} + R.F.M_{Ext} \quad (10)$$

Where F is the assumed fraction of the wall thermal mass that is coupled to the interior zone temperature. A factor of 0.9 is applied to correct for the difference in interior and gross floor area. R is the ratio of exterior wall area (excluding windows) to floor area as defined by:

$$R = \frac{A_{Wall}(1 - WWR)}{A_{Floor}} \quad (11)$$

Where A_{Wall} is the area of the wall envelope, *WWR* is the window-to-wall ratio, and A_{Floor} is the gross floor area of the building. The wall area can be calculated from building form factors as follows:

$$A_{Wall} = 2.h_{floor}\sqrt{\frac{A_{Floor}}{R_{Aspect}}}.\left(R_{Aspect} - 1\right) \quad (12)$$

Where h_{floor} is the floor-to-floor height of the building and R_{Aspect} is the building's floorplan aspect ratio. The resulting distribution of the total thermal mass per floor area is shown in Figure 36. The values are generally consistent with prior unpublished PNNL studies that used a nominal value of 3.9 Btu/^{o}F-ft^2 which was varied randomly over a range of $\pm$50% as well as the default GridLAB-D value of 3.5 Btu/^{o}F-ft^2 (GridLAB-D 2017).

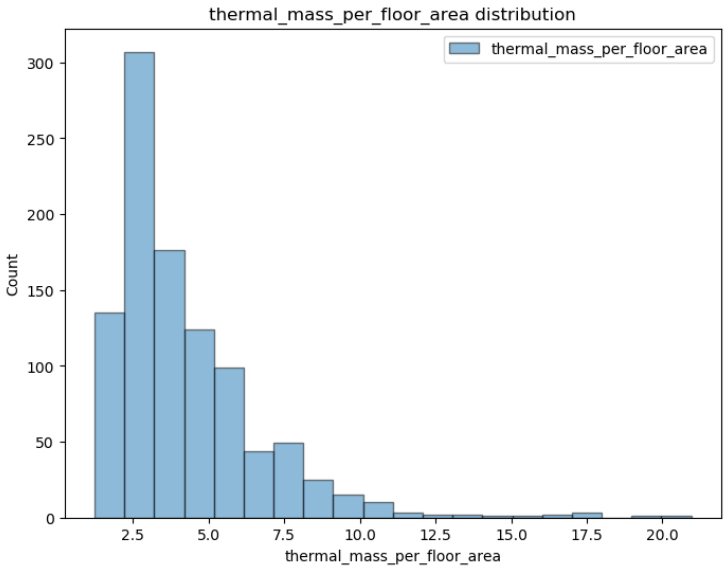

Figure 36. Example distribution of total thermal mass per floor area (BTU/F-ft^2) for a population of 1,000 commercial buildings.

7.4 Determining Building Schedules and Internal Gains

The building occupancy schedules were informed by the distribution of hours buildings were open per week as reported in CBECS 2012 data. The average operating hours per week as well as the average schedule for each building type are shown in Table 38.

Table 38. Summary of percent of time buildings are occupied and internal gains loads.

						Internal Gains			
Building Type	Open 24/7	Mean Occupancy	Modeled Occupancy	Plug Load Ratio	Lighting Load Ratio	Lighting W/ft2	Large Refrigeration W/ft2	Plug/MEL Loads W/ft2	Occupancy Occ / ft2
Office, Large (> 50,000 sq. ft.)	8%	28%	30%	56%	31%	1.01	0.00	1.44	0.00
Office, Medimum/Small (<50,000 sq ft)	8%	28%	30%	56%	31%	1.01	0.00	1.44	0.01
Warehouse and Storage	19%	24%	30%	56%	31%	0.78	0.00	0.81	0.00
Big box	5%	30%	50%	65%	38%	1.16	0.00	1.29	0.02
Strip	15%	31%	50%	65%	38%	1.01	0.00	2.00	0.01
Education	4%	27%	30%	56%	31%	0.57	0.00	1.09	0.03
Food Service	4%	42%	50%	65%	38%	0.90	2.09	3.96	0.05
Food Sales	21%	52%	50%	65%	38%	1.07	3.94	1.43	0.02
Lodging	89%	-	100%	100%	100%	0.23	0.00	1.14	0.01
Heathcare Inpatient	100%	-	100%	100%	100%	0.56	0.00	1.61	0.00
Low Occupancy	2%	13%	17%	52%	27%	0.18	0.00	0.44	0.03
1) Mean and modeled occupancy levels exclude buildings that are open 24/7									
2) Load ratio is the ratio of occupied load levels to annual average levels									
3) All internal gains values are for occupied periods except large refrigeration which is 24/7									

Summary data of the weekly occupancy level and internal gains are also shown in Table 37. CBECS reports the number of buildings that are open 24/7. This percentage was assigned an ‘always occupied’ schedule with no setbacks. All lodging and healthcare inpatient buildings were assumed to be always occupied. Then for each building type the mean percent of time that the buildings were in use per week was calculated excluding always occupied buildings. Based on these results the building types were split into three occupancy schedules: ‘office’ for building types that had occupancy rates less than 30% and were assumed to have lower use on the weekend (this included office, warehouse, and education building types); retail, for buildings

with occupancy greater than 30% and assumed to have identical use on the weekends as during the week (this included big box, strip mall, food service, and food sales);and a 'low occupancy' schedule specifically for the low occupancy building type. The normalized load profile shapes used for the lighting and plug loads profile are shown in Figure 37. Only office schedules had a different operation on the weekends. The ratios of occupied and unoccupied loads are based on the field measurements of Taylor and Pratt (1989). Finally, to ensure a distribution of schedules the start time of each building was varied to start up to 1.5 hours before the base schedule.

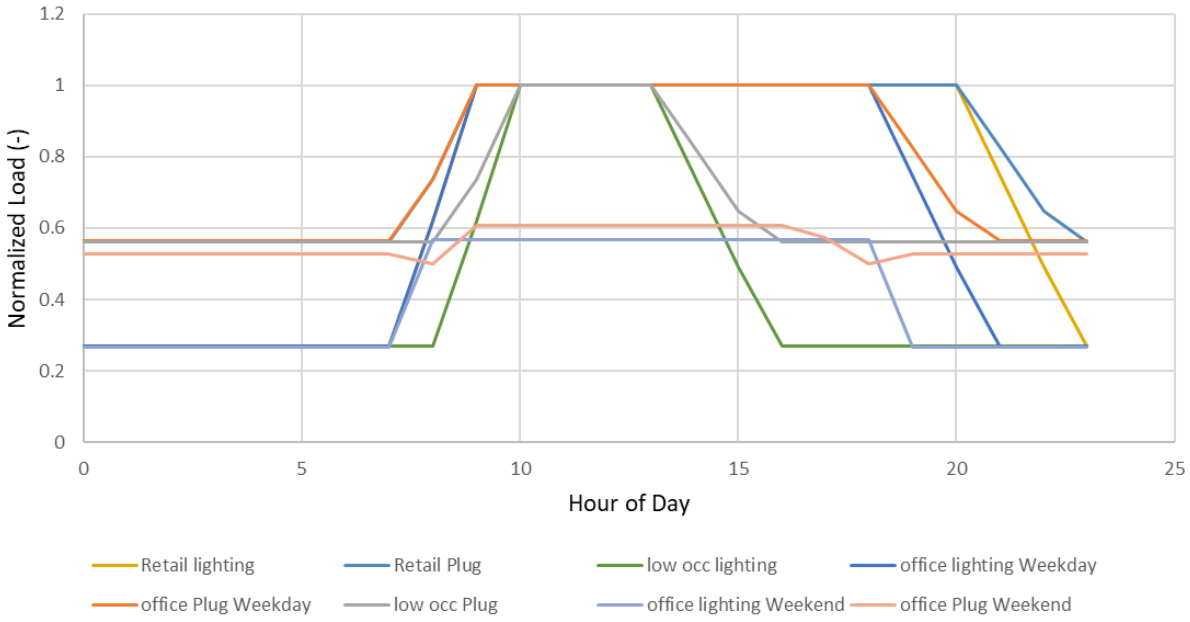

Figure 37. Example normalized internal load schedules.

These normalized load shapes are multiplied by the building type relevant internal gains loads shown in Table 37. The lighting, miscellaneous electric loads, and refrigeration loads are all based on estimates provided by the CBECS for annual average energy usage intensity. These values are scaled from an annual average value to the peak occupied value using the following equation:

$$Load_{occ} = \frac{Load_{Ave}}{\left(f_{occ} + R_{\frac{occ}{un}} - f_{occ}R_{\frac{occ}{un}}\right)} \quad (13)$$

Where f_{occ} is the fraction of the time where the building is occupied and $R_{occ/un}$ is the ratio of load values between occupied and unoccupied periods.

The thermostat set points were considered the same for all buildings with heating set points of 70°F occupied and 60°F unoccupied and summer setpoints of 75°F occupied and 80°F unoccupied. The occupied period for the HVAC system was identical to the load shape shown in Figure 36 for the loads.

Food sale and food service buildings reported in the CBECS contain a nontrivial number of major refrigeration systems and walk-in coolers. Since these consume electrical base load but have heat rejected directly to the ambient (and not contribute to internal gains) these major

refrigeration loads were accounted for separately in the analysis and considered to be independent of occupancy. The minor refrigeration loads of the other building types were lumped into the plug load and miscellaneous electric load category and varied in value with occupancy status.

The occupancy density is based on the DOE reference building definitions and the heat gains from the occupants were assumed to be 250 Btu/hr (73 W) each. All internal loads (occupancy, lighting, miscellaneous electric load, and refrigeration) are randomly varied with a Gaussian distribution and standard deviation of 10%.

7.5 Determining HVAC Equipment Parameters

7.5.1 Packaged HVAC Unit Parameters

The majority of building types are assumed to have their cooling loads served by packaged rooftop HVAC units. Efficiency is based on the age of the unit. Prior to 2010 the seasonal EER performance was assumed to be an extrapolation of Air Conditioning, Heating, and Refrigeration Institute (AHRI) data (Hart et al. 2008). More recent AHRI statistics that provided seasonal EER values could not be found, so it was assumed that units shipped since then meet the minimum EER requirement for their respective size weighted by shipping volumes. The efficiency of heat pump operation was assumed to be the same as that of cooling operation based on the similarity of values reported by DOE-EIA (2018, Appendix A). A random Gaussian distribution with a standard deviation of 5% was applied to all COP values. As shown in Figure 38, COP was calculated from seasonal EER using the following equation:

$$COP = 0.3796*SEER-0.0076*SEER^2 \quad (14)$$

It should be noted that GridLAB-D automatically adjusts unit efficiency and capacity as a function of ambient air temperature.

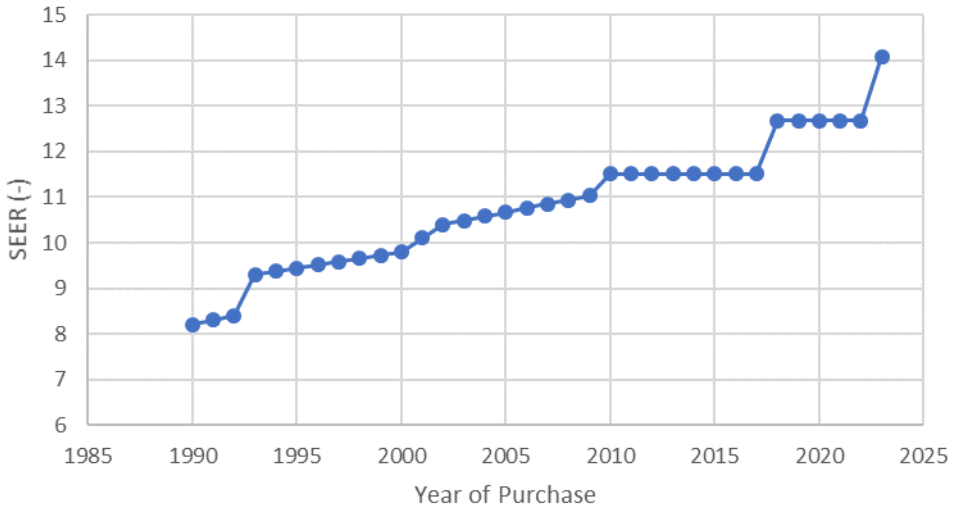

Figure 38. Assumed seasonal EER value as a function of rooftop terminal unit (RTU) age.

The efficiency of the RTU fleet will be affected by the unit age distribution. There are a number of published estimates of average RTU lifetime. Northeast Energy Efficiency Partnerships

(NEEP 2014) established a weighted-average lifetime of 20.6 years, whereas EIA (Navigant 2018) assumes a lifetime of 21 years and DOE has used 18.4 years in proposed rulemaking (DOE-EERE 2014). We have assumed an average RTU life of 20 years. As such buildings constructed since 1999 have RTUs with performance consistent with the year of construction. Buildings older than that are assumed to have upgraded units on a 20-year refresh cycle.

The oversizing of RTUs is an important feature that impacts the cycling and pulldown capability of the unit. Felts and Bailey (2000) found in a field survey of 250 RTUs that slightly less than 40% where correctly sized for peak load conditions, 20% where no more than 25% oversized, and 10% being more than 50% oversized. Based on this description, the median oversizing is assumed to be 20% with a standard deviation of 20% and limits on the distribution of 0% and 60% oversizing. Examples of RTU COP and oversizing distributions are shown in Figure 39.

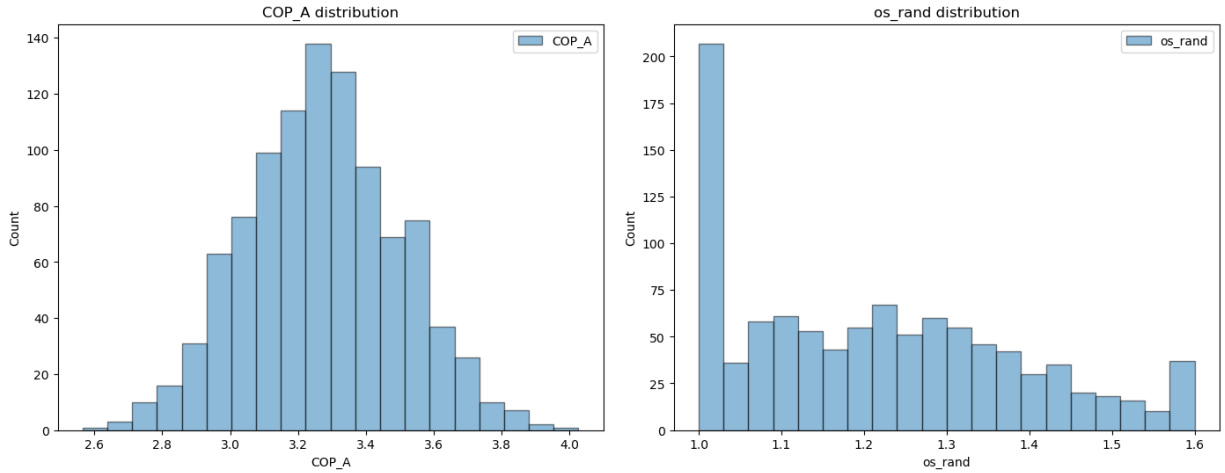

Figure 39. Example distributions of rooftop unit COP and oversizing factor for a distribution of buildings.

7.5.2 Prevalence of Electric Heating

The number of buildings that primarily used electricity for heating was based on 2012 CBECS data by building type. Furthermore, it was assumed that commercial buildings in rural locations (which is assumed to be 13% of the population) have half the rate of non-electric primary heating sources than urban and suburban locations. This assumption is based on the reported gas heating rates for residential buildings in urban, suburban, and rural locations. The prevalence of heat pumps (versus resistive electric heating) was also based on CBECS reported data. This information is summarized in Table 39.

Table 39. Summary of electric heating prevalence and types.

	Primary Electric Heating				Electric Heating System Type
Building Type	Total	Urban	Suburban	Rural	[Heat Pump Resistance]
Office, Large (>50,000 ft^2)	46%	46%	–	–	[20% 80%]
Office, Medium/Small	46%	42%	42%	71%	[20% 80%]
Warehouse and Storage	18%	12%	12%	56%	[22% 78%]
Big Box	32%	27%	27%	64%	[22% 78%]
Strip	39%	35%	35%	67%	[0% 100%]
Education	51%	48%	48%	74%	[8% 92%]

Building Type	Primary Electric Heating				Electric Heating System Type
	Total	Urban	Suburban	Rural	[Heat Pump Resistance]
Food Service	50%	46%	46%	73%	[6% 94%]
Food Sales	67%	65%	65%	82%	[0% 100%]
Lodging	63%	60%	60%	80%	[40% 60%]
Healthcare Inpatient	29%	29%	–	–	[31% 69%]
Low Occupancy	35%	30%	30%	65%	[20% 80%]
Weighted Average	**38%**	**33%**	**33%**	**65%**	**-**

7.6 Definition of Larger Multizone Commercial Buildings

7.6.1 GridLAB-D Treatment of Larger Commercial Buildings

Commercial buildings larger than 10,000 sq. ft. are subdivided into multiple zones, each of which is treated as a GridLAB-D house object with appropriately adjusted interior to exterior wall ratios for each zone. The approaches used below are based on the treatment of office buildings and big box stores used in prior studies (Fuller et al. 2012, Appendix B.2.2).

For commercial buildings between 10,000 and 30,000 sq. ft. of gross floor area, a prototypical six-zone building with an aspect ratio of 1.28 was simulated. The floor plan of the building is illustrated in Figure 40. The loads for all six zones were combined as one customer meter and account. Each zone was thermally independent, corresponding to an assumption that single-zone packaged HVAC units supply conditioned air for each zone, with no mixing of return air. All other building parameters were calculated as described in the above sections and are identical for all zones in the building.

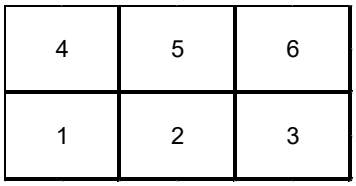

Figure 40. Floor plan of commercial buildings between 10,000 and 30,000 sq. ft.

For commercial buildings larger than 30,000 sq. ft. (but excluding large offices and hospitals), a three-story, fifteen-zone office building with an aspect ratio of 1.5 was simulated. The floor plan of the prototypical building is shown in Figure 41. The loads for all fifteen zones were combined as one customer meter and account. Each zone was thermally independent, corresponding to an assumption that single-zone packaged HVAC units supply conditioned air for each zone, with no mixing of return air.

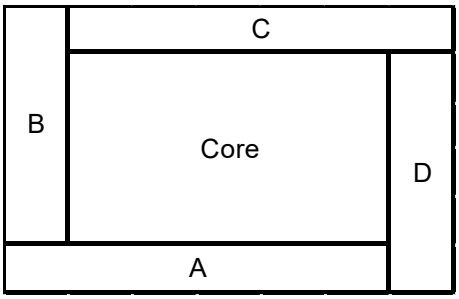

Figure 41. Floor plan of commercial buildings over 30,000 sq. ft.

8.0 Summary of Building Load Results

This section presents total system and building load results for the MR BAU case and compares them to actual ERCOT load profiles and expected values. Ultimately the goal of this comparison is to illustrate how well the simulation can capture overall system load values, load shapes, and contributions by load type and customer class. Annual simulations were run for both 200-bus and 8-bus configurations of the model. For the 8-bus model, the simulation contained 11,929 buildings (11,190 residential and 739 commercial), 13,162 HVAC units, and 7,325 water heaters, representing a 1:952 scale (and hence the weighting factor) of the ERCOT system. For the 200-bus model, the simulation contained 63,729 buildings (58,453 residential and 5,273 commercial), 73,704 HVAC units, and 36,624 water heaters, representing a 1:172 scale of the ERCOT system. Overall load profiles were similar between both models. The results presented here are for the 200 bus model unless otherwise stated.

8.1 Load Demand by End-Use and Device

Example load profiles (by end-load type) are shown in Figure 42 for the weeks with maximum and minimum actual ERCOT loads.

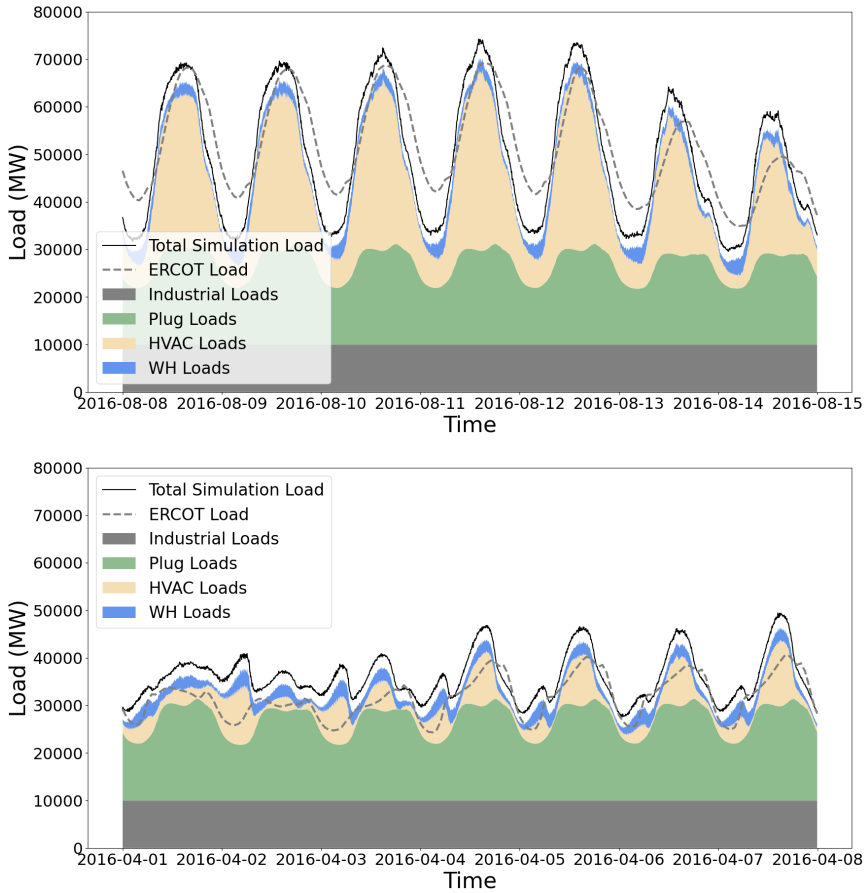

Figure 42. System load contributions by end use for (a) peak load (top) and (b) minimum system load (bottom). Total simulation load (solid line) is shown in comparison to the actual load experienced in ERCOT (dotted line). (8-bus model.)

The overall system load compares well with the actual ERCOT peak load (summer) week but overpredicts the reduction in load at night. During the minimum load week (spring), the load shape is trend-wise accurate but overpredicted. As discussed in Section 5.4.1, the industrial load is assumed to be constant. The plug and miscellaneous electrical loads are based on predefined schedules with weekday and weekend dependence. The water heater load shape is primarily driven by assumed usage (water draw) profiles. Finally, the HVAC load is driven by ambient weather conditions and occupancy schedules. Annual end-load consumption is shown in Table 40. HVAC accounted for 24% of total annualized distribution system load (excluding losses) versus CBECS/RECS-based estimates of 29.6%, and residential water heating contributed 5.7% versus RECS-based estimates of 5.2%. (Note that the CBECS- and RECS-based values are based on West South Central Census Region data that is then corrected for building class contributions. For example, water heating is estimated by RECS to account for 12% of residential load in the region. Given that residential customers represent 43% of ERCOT load we would expect water heaters to present 5.2% of load not including distribution losses.)

Table 40. Summary of simulated end-use device number and loads (prior to system losses).

	Simulated		Scaled		Building Load	
Building Type	Number	%	Number	%	Load (MW-hr)	%
HVAC	73,704	66.8%	11,627,729	66.4%	64,605,889	23.6%
Water Heaters	36,624	33.2%	5,871,794	33.6%	15,507,344	5.7%
Plug Loads	-	-	-	-	130,873,225	47.7%
Industrial Loads	-	-	-	-	63,257,981	23.1%
Total	110,328	100%	17,499,523	100%	274,244,439	100%

8.2 Load Demand by Customer Class and Building Type

Figure 43 shows similar system load profile examples but broken out by customer class and building type. Table 41 shows that residential and commercial buildings loads compared well to ERCOT utility data in terms of both overall contributions and the average value per building. While utility data were not available for load factor (the ratio of building average load to peak load), the values are comparable (but higher) than those reported by (New et al. 2019) based on >170,000 buildings in Tennessee, with load factors of 0.23 versus 0.16 for residential buildings and 0.37 versus 0.27 for commercial buildings.

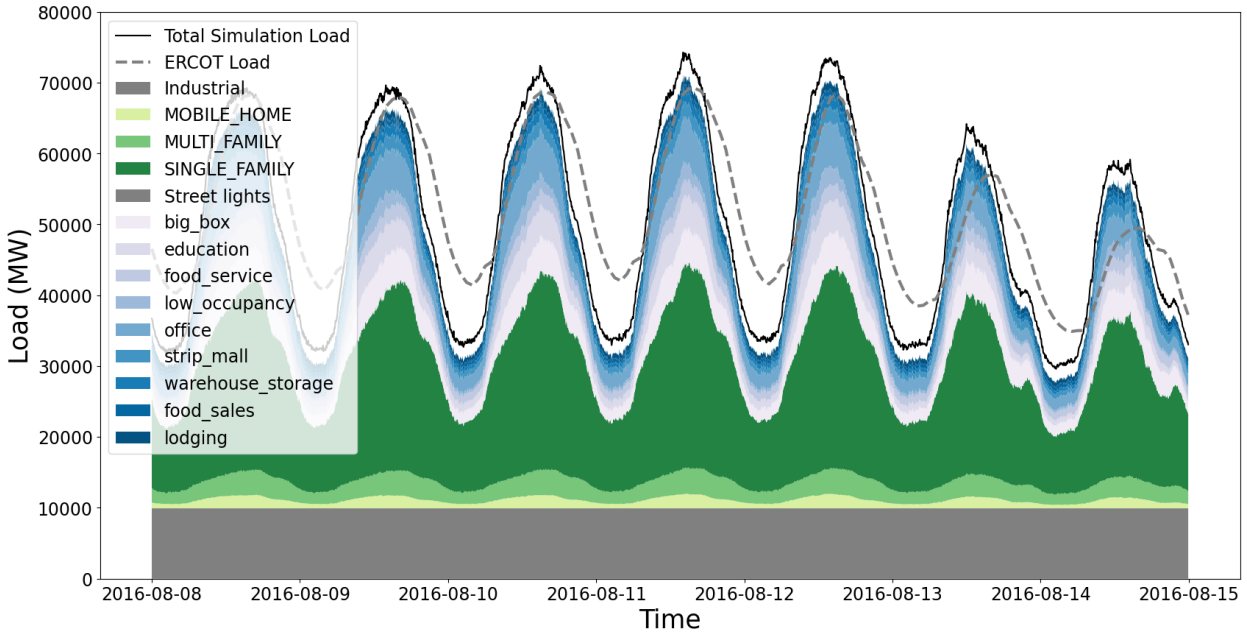

Figure 43. System demand by customer class (green for residential, blue for commercial, and gray for industrial) and building type for the week of peak load.

Table 41. Comparison of results by customer class.

	Residential			Commercial		
Statistic	Simulation	Actual	Diff (%)	Simulation	Actual	Diff (%)
End load (%)	45.2%	43.3%	4.4%	30.7%	31.2%	1.5%
Average load per Customer (kW)	1.73	1.59	8.9%	9.30	9.00	3.5%

Table 42 shows the number, proportion, and load by building type in the simulation before and after the weighting factors are applied. Residential buildings account for >90% of the customer buildings and >60% of the load (excluding industrial load). This is dominated by single-family homes (70% of the buildings and 50% of the load). Significantly more diversity in building type is seen in the commercial customers. The most prominent commercial building types are office buildings and bog-box retail buildings each representing 8-9% of non-industrial load.

Table 42. Summary of simulated building number and load by type and customer class.

		Simulated		Scaled		Building Load	
Customer Class	Building Type	Number	%	Number	%	Load (MW-hr)	%
Residential	Single Family	44,019	69.1%	7,496,214	70.7%	107,514,838	50.0%
	Mobile Home	4,485	7.0%	438,043	4.1%	5,464,985	2.5%
	Multifamily	9,949	15.6%	2,133,030	20.1%	17,992,707	8.4%
	Total	58,453	92%	10,067,287	95%	130,972,530	60.9%
Commercial	Office	1,074	1.7%	117,416	1.1%	16,509,851	7.7%
	Warehouse & Storage	898	1.4%	93,846	0.9%	8,173,540	3.8%
	Big Box	1,246	2.0%	128,967	1.2%	18,693,237	8.7%

		Simulated		Scaled		Building Load	
	Strip Mall	110	0.2%	12,520	0.1%	6,996,139	3.3%
	Education	395	0.6%	46,529	0.4%	11,184,126	5.2%
	Food Service	317	0.5%	28,821	0.3%	8,087,731	3.8%
	Food Sales	193	0.3%	17,770	0.2%	5,149,110	2.4%
	Lodging	152	0.2%	11,568	0.1%	4,241,945	2.0%
	Healthcare Inpatient	1	0.0%	201	0.0%	228,624	0.1%
	Low Occupancy	887	1.4%	82,450	0.8%	4,994,222	2.3%
	Total	5,273	8%	540,088	5%	84,258,525	39.1%
Total		63,726	-	10,607,375	-	215,231,055	-

8.3 Summary of Annual Load Demand

Summaries of load and daily change in load by month are provided in Figure 44 and an overall summary is provided in Table 43. This confirms that while the overall average load is accurately captured (within ~5% percent), the daily variation in load is overpredicted (on average by ~37%), and the minimum total load is overpredicted by ~10%.

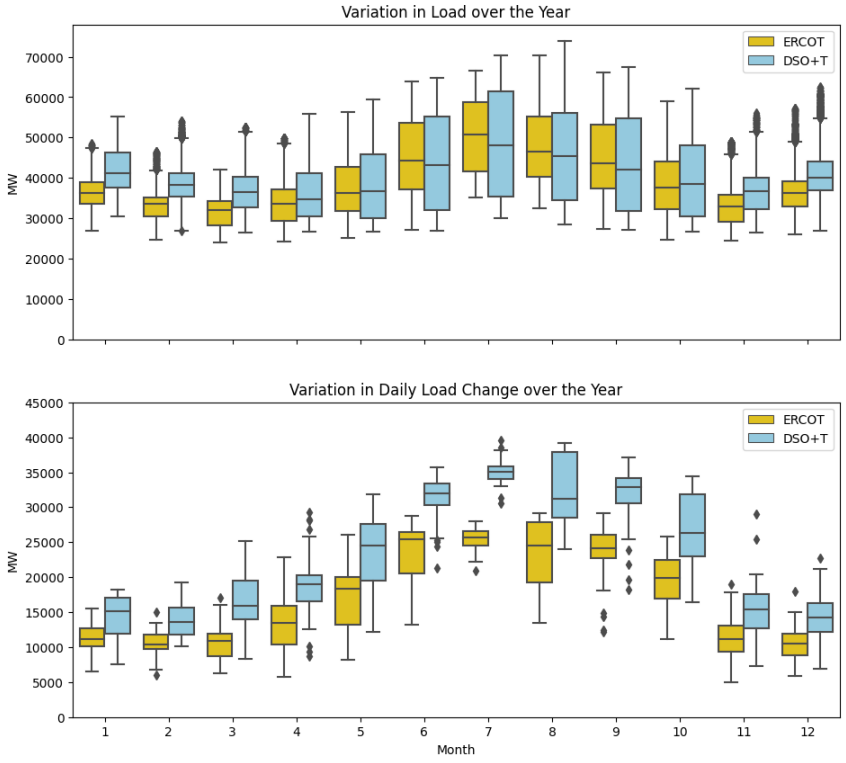

Figure 44. Comparison of system total load (top) and daily range in total load (bottom) between simulation (DSO+T) and actual (ERCOT).

Table 43. Comparison of the simulated grid load.

System Load (MW)	DSO+T	ERCOT	% Diff
Average	40,998	39,191	4.6%
Max	73,938	70,359	5.1%
Min	26,545	24,098	10.2%
Average daily range	23,049	16,795	37.2%
Max daily range	39,588	29,146	35.8%
Min daily range	6,861	5,036	36.2%

8.4 Discussion and Lessons Learned

8.4.1 Simulation Accuracy

The simulation results have two main inaccuracies: the overprediction of the daily load range (especially in the summer) and the overprediction of electric loads in the winter heating season. Work by NREL (Hale et al. 2018) has also overpredicted the daily swing. This suggests that the use of a higher fidelity simulation tool (e.g., EnergyPlus) or more detailed building survey data (ComStock and ResStock databases) would be unlikely to resolve this issue. The overprediction in the daily change in building load could be due to overly optimistic assumptions about the nighttime reduction of miscellaneous electric loads and building thermostat schedules. Lower diurnal variation of each of these would improve the agreement with actual loads. In addition, increased nighttime HVAC operation could be explained by a desire to address latent cooling rather than sensible cooling objectives. In addition, there are a number of building parameters that do not have well-characterized probability distributions in the literature that could contribute to this issue. These include infiltration and natural ventilation (including behavioral modeling of window opening rates), shading and its impact on solar loads, and accurate distributions of buildings' internal thermal mass and heat transfer coefficient.

The overprediction of winter loads likely arises from inaccuracies in estimating the proportion of homes with gas heat. Using calibration methods to fine-tune input parameters could address this. For example, changing the proportion of homes with gas heat from ~40% to ~60% reduced the average load error to less than 5% and minimum system load error to less than 10%. It also improved the average residential load error to 0.3%. However, this resulted in a substantial reduction in the load contribution from electric water heaters and HVAC, increasing the risk that their contribution to load flexibility would be underrepresented. Auto-calibration techniques could result in improved load shape accuracy at the risk of substantial losses in the contribution representativeness of end loads and customer classes. Prior work (Fuller et al. n.d.) has shown that detailed calibration of GridLAB-D building models with customer data can reduce load shape inaccuracies but still reported a >14% mean average percentage error.

8.4.1 Lessons Learned

Co-simulating dynamic building models with a full grid operation and market model can present unique requirements and challenges. First, care is required that all boundary conditions, operating inputs, and initialization values are sufficiently randomized and piecewise continuous in time. For example, a population-wide discontinuity in set-point temperature schedule between weekend and weekday operation can cause a large portion of the HVAC fleet to turn on at once, resulting in a large spike in system load. Such dynamic transients would typically be averaged out in energy efficiency modeling but can cause significant problems for grid operation.

Care is also needed when reconciling and normalizing data from various sources. For example, energy data from EIA are denominated per building, while utility data are denominated per customer. While these values are typically consistent for the residential market, they are not consistent for the commercial market, where data suggest more than two commercial customers per commercial building. If such discrepancies are not identified and harmonized, the overall loads and contributions of specific customer classes can be significantly over or underrepresented.

8.4.2 Future Research Needs

As building modeling continues to transition its focus from quasi-steady modeling of energy efficiency benefits to fully dynamic modeling to investigate advanced control solutions for grid interaction, further work is needed in three areas. First, an investigation is needed into identifying and resolving the overprediction of the daily change in system load. This load variation, most prominent in the summer, drives the need for electrical generation flexibility and the resulting variation in dynamic wholesale electric prices. Second, the variation of key building parameters that directly affect their dynamic response and the flexibility of end loads (such as building internal thermal mass) needs to be better characterized for the actual national building stock. Finally, an open and simulation tool-agnostic summary of building parameter distributions suitable to be adapted to different regions of the country and future scenarios would be of great value to the research community.

9.0 Battery Characteristics

This section documents the battery performance characteristics and underlying assumptions used for the battery case in the DSO+T study.

9.1 Battery Modeling

A battery is defined as a direct current electrochemical storage device. A storage system consists of a battery and an inverter. The battery model used here does not explicitly represent a specific battery chemistry, but rather is a generic energy storage device. Let the battery be rated by its (direct current) energy storage capacity, E_{bat} (kWh), and maximum charging (R^c) and discharging (R^d) power in kW. We assume that R^c and R^d are same for the battery. The capacity duration of battery at rated output, T_{bat} (hours) can be given as

$$T_{bat} = E_{bat}/R^c. \quad (15)$$

The inverter's rated power is assumed to be same as the battery rating. The battery is capable of storing energy (C) within the given maximum (C^{max}) and minimum (C^{min}) allowable amount of energy in kWh. The energy stored in the battery can be altered by the inverter, given its combined limitations of maximum charging (R^c) and discharging (R^d) rate in kW. The energy stored in the battery at any time t can be written as

$$C(t) = C(t-1) + E^{in}(t) \times \eta_{in} - E^{out}(t)/\eta_{out} \quad (16)$$

where $E^{in}(t)$ and $E^{out}(t)$ are the kWh energy flowing into (charging) and out (discharging) of the storage system at time t and are limited by the rating R^c and R^d. The efficiencies of the process of charging and discharging the storage system are represented by η_{in} and η_{out}. These efficiencies can be modeled as

$$\eta_{in} = (1 - L^{in}) \times \eta_{inv} \quad (17)$$

$$\eta_{out} = (1 - L^{out}) \times \eta_{inv} \quad (18)$$

where the battery losses are split as charging losses (L^{in}) and discharging losses (L^{out}) in percentage. Similarly, the inverter losses are modeled in terms of their efficiency, given as η_{inv}. Thus, the overall system roundtrip efficiency can be defined as

$$\eta = \eta_{in} \times \eta_{out}. \quad (19)$$

9.2 Battery Population Instantiation Strategy

In this study, a diverse population of battery systems are instantiated throughout the feeders with no more than 1 battery system per building. Residential buildings are selected randomly to have a battery system installed based on the target storage participation rate.

The Tesla PowerWall specifications were used as mean values to model the battery system (Tesla 2019) as shown in Table 44. Further, a range is assigned to create a uniform distribution of battery parameters to be able to instantiate a diverse battery population among the selected

buildings. There is no correlation assumed between the residential load and the installed battery capacity. All selected residential buildings are randomly assigned a battery system.

Table 44. Specifications to model and instantiate a population of residential battery systems.

Characteristics	Mean Value	Deviation Range
Capacity (kWh)	13.5	$\pm$ 20%
Battery rated charging power (R^c, kW)	5	$\pm$ 20%
Battery rated discharging power (R^d, kW)	Same as R^c	
Capacity (hours)	Calculated as Eq (15) – (mean: 2.7)	
Inverter Efficiency (%)	98	-
Battery charging efficiency ($1 - L^{in}$, %)	96	$\pm$ 3
Battery discharging efficiency ($1 - L^{out}$, %)	Same as L^{in}	
System Round Trip Efficiency (%)	Calculated as Eq (17)(18)(19) – (mean: 89)	
Battery minimum allowed state of charge (C^{min}, %)	100	-
Battery maximum allowed state of charge (C^{max}, %)	20	-

Commercial buildings used the same battery parameter definitions as above but the battery was sized to represent multiple batteries for larger buildings. One battery unit was assumed for every 10,000 sq. ft. (or portion of). For example, a 5,000 sq. ft. commercial building would have one battery unit (similar to a residential building), a 16,000 sq. ft. building would have a battery twice the size, etc.

10.0 Electric Vehicle Charging Characteristics

10.1 Availability and Usage Patterns

This study assumes that EVs are only available for charging and discharging when plugged in at a residential building. Therefore, EVs are not assumed to charge at commercial buildings or charge and discharge at more than one location. Residential car driving schedules are gathered from the 2017 National Household Travel Survey. These schedules are assumed to represent residential EV behavior. Each schedule consists of the parameters defined in Table 45.

Table 45. EV usage parameters.

Plug-in time	t_{in}	the latest time the EV arrives home
Plug-out time	t_{out}	the earliest time the EV leaves home
Plug-in duration	T_p	time elapsed between t_{in} and t_{out}
Miles traveled	d	daily total miles driven

Two histograms of t_{in} (arriving home) and t_{out} (leaving home) for residential EVs are shown in Figure 45. It can be observed that most EVs are available for charging and discharging between 6 p.m. and 7 a.m. Similarly, histograms of plug-in duration and miles traveled daily are shown in Figure 46 and Figure 47.

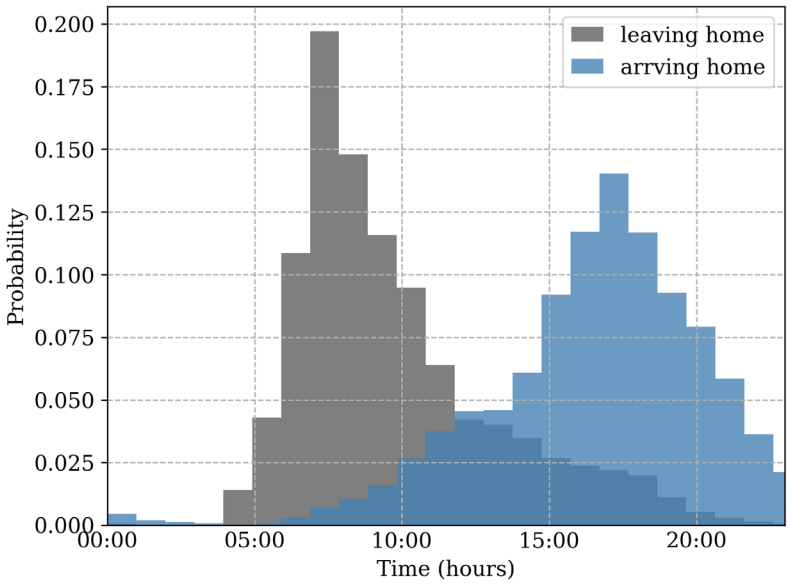

Figure 45. Histogram of arrival and departure hours of residential EVs from NHTS 2017 survey.

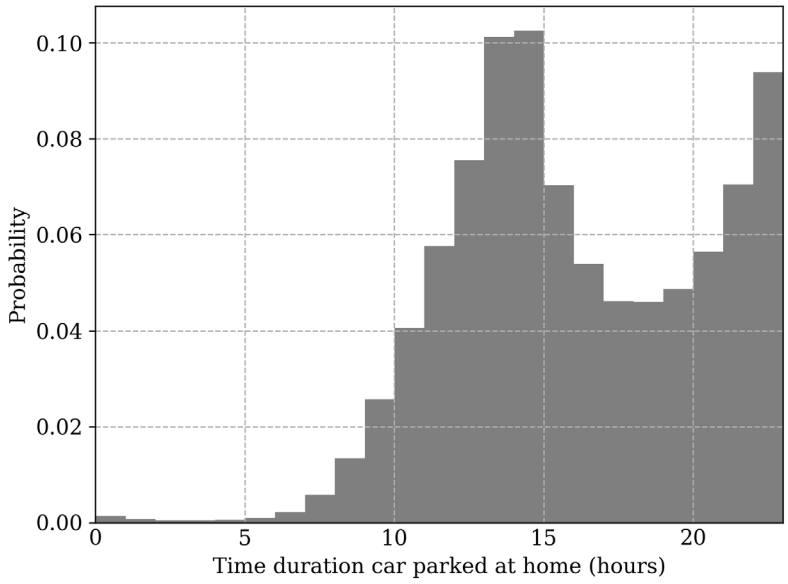

Figure 46. Histogram of EV availability duration for charging based on NHTS 2017 survey.

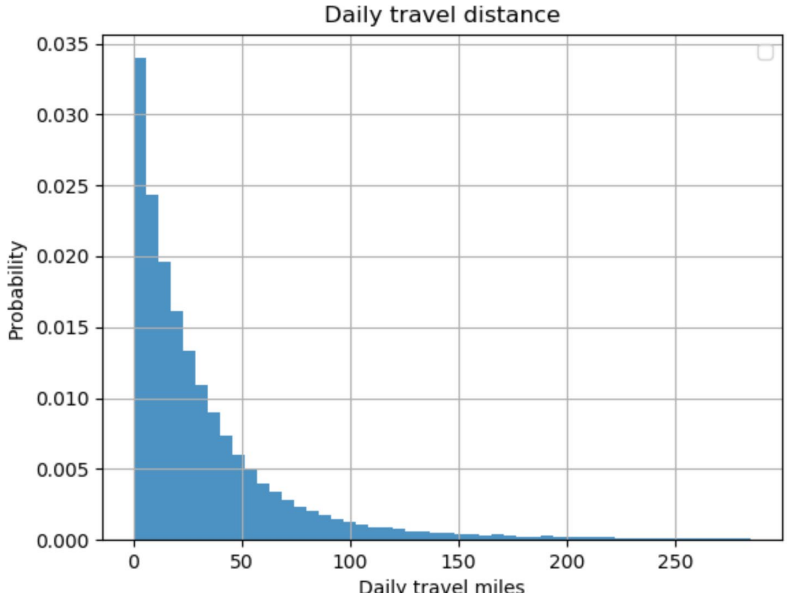

Figure 47. Histogram of miles traveled daily by residential EVs based on NHTS 2017 survey.

10.2 EV Device Model

10.2.1 Physical Parameters

The physical model of an EV can be sufficiently characterized using the parameters shown in Table 46.

Table 46. EV and charger performance parameters.

Range (miles)	r	maximum miles the EV can drive per one full charge cycle
Mileage efficiency (miles/kWh)	m	discharge rate while driving, given in miles/kWh.
Charging rating (kW)	E_{max}^{in}	maximum power a charger can transfer from grid to EV
Discharging rating (kW)	E_{max}^{out}	maximum power a charger can transfer from EV to grid
Charging efficiency	η_{in}	Conversion ratio of the energy addition in EV to the energy input from the grid in V1G mode
Discharging efficiency	η_{out}	Conversion ratio of energy transferred to the grid to the energy depletion in EV in V2G mode

These physical parameters for various EV models are sourced from DOE's publicly available data (Gohlke and Zhou 2020) (www.fueleconomy.gov n.d.) and are tabulated in Table 47.

Table 47. Sales data and physical parameters for commercially available EVs 2016-2019.

EV Model	2016-2019 Sales %	Range (miles)	Charger Rating (kW)	Mileage Efficiency (miles/kWh)
Tesla Model 3	44.11%	220	11.5	3.846
Tesla Model S	14.52%	285	11.5	3.333
Tesla Model X	12.92%	258	11.5	2.857
Chevy Bolt	8.66%	238	3.3	3.571
Nissan Leaf	7.79%	151	3.3	3.333
BMW i3	3.70%	153	7.4	3.846
VW e-Golf	2.04%	125	7.2	3.571
Fiat 500E	1.48%	84	6.6	3.333
Audi e-tron	0.80%	204	11	2.174
Kia Soul EV	0.76%	111	6.6	3.226
Ford Focus EV	0.49%	115	6.6	3.226
Smart ED	0.46%	58	3.3	3.226
Chevy Spark	0.46%	84	3.3	3.571
Jaguar I-Pace	0.44%	234	7	2.273
Honda Clarity BEV	0.42%	89	7.7	3.333
Hyundai Kona Electric	0.26%	258	6.6	3.571
Kia Niro EV	0.23%	239	7.4	3.333
Mercedes B-Class (B250e)	0.23%	87	7	2.5
Hyundai Ioniq EV	0.23%	124	7	4
Mitsubishi I EV	0.01%	59	3.3	3.333

Since a level 1 charger is too slow for the new EV models, we consider a level 2 charger for all EVs and their ratings are shown in Table 46. The ratings for charging (V1G) and discharging (V2G) is considered the same in this study. The 90% charger efficiency is considered for all EV models to account for losses.

10.2.2 EV Fleet Population and Driving Schedule Mapping

To create a diverse EV population, a model is picked from a random distribution based on 2019 EV sales data probability, as shown in Table 46. Then we pick a random driving schedule from NHTS 2017 data (distribution shown in Figure 46) and associate it to the selected model. While picking a random driving pattern, it is ensured that:

a) $d < r$:: The daily miles traveled are not more than the range of the EV model.

b) $T_p . E_{max}^{in} < \frac{r}{m}$: The plug-in duration is sufficient to charge the EV fully before it leaves home every day.

10.2.3 Assumptions

In this model, both the weekday and weekend schedules are weighted together to provide a combined dataset of driving patterns and EV availability rather than treating them separately. It is assumed that all residential EV owners have level 2 charging available as level 1 charging is too slow for new EV models with longer range. The EV charging facility is only assumed to be available at home, therefore work charging or highway charging is not considered. Further, based on the NHTS 2017 vehicle trips data, the charging duration is only considered between the latest home arrival time and the earliest home leaving time of a day. The EV is not considered available for charging outside this period. The BAU charging strategy starts charging to 100% with the maximum charger rating as soon as the EV arrives home. Similarly, the BAU boundary condition is that an EV must have 100% state of charge (SOC) every day before leaving home.

10.2.4 Physical Equations and Constraints

To model EV behavior we defined a set T of all 24 hours and a set T_{trans} that contains all transactive hours, i.e., when the EV is parked at home and available for charging or discharging, excluding the boundary hours t_{in} and t_{out}. $E^{in}(t)$ and $E^{out}(t)$ are the charging and discharging energy amount in kWh exchanged by the EV with the grid. During nontransactive hours, the energy exchanged between grid and EV is 0, that is

$$E^{in}(t) = E^{out}(t) = 0 \; \forall t \in T - T_{Trans}. \quad (20)$$

During transactive hours, the energy exchange can range from zero and the maximum amount permissible by the charger rating

$$0 \leq E^{in}(t) \leq E_{max}^{in} \; \forall t \in T_{trans} \quad (21)$$

$$0 \leq E^{out}(t) \leq E_{max}^{out} \; \forall t \in T_{trans}. \quad (22)$$

Note that E^{out} is nonzero only in the V2G case where the EV can discharge to provide energy to the grid. The BAU charging strategy considers only the V1G mode with constant charging rate ($E^{in} = E_{max}^{in}$) until the EV is fully charged. Note that the energy exchange recorded by the net meter is different from what the EV experiences since it also accounts for losses. Metered energy is $E^{in} \div \eta_{in}$ and $E^{out} \times \eta_{out}$ in case of charging and discharging.

The SOC at any time t is denoted by $C(t)$ and is governed by different equation during different time periods as

$$C(t) = C(t-1) + \left(E^{in}(t) - E^{out}(t)\right) \; \forall t \in T_{trans} \quad (23)$$

$$C(t) = C(t-1) - \frac{Q_d}{2} \; \forall t \in \{t_{in}, t_{out}\} \quad (24)$$

$$C(t) = C(t-1) \; \forall t \in T - T_{trans} - \{t_{in}, t_{out}\} \quad (25)$$

Equation (25) denotes the change in SOC during transactive hours when EV is exchanging energy with the grid. We assume the daily driving charge $Q_d = d/m$ is drained equally at the departure and arrival hours as modeled in Equation (26). SOC remains unaffected for the rest of the hours as reflected in Equation (27). For the base case, the boundary condition of SOC is defined as the EV should be fully charged before it leaves home and can be written as:

$$C(t-1) = C^{max} \; \forall t \in \{t_{out}\} \qquad (26)$$

where C^{max} is the maximum permissible stored charge in an EV.

10.2.5 EV Charging Profiles

Using the above modeling and dataset, 200 EVs were populated in different houses in GridLAB-D. A resultant average BAU charging profile of all EVs is shown in Figure 48. It can be seen that the peak occurs in the evening when most EVs return home from work.

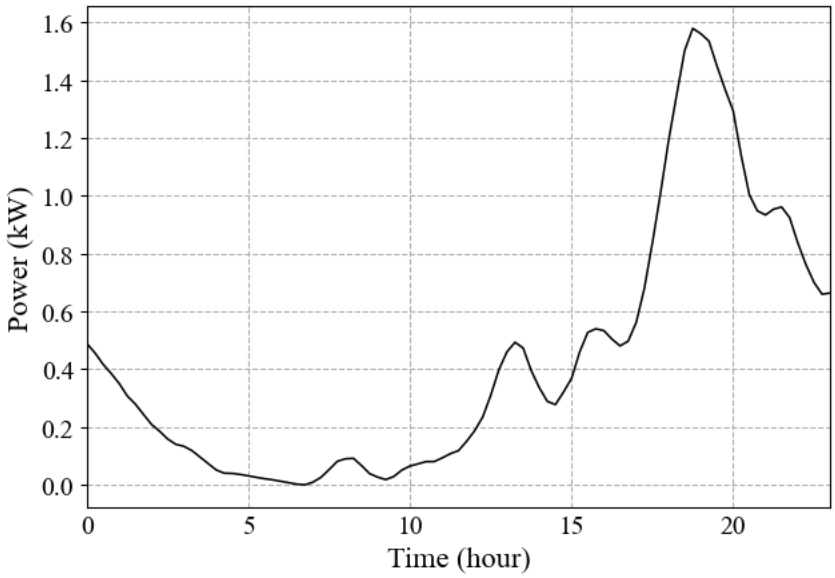

Figure 48. A daily EV charging profile representing an average of a population of 200 residential EVs.

A corresponding mean SOC profile is shown in Figure 49. It is worth noting that, on average, only a small portion of EV battery capacity is used during regular daily travel in the BAU case charging strategy. It suggests that the transactive bidding strategy can significantly enhance the EV utility particularly in V2G operation. Results of transactive control for EV V2G operation are provided in (Singhal et al. 2021).

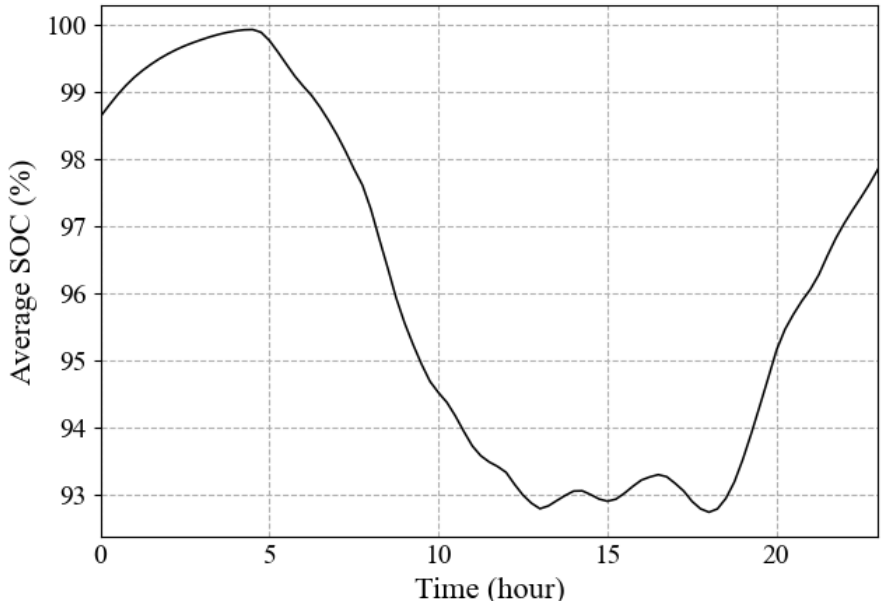

Figure 49. An average SOC profile of a population of 200 residential EVs.

11.0 Conclusions

The co-simulation model developed for the DSO+T study demonstrated the ability to model the entire electricity delivery system from bulk generation to individual end loads. Comparison to real-world performance demonstrated that the resulting models represent average load and price values and their daily and seasonal trends well. The large scale of the simulation, in terms of number of cases, full annual analysis, and large number of building and flexible asset models, combined with the fully integrated nature of the simulation challenged the robustness and computational efficiency of both the distribution and bulk system simulation tools. Debugging integration and performance issues within such a computationally heavy, integrated, and multidisciplinary environment is challenging and would benefit from improved diagnostic tools. Simulating the integrated market operation for the HR scenario was particularly challenging and we expect that modeling annual performance of more aggressive decarbonization scenarios (at relevant grid dynamics and market time scales) will be even more difficult. Despite these challenges, the study identified and implemented many robustness, computational efficiency, integration, and accuracy improvements through the course of executing the simulation.

There are key three areas that warrant improvement. First, while the overall simulated load shapes captured aggregate daily and seasonal demand trends well, the daily change in load was consistently over predicted. Better capturing these daily changes in load is important to capture the absolute rate of change of system load and resulting ramping requirements on the providers of flexibility, whether they be the generation fleet or distributed assets. Efforts by the United States Department of Energy (DOE 2019) on updating and improving the understanding of commercial and residential building load profiles could aid in this. Better representations of industrial customers and their load profiles are also needed.

Second, the wholesale market model captured overall price trends but did not capture price excursions. This results in a substantial underprediction in the average daily price range, likely resulting in conservative estimates of the wholesale energy market benefits of demand flexibility. A better understanding of the factors causing wholesale price volatility, and which (if any) can be captured in an improved market model, is important to better estimate the overall value of transactive energy approaches and to evaluate the performance of distributed assets coordinated using signals based on these wholesale market prices. Improved market price modeling will become more important as the continued deployment of renewables increases periods of negative prices, and more frequent extreme events result in prices hitting market caps. Achieving these improvements will likely require improved understanding of representing transmission constraints, generation fleet performance, and dispatch and curtailment strategies for renewable generation.

Finally, this study includes flexible assets that currently have lower levels of deployment (such as EVs and batteries). As more data is collected on their real-world operation improvements in how they are modeled may be required. For example, a limitation of the current modeling platform requires that EVs only charge and discharge at a single location (in this study at a residence). If data suggests a substantial fraction of EVs charge in multiple locations (fully realizing the EV ability to move demand in space and time) updates to the modeling platform will be warranted. There are also many other end-use loads (e.g., appliances, commercial refrigeration, lighting, pumping and irrigation) that were not included in this study that offer flexibility potential.

12.0 References

AMES n.d., Agent-Based Modeling of Electricity Systems source code. Accessed at: https://github.com/ames-market/AMES-V5.0

Ang YQ, ZM Berzolla, and CF Reinhart. From concept to application: A review of use cases in urban building energy modeling. *Applied Energy*, Volume 279, 1 December 2020, Article number 115738

Battula S, L Tesfatsion, and TE McDermott. 2019. A test system for ERCOT market design studies: Development and application. Iowa State University; 2019. https://lib.dr.iastate.edu/econ_workingpapers/79/.

Battula S, L Tesfatsion, and TE McDermott. 2020. "An ERCOT Test System for Market Design Studies." Applied Energy 275. PNNL-SA-147701. doi:10.1016/j.apenergy.2020.115182

Bender SR, MR Oster, TD Hardy, JT Holzer, and JD Follum. 2019. *Future Grid State Modeling for Transactive Systems*. PNNL-28596. Pacific Northwest National Laboratory, Richland, WA.

Blair N, N DiOrio, J Freeman, P Gilman, S Janzou, T Neises, and M Wagner. 2018. *System Advisor Model (SAM) General Description (Version 2017.9.5)*. National Renewable Energy Laboratory, Golden, CO. NREL/ TP-6A20-70414.https://www.nrel.gov/docs/fy18osti/70414.pdf.

Briggs RS, DB Crawley, and JS Schliesing. 1987. *Analysis and Categorization of the Office Building Stock, Topical Report*. Gas Technology Institute, Des Plains, IL. GRI-87/0244

Chen P, T Pedersen, B Bak-Jensen, and Z Chen. 2010. “ARIMA-Based Time Series Model of Stochastic Wind Power Generation.” *IEEE Transactions on Power Systems*, 25(2), 667-676. https://doi.org/10.1109/TPWRS.2009.2033277

Curcija DC, M Yazdanian, C Kohler, R Hart, R Mitchell, and S Vidanovic. 2013. *Energy Savings from Window Attachments.* DOE/EE-0969. Accessed at: https://www.energy.gov/sites/prod/files/2013/11/f5/energy_savings_from_windows_attachments.pdf

Deaver P. 2019. *Updating Thermal Power Plant Efficiency Measures and Operational Characteristics for Production Cost Modeling*. California Energy Commission. https://ww2.energy.ca.gov/2019publications/CEC-200-2019-001/CEC-200-2019-001.pdf

Deru M, K Field, D Studer, K Benne, B Griffith, P Torcellini, B Liu, M Halverson, D Winiarski, M Rosenberg, M Yazdanian, J Huang, and D Crawley. 2011. *U.S. Department of Energy Commercial Reference Building Models of the National Building Stock*. NREL/TP-5500-46861, National Renewable Energy Laboratory, Golden, CO. Accessed at: https://www.nrel.gov/docs/fy11osti/46861.pdf

DOE. 2019. End-Use Load Profiles for the U.S. Building Stock: Market Needs, Use Cases, and Data Gaps. Accessed at: https://www.nrel.gov/docs/fy20osti/75215.pdf

DOE-EERE. 2014. Energy Conservation Program: Energy Conservation Standards for Small, Large,and Very Large Air-Cooled Commercial Package Air Conditioning and Heating

Equipment. Accessed at: https://www.energy.gov/sites/prod/files/2014/09/f18/2014-09-18%20Issuance%20cauc_noticeofproposedrulemaking.pdf

DOE-EIA. 2012. COMMERCIAL BUILDINGS ENERGY CONSUMPTION SURVEY (CBECS). Accessed at: https://www.eia.gov/consumption/commercial/data/2012/

DOE-EIA. 2015 RESIDENTIAL ENERGY CONSUMPTION SURVEY (RECS), Accessed at: https://www.eia.gov/consumption/residential/data/2015/

DOE-EIA. 2017. “Rising solar generation in California coincides with negative wholesale electricity prices”. https://www.eia.gov/todayinenergy/detail.php?id=30692.

DOE-EIA n.d. Annual Electric Power Industry Report, Form EIA-861, 2016 data accessed from: https://www.eia.gov/electricity/data/eia861/

El Kontar R, B Polly, T Charan, K Fleming, N Moore, N Long, and D Goldwasser. 2020. URBANopt: An Open-Source Software Development Kit for Community and Urban District Energy Modeling: Preprint. National Renewable Energy Laboratory, Golden, CO. NREL/CP-5500-76781 https://www.nrel.gov/docs/fy21osti/76781.pdf

ERCOT. n.d. “Hourly Load Data Archives.” Accessed March 22, 2019. http://www.ercot.com/gridinfo/load/load_hist/.

Felts DR and P Bailey. 2000. “The state of affairs - packaged cooling equipment in California, Proceeding of American Control for an Energy-Efficient Economy 3, p. 137-148.

Fuller JC, N Prakash Kumar, and CA Bonebrake. 2012. *Evaluation of Representative Smart Grid Investment Project Technologies: Demand Response*. PNNL-20772. Pacific Northwest National Laboratory, Richland, WA. https://www.pnnl.gov/main/publications/external/technical_reports/PNNL-20772.pdf

Fuller J, K Schneider, A Guerra, S Collins, and A Gebeyehu, A. n.d., Characterization & Modeling of Representative Distribution Circuits in GridLAB-D, California Solar Initiative Project, Advanced Distribution Analytic Services Enabling High Penetration Solar PV. Accessed at: https://calsolarresearch.ca.gov/images/stories/documents/Sol4_funded_proj_docs/SCE4/CSI-RDD_Sol4-SCE_Task_3_Technical_Report_1_v6.pdf

Gohlke D and Y Zhou. 2020. Impacts of Electrification of Light-Duty Vehicles in the United States, 2010 – 2019. Alternative Fuels Data Center, DOE, Washington, D.C. https://afdc.energy.gov/data/10567

Graham P, T Brinsmead, S Dunstall, J Ward, L Reedman, T Elgindy, J Gilmore, N Cutler, G James, A Rai, and J Hayward. 2013. *Modelling the Future Grid Forum Scenarios.* CSIRO and Roam Consulting.

GridLAB-D. 2017. Residential Module User’s Guide. Accessed at: http://GridLAB-d.shoutwiki.com/wiki/Residential_module_user%27s_guide

Hale E, H Horsey, B Johnson, M Muratori, E Wilson, B Borlaug, C Christensen, A Farthing, D Hettinger, A Parker, J Robertson, M Rossol, G Stephen, E Wood, and B Vairamohan. 2018. *The*

Demand-side Grid (dsgrid) Model Documentation. National Renewable Energy Laboratory, Golden, CO. NREL/TP-6A20-71492. https://www.nrel.gov/docs/fy18osti/71492.pdf

Hammerstrom DJ, R Ambrosio, J Brous, TA Carlon, DP Chassin, JD DeSteese, RT Guttromson, GR Horst, OM Järvegren, R Kajfasz, S Katipamula, L Kiesling, NT Le, P Michie, TV Oliver, RG Pratt, SE Thompson, M Yao. 2007. *Pacific Northwest GridWise™ Testbed Demonstration Projects: Part I. Olympic Peninsula Project.* PNNL-17167. Pacific Northwest National Laboratory, Richland, WA.

Hart R, D Morehouse, W Price, J Taylor, H Reichmuth, and M Cherniack. 2008. “Up on the roof: From the past to the future.” Proceedings of the 2008 ACEEE Summer Study on Energy Efficiency in Buildings, Pacific Grove, CA, August 17–22 1:3–119.

Hodge B, D Lew, M Milligan, H Holttinen, S Sillanpää, E Gómez-Lázaro, R Scharff, L Söder, XG Larsén, G Giebel, D Flynn, and J Dobschinski. 2012. *Wind Power Forecasting Error Distributions: An International Comparison.* Preprint. https://www.nrel.gov/docs/fy12osti/56130.pdf

Huang Q, TE McDermott, Y Tang, A Makhmalbaf, DJ Hammerstrom, AR Fisher, LD Marinovici, and T Hardy. 2019. "Simulation-Based Valuation of Transactive Energy Systems," in *IEEE Transactions on Power Systems*, vol. 34, no. 5, pp. 4138-4147, Sept. 2019, doi: 10.1109/TPWRS.2018.2838111.

HUD. 2009. Manufactured Home Construction and Safety Standards. 2009 Title 24, Volume 5, Chapter XX, Part 3280 Subpart F: Thermal Protection.

Goldenberg C, M Dyson, and H Masters. 2018. *Demand Flexibility: The Key to Enabling a Low-Cost, Low-Carbon Grid.* Rocky Mountain Institute. Boulder, CO.

Gonzalez-Salazar MA, T Kirsten, and L Prchlik. 2018. Review of the operational flexibility and emissions of gas- and coal-fired power plants in a future with growing renewables. *Renewable and Sustainable Energy Reviews*, Volume 82, Part 1, 2018, Pages 1497-1513, ISSN 1364-0321, https://doi.org/10.1016/j.rser.2017.05.278.

Gotseff P and B Lundstrom. 2017. "Data-Driven Residential Load Modeling and Validation in GridLAB-D," 2017 Ninth Annual IEEE Green Technologies Conference (GreenTech), Denver, CO, pp. 20-25, doi: 10.1109/GreenTech.2017.9.

James P, JE Cummings, J Sonne, R Vieira, and J Klongerbo. 1997. “The Effect of Residential Equipment Capacity on Energy Use, Demand, and Run-Time,” *ASHRAE Transactions*, Vol 103, Pt. 2., American Society of Heating, Refrigerating, and Air- Conditioning Engineers, Inc., Atlanta, GA.

Johra H and P Heiselberg. 2017a. Influence of internal thermal mass on the indoor thermal dynamics and integration of phase change materials in furniture for building energy storage: A review, *Renewable and Sustainable Energy Reviews*, Volume 69, 2017, Pages 19-32, ISSN 1364-0321, https://doi.org/10.1016/j.rser.2016.11.145.

Johra H, P Heiselberg, and J Le Dréau. 2017b. Numerical Analysis of the Impact of Thermal Inertia from the Furniture / Indoor Content and Phase Change Materials on the Building Energy Flexibility. Proceedings of the 15th IBPSA Conference San Francisco, CA, USA, Aug. 7-9, 2017

Kohler C, Y Shukla, and R Rawal. 2017. "Calculating the Effect of External Shading on the Solar Heat Gain Coefficient of Windows." Building Simulation 2017. San Francisco, CA, 2017. LBNL-2001057.

Kumar N, P Besuner, S Lefton, D Agan, and D Hilleman. 2012. *Power Plant Cycling Costs.* National Renewable Energy Laboratory, Golden, CO. No. NREL/SR-5500-55433. https://www.nrel.gov/docs/fy12osti/55433.pdf

Lei X, Y Ye, J Lerond, and J Zhang. 2021. A modularized Urban Scale Building Energy Modeling Framework Designed with an Open Mind. To be published at 2021 ASHRAE Winter Conference.

Lew D, G Brinkman, E Ibanez, A Florita, M Heaney, BM Hodge, M Hummon, G Stark, J King, SA Lefton, N Kumar, D Agan, G Jordan, and S Venkataraman. 2013. *The Western Wind and Solar Integration Study Phase 2*. Office of Scientific and Technical Information. https://doi.org/10.2172/1220243. https://www.osti.gov/servlets/purl/1220243.

Meyn S, T Sarmad, I Hiskens, and J Stoustrup. 2018. *Energy Markets and Responsive Grids: Modeling, Control, and Optimization*. Springer, New York, NY

Mukherjee M, LD Marinovici, TD Hardy, and J Hansen. (2020). “Framework for large-scale implementation of wholesale-retail transactive control mechanism”. *International Journal of Electrical Power and Energy Systems*, Volume 115, 2020. https://www.sciencedirect.com/science/article/pii/S0142061519306258

Navigant. 2015. Residential End Uses: Area 1: Historical Efficiency Data. Navigant Consulting, Inc. Chicago, IL. Accessed at: https://www.eia.gov/analysis/studies/residential/pdf/res_ee_fuel_switch.pdf

Navigant. 2018. EIA - Technology Forecast Updates - Residential and Commercial Building Technologies – Reference Case. Navigant Consulting, Inc. Chicago, IL. Accessed at: https://www.eia.gov/analysis/studies/buildings/equipcosts/pdf/appendix-a.pdf

NEEP. 2014. Northeast and Mid-Atlantic High Performance Rooftop Unit Market Transformation Strategy Report. Northwest Energy Efficiency Partnerships, Lexington, MA. Accessed at: https://neep.org/sites/default/files/resources/NEEP%20RTU%20Market%20Transformartion%20Strategy%20Report%202016.pdf

New JR, M Adams, E Garrison, W Copeland, B Smith, and A Campbell. 2019. "Nailing the Peak: City-Scale, Building-Specific Load Factor and Contribution to a Utility's Hour of Critical Generation." Proceedings of the IBPSA Building Simulation Conference, Rome, Italy, Sept. 2-4, 2019 http://web.eecs.utk.edu/~jnew1/publications/2019_IBPSA_Peak.pdf

Pratt RG, CC Conner, EE Richman, KG Ritland, WF Sandusky, and ME Taylor. 1989. *Description of Electric Energy Use in* Single *Family Residences in the Pacific Northwest*. DOE/BP 13795 21, Bonneville Power Administration, Portland, OR.

Pratt RG, SR Bender, HM Reeve, SE Barrows, T Yin, and TD Hardy. 2022. *DSO+T Study Volume 4: Valuation Methodology and Economic Metrics.* PNNL-SA-32170-4. Pacific Northwest National Laboratory, Richland, WA.

Potomac Economics. 2017. *2016 State Of The Market Report For The Ercot Electricity Markets*. Accessed at: https://www.potomaceconomics.com/wp-content/uploads/2017/06/2016-ERCOT-State-of-the-Market-Report.pdf

PYPOWER. 2020. https://github.com/rwl/PYPOWER. Accessed Jan 2021.

Reeve HM, SE Widergren, RG Pratt, B Bhattarai, S Hanif, SR Bender, TD Hardy, and M Pelton. 2022a. *The Distribution System Operator with Transactive Study Volume 1: Main Report.* PNNL-SA-32170-1. Pacific Northwest National Laboratory, Richland, WA.

Reeve HM, et al. 2022b. *DSO+T Study Volume 5: Study Results.* PNNL-SA-32170-5. Pacific Northwest National Laboratory, Richland, WA.

Sengupta M, Y Xie, A Lopez, A Habte, G Maclaurin, and J Shelby. 2018. "The National Solar Radiation Data Base (NSRDB)." *Renewable and Sustainable Energy Reviews* 89 (June): 51-60.

Schneider KP, DW Engel, Y Chen, SE Thompson, DP Chassin, and RG Pratt. 2008. *Modern Grid Initiative Distribution Taxonomy Final Report.* PNNL-18035. Pacific Northwest National Laboratory, Richland, WA. Accessed at: https://pdfs.semanticscholar.org/b7d2/946e73aa2cba6c321f7802aefb375112439d.pdf

Schneider KP, E Sortomme, SS Venkata, MT Miller, and L Ponder. 2016. "Evaluating the magnitude and duration of cold load pick-up on residential distribution using multi-state load models," in *IEEE Transactions on Power Systems*, vol. 31, no. 5, pp. 3765-3774, Sept. 2016, doi: 10.1109/TPWRS.2015.2494882.

Singhal A, B Bhattarai, FB dos Reis, HR Reeve, and RG Pratt. 2021. Transactive EV Agent: Design and Performance Evaluation. IEEE PES General Meeting. IEEE.

Taylor ZT and RG Pratt. 1989. *Summary of Electrical Energy Use in the Commercial Sector.* DOE/BP 13795 22, Bonneville Power Administration, Portland, Oregon.

Taylor ZT, Y Xie, CD Burleyson, N Voisin, and I Kraucunas. 2019. A multi-scale calibration approach for process-oriented aggregated building energy demand models. *Energy and Buildings*, 191, 82–94. https://doi.org/10.1016/j.enbuild.2019.02.018

Tesla. 2019. Tesla PowerWall Dataset. Tesla, Inc. Austin, TX. https://www.tesla.com/sites/default/files/pdfs/powerwall/Powerwall%202_AC_Datasheet_en_northamerica.pdf

TESP n.d., Transactive Energy Simulation Platform (TESP) Documentation. Accessed at: https://tesp.readthedocs.io/en/latest/

TESP n.d. b, Transactive Energy Simulation Platform (TESP) Code. Accessed at: https://github.com/pnnl/tesp

Texas Comptroller State Energy Conservation Office. n.d. “Commercial and Multi-family Construction.” Accessed October 6, 2019 at: https://comptroller.texas.gov/programs/seco/code/commercial.php

Vibrant Clean Energy. 2019. *Colorado Electrification & Decarbonization Study*. Boulder, Colorado. https://www.vibrantcleanenergy.com/wp-content/uploads/2019/11/CEDS-CEI-VCE-FullReport.pdf

WECC. 2020. “Data Development and Validation Manual (DDVM).” Accessed January 11, 2021 at: https://www.wecc.org/Reliability/ADS_Data_Development_and_Validation_Manual_6-30-2020_V3.0.pdf

Widergren SE, DJ Hammerstrom, TE Mcdermott, Q Huang, K Kalsi, D Sivaraman, Y Tang, J Lian, A Veeramany, A Makhmalbaf, and JT Woodward. 2017. Transactive Systems Simulation and Valuation Platform Trial Analysis. PNNL-26409. Pacific Northwest National Laboratory, Richland, WA. 10.13140/RG.2.2.10508.82561.

Widergren SE, B Bhattarai, RG Pratt, S Hanif, A Singhal, A Tbaileh, F Bereta dos Reis, and HM Reeve. 2022. *DSO+T Study Volume 3: Transactive Energy Coordination Framework.* PNNL-SA-32170-3. Pacific Northwest National Laboratory, Richland, WA.

Zhang J, BM Hodge, S Lu, HF Hamann, B Lehman, J Simmons, E Campos, V Banunarayanan, J Black, and J Tedesco. 2015. Baseline and target values for regional and point PV power forecasts: Toward improved solar forecasting, *Solar Energy*, Volume 122, 2015, Pages 804-819, ISSN 0038-092X, https://doi.org/10.1016/j.solener.2015.09.047.

Pacific Northwest National Laboratory

902 Battelle Boulevard
P.O. Box 999
Richland, WA 99354
1-888-375-PNNL (7665)

www.pnnl.gov